A review of the Geodynamic Evolution of Flat Slab Subduction in Mexico, Peru and Chile

Article *in* Tectonophysics · January 2017

DOI: 10.1016/j.tecto.2016.11.037

7 authors, including:

vlad constantin Manea
Universidad Nacional Autónoma de México
93 PUBLICATIONS **1,680** CITATIONS
SEE PROFILE

Marina Manea
Universidad Nacional Autónoma de México
76 PUBLICATIONS **1,051** CITATIONS
SEE PROFILE

Luca Ferrari
Universidad Nacional Autónoma de México
149 PUBLICATIONS **5,024** CITATIONS
SEE PROFILE

Teresa Orozco Esquivel
Universidad Nacional Autónoma de México
31 PUBLICATIONS **929** CITATIONS
SEE PROFILE

Tectonophysics 695 (2017) 27–52

Contents lists available at ScienceDirect

Tectonophysics

journal homepage: www.elsevier.com/locate/tecto

A review of the geodynamic evolution of flat slab subduction in Mexico, Peru, and Chile

V.C. Manea [a,b,*], M. Manea [a,b], L. Ferrari [b], T. Orozco [b], R.W. Valenzuela [c], A. Husker [c], V. Kostoglodov [c]

[a] National Institute for Earth Physics, Măgurele, 12 Călugăreni str., 077125, Ilfov, Romania
[b] Computational Geodynamics Laboratory, Centro de Geociencias, Universidad Nacional Autónoma de México, Campus Juriquilla, Querétaro, Qro. 76230, Mexico
[c] Departamento de Sismología, Instituto de Geofísica, Universidad Nacional Autónoma de México, 04510, Mexico City, D. F., Mexico

ARTICLE INFO

Article history:
Received 7 January 2016
Received in revised form 21 November 2016
Accepted 29 November 2016
Available online 06 December 2016

Keywords:
Subducting slabs geometry
Flat-slab subduction
Oceanic plate and overriding plate structure
Numeric modeling of slab flattening

ABSTRACT

Subducting plates around the globe display a large variability in terms of slab geometry, including regions where smooth and little variation in subduction parameters is observed. While the vast majority of subduction slabs plunge into the mantle at different, but positive dip angles, the end-member case of flat-slab subduction seems to strongly defy this rule and move horizontally several hundreds of kilometers before diving into the surrounding hotter mantle. By employing a comparative assessment for the Mexican, Peruvian and Chilean flat-slab subduction zones we find a series of parameters that apparently facilitate slab flattening. Among them, trench roll-back, as well as strong variations and discontinuities in the structure of oceanic and overriding plates seem to be the most important. However, we were not able to find the necessary and sufficient conditions that provide an explanation for the formation of flat slabs in all three subduction zones. In order to unravel the origin of flat-slab subduction, it is probably necessary a numerical approach that considers also the influence of surrounding plates, and their corresponding geometries, on 3D subduction dynamics.

Contents

* Corresponding author at: National Institute for Earth Physics, Măgurele, 12 Călugăreni str., 077125, Ilfov, Romania.

http://dx.doi.org/10.1016/j.tecto.2016.11.037
0040-1951/

1. Introduction

In the framework of plate tectonics, subduction zones are among the major tectonic features where Earth's lithospheric plates return to the mantle. One tectonic consequence of the subduction process is the occurrence of inter-plate and intra-plate earthquakes which define Wadati-Benioff zones, in other words, the present-day shape of sinking slabs. This valuable information combined with tomographic anomalies provide a powerful tool used to provide a short-term snapshot of the subduction process where the cold oceanic lithosphere sinks into the fluid-like mantle with a variety of dips and shapes. Traditionally, subduction zones were classified in two main categories: the Marianas type and the Peru-Chile type (Uyeda and Kanamori, 1979). Whereas the Marianas subduction zone is characterized by an old oceanic plate that is subducting at an almost vertical angle, the Peru-Chile type is known for its relatively fast and young oceanic plate that subducts beneath the South American plate less steeply, including horizontal slab segments (e.g., Barazangi and Isacks, 1976; Cahill and Isacks, 1992; Ramos and Folguera, 2009). This particular phenomenon of flat subduction in known to occur only in three places worldwide: Central Mexico, Peru and Central Chile (Fig. 1). In other locations where it was previously suggested the slab dip angle is shallow rather than horizontal (e.g., Cascades, McCrory et al., 2012; Nankai Trough, Matsubara et al., 2008; Ecuador, Yepes et al., 2016) or with a complex geometry because of the proximity to a triple point (eastern part of the Alaska subduction zone, Ratchkovski and Hansen, 2002, Jadamec and Billen, 2012). On the basis of their particular, but rather similar slab geometries and subduction settings, in this review we discuss only the Mexican, Peruvian and Pampean (Chilean) flat-slab subduction zones.

In this paper we review the recent progress in understanding how flat-slabs form, evolve and interact with the surrounding mantle over geological time scales. Although clues to the dynamics of the flat-slab subduction processes can be found in several measurable parameters, as convergence rates or incoming plate ages, their long-term dynamic evolution is still uncertain due to its transient character. Lifetime of the South America and Mexico flat-slab segments is <20 Myr (Ramos and Folguera, 2009; Ferrari et al., 2012), and present-day observations are insufficient to understand subduction dynamics without additional insights provided by complementary observations and techniques, as geochemistry, tectonic records, geochronology and numerical modeling. However, in the last decade, knowledge of the flat-slab subduction dynamics has considerably increased (e.g. Espurt et al., 2008; Pérez-Campos et al., 2008; Gerya et al., 2009; Manea et al., 2012; Skinner and Clayton, 2013; Kusky et al., 2014; Eakin et al., 2015; Gérault et al., 2015; Hu et al., 2016). While the vast majority of subducted slabs plunge into the mantle at different, but positive dip angles, the end-member case of flat-slab subduction seems to strongly defy this rule as the slab moves horizontally several hundreds of kilometers before diving into the surrounding hotter mantle. Recent improvement in geological, petrological, and geochemical records, coupled with computational algorithms and fast growing computing resources, has contributed to first-order understanding of the evolution of subduction zones in general, and flat-slab subduction systems in particular. Although several alternative mechanisms have been proposed to explain this particular type of subduction (e.g. Cross and Pilger, 1982; van Hunen et al., 2002; Manea and Gurnis, 2007; Manea et al., 2012), the analysis of real cases of flat-slab subduction has been somewhat limited.

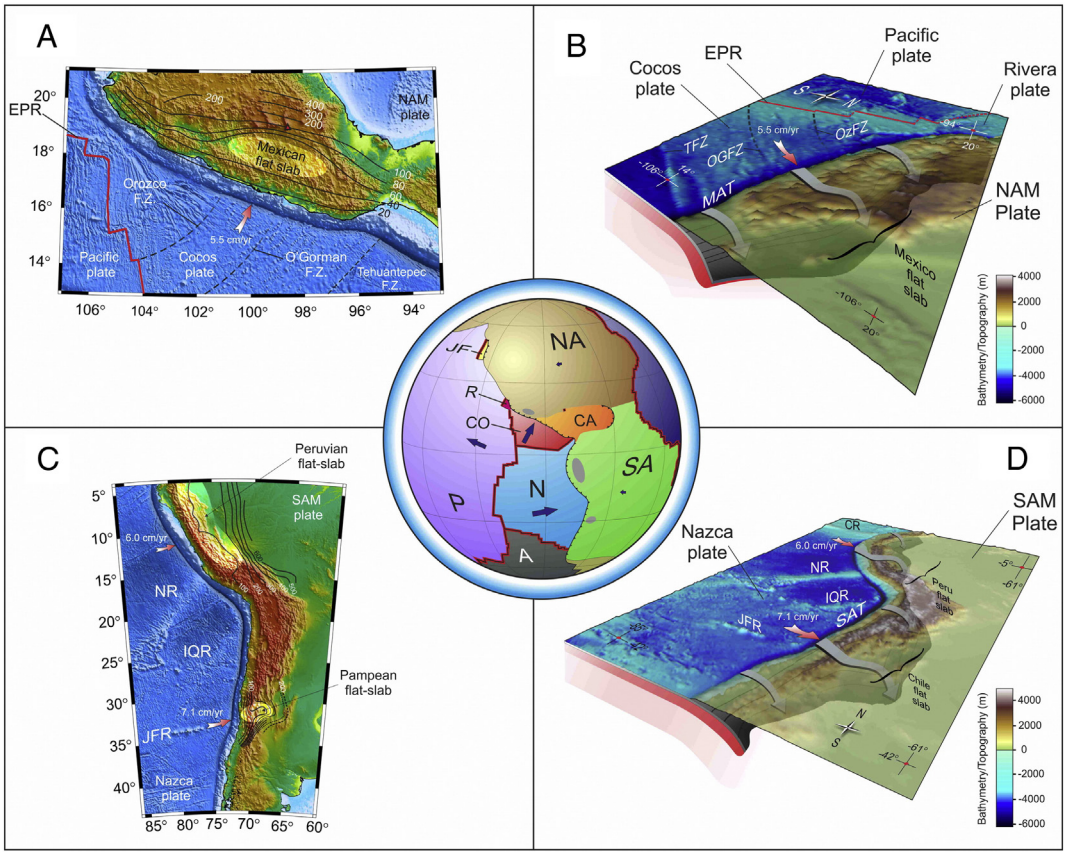

Fig. 1. The Mexican, Peruvian and Chilean flat-slab bathymetric and topographic maps (A, C). Three-dimensional visualization of the Mexican and Andean subduction zones (B, D). Large curved gray arrows are used to facilitate viewing of subducting slabs geometry beneath Mexico and South America. Surface relief is shown as a semi-transparent layer. Labeled black contours indicate depths to the slab surface from the Earth's surface. Red arrows show the direction of the Cocos and Nazca plates movement relative to North (NAM) and South America (SAM) plates. EPR – East Pacific Rise, MAT – Middle America Trench, SAT – South America Trench, NR – Nazca Ridge, IQR – Iquique Ridge, JFR – Juan Fernandez Ridge. Central inset – global view of present day tectonic plates: JF – Juan de Fuca, Co – Cocos, R – Rivera, NA – North America, P – Pacific, SA – South America, CA – Caribbean, N – Nazca.

Here we address advances in the overall understanding of flat-slab structure and evolution, with a focus on the Mexican, Peruvian, and Chilean flat-slab subduction zones. By comparing these three particular cases of modern flat-slab subduction we hope to contribute to the understanding of this rather enigmatic case of subduction. We first examine the present-day configuration and structure of the Mexican, Peruvian, and Chilean flat-slabs, and then review the Neogene tectonic history of the Cocos and Nazca plates. Next, we analyze the geochemical signature and evolution of volcanism associated with the process of slab flattening. Following this section is a review of seismic anisotropy and mantle flow in areas of flat subduction, and then we highlight some of the models that best fit the observations. In the end, we present published dynamic numeric models that have tried to explain the slab flattening process, and present a comparative summary table of subduction parameters for the three flat-slab subduction zones.

2. Tectonic setting

Despite the fact that recent geophysical experiments started revealing the hidden subduction structure at a level of detail never seen before, the tectonic environment around the subduction of Cocos and Nazca plates beneath North and South America is still not entirely understood, especially in the flat-slab subduction areas. In this chapter, we will briefly review the offshore and onshore first-order tectonic elements specific for the Mexican, Peruvian, and Chilean flat-slabs.

2.1. The Mexican flat-slab

In Mexico, the Cocos plate is a remnant of the large Farallon plate who began to split into a series of smaller plates since ~28 Myr ago when the East Pacific Rise (EPR) began to interact with the North American Plate (Atwater and Stock, 1998). The approaching of the EPR to the North and South America subduction zones during the Early Paleogene resulted in an increasingly narrow Farallon plate with a subduction boundary in excess of 10,000 km length and a lateral variation in slab age and convergence direction (Wright et al., 2016). Apparently, this produced a highly tensional stress field within the Farallon plate (Wortel and Cloetingh, 1981) that eventually led to its fission into the Cocos and Nazca plates around 23 Myr ago (Lonsdale, 2005). Afterward, at ~10 Ma the Rivera plate split from the westernmost part of the Cocos plate and start acting as an independent microplate since then (DeMets and Traylen, 2000). The triangular shaped Cocos plate is bordered to the northeast by the North American plate and the Caribbean plate, to the west by the Pacific plate and to the south by the Nazca plate (Fig. 1 – inset). The present flat-slab area is located along the central part of the Cocos-North America plate boundary (Fig. 1A,B). Despite the fact that the convergence rate between Cocos and North America and the plate age increases only slightly to the southeast along the Middle America Trench (MAT) (~5 to ~6 cm/yr, ~10 to 18 Ma, respectively) (Schellart et al., 2008; Sdrolias and Muller, 2006), the dip of the subducting slab varies strongly, from steep to flat (Fig. 1B). In this review paper, we use velocities for tectonic plates that were calculated using the relative plate motion model in the Indo-Atlantic hotspot reference frame of O'Neill et al. (2005). This reference frame is widely used in studies where evolution of subducting plates is investigated by numerical means (Schellart et al., 2008), and it is the one that best describes plate motions, subduction kinematics and mantle flow (Schellart et al., 2011).

Using hypocenters of local and teleseismic earthquakes, Pardo and Suárez (1995) first showed the geometry of the subducting Cocos slab in Mexico and the extension of the flat-slab segment. However, it was only recently that the accurate geometry of the Mexican flat-slab was revealed by the receiver function study of Pérez-Campos et al. (2008). The flat-slab segment runs almost perfectly horizontal at ~45 km depth some 300 km inland from the MAT before sinking at a fairly steep angle of ~75° into the asthenosphere (Husker and Davis, 2009).

According to Schellart et al. (2008), the MAT in the flat-slab area retreats (rolls back) at a rate of 0.6–0.7 cm/yr. The Quaternary erosion rate along the MAT in Mexico is quite small, only 0.1 cm/yr (Mercier de Lépinay et al., 1997; Vannucchi et al., 2013), and most of the ~200 m thin layer of oceanic sediments enters the subduction zone (Manea et al., 2003). The Cocos plate contains a series of well-defined oceanic fracture zones created by the physical extension of transform faults between offset spreading centers along EPR. These are the Orozco, O′ Gorman, and farther south and distant from the flat-slab area, the Tehuantepec fracture zone (Fig. 1A). Apart from fracture zones, the Cocos plate morphology is characterized by abundant seamounts that roughen the oceanic crust surface in different regions. However, offshore the flat-slab area, between the Orozco and the O′Gorman fracture zones, the oceanic plate surface is rather smooth (Fig. 1B) compared with the rugged surface of the neighboring regions (Kanjorski, 2003). The bathymetry along the entire MAT reflects a complex response of the crust to the subduction process, with the abyssal-hill fault system reactivated due to the plate bending. Ranero et al. (2003) showed that through these faults that cut across the oceanic crust and uppermost mantle, a large quantity of fluids is transported into the subduction zone.

The overriding plate is part of the North American plate, which above the flat slab area moves almost westward at a rate of 1.8–2.0 cm/yr (Schellart et al., 2007). The continental crust in Mexico is composed by an assemblage of several terranes with different age and thickness (Sedlock et al., 1993; Ferrari et al., 2012). In particular, the continental crust underlain by the flat slab area belongs to the Guerrero, the Mixteco, the Oaxaca and the Xolapa terranes (Fig. 2A). The Guerrero terrane consists of Mesozoic volcano-sedimentary, low-grade metamorphic assemblages thrusted onto Paleozoic and Precambrian crystalline rocks of the Mixteco and Oaxaca terranes, which constitute the oldest core of continental Mexico. Bounding the Guerrero, Mixteco and Oaxaca terranes is the trench parallel belt of low- to medium-grade metamorphic and plutonic rocks of the Xolapa terrane, which is considered to have formed by the exhumation of the terranes to the north during the Oligocene (Herrmann et al., 1994; Ratschbacher et al., 2009; Ducea et al., 2004).

2.2. The Peruvian flat-slab

Several seismic studies documented the existence of a large (>1500 km in length) flat-slab segment in central-northern Peru (Barazangi and Isacks, 1976; Hasegawa and Sacks, 1981; Suárez et al., 1983; Grange et al., 1984; Cahill and Isacks, 1992). In this region the Nazca plate subducts obliquely beneath the South American plate at a rate of ~6 cm/yr (Schellart et al., 2008) (Fig. 1C). The Nazca plate contains a series of well-defined bathymetric highs corresponding to aseismic ridges and fracture zones. Among them, the one that is of particular interest for the Peruvian flat-slab is the aseismic Nazca ridge (Fig. 1C,D), which has been proposed to contribute to slab flattening beneath Peru (Pilger, 1981) together with the hypothetical, and now completely subducted, Inca plateau (Gutscher et al., 1999; Gutscher, 2002). Offshore the region of flat-slab, the age of the Nazca plate increases along the Peru-Chile trench from ~30 Ma to the north (at ~5°S latitude) to ~45 Ma in the southern (at ~15°S latitude) part of the flat slab area (Sdrolias and Muller, 2006) (Fig. 1C). Strong variations in the erosion/shortening rates along the trench in the Peru-Chile flat-slab area produced a counterclockwise rotation of the trench. Whereas in the northern part the trench rolls back at a rate of ~1.3 cm/yr, in the southern part the trench actually rolls forward at a high rate of ~ − 0.7 cm/yr (Schellart et al., 2008). The geometry of the subducted plate in the Peruvian Andes is similar to that reported for the Mexican flat-slab although at different depth. The slab initially descends at an angle of ~30° down to ~100 km depth, and then it flattens out for several hundred of km beneath Sierras Pampeanas, before plunging into the mantle (Dorbath et al., 1991; Gutscher et al., 2000).

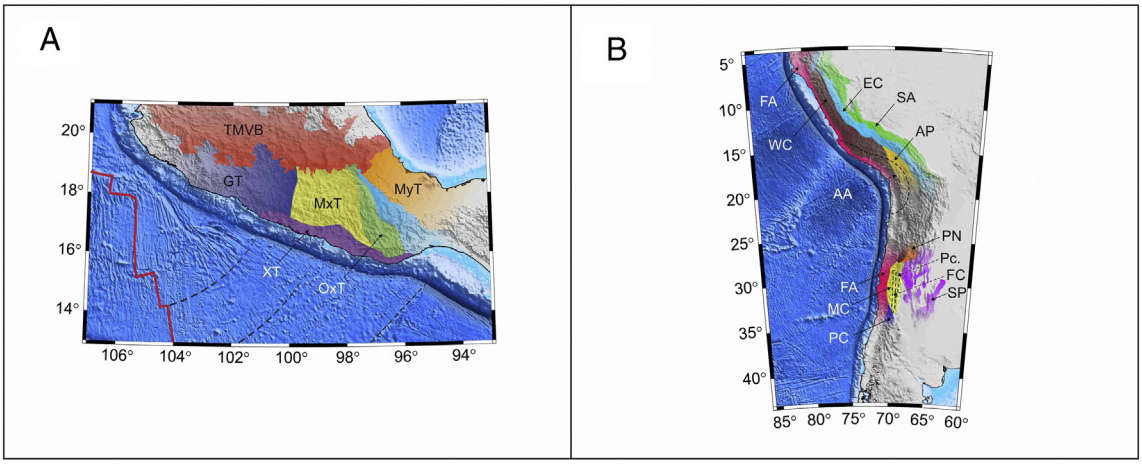

Fig. 2. A. Main crustal units corresponding to the Mexico flat-slab region: TMVB – Trans Mexican Volcanic Belt, GT – Guerrero Terrane, MxT – Mixteco Terrane, MyT – May Terrane, XT – Xolapa Terrane, OxT – Oaxaca Terrane. B. Major morphotectonic provinces in South America corresponding to flat-slab areas in Peru and Chile: FA – Forearc, WC – Western Cordillera, EC - Eastern Cordillera, SA – Subandes, AP – Altiplano, AA – Arequipa-Antofalla coastal block, PN – Puna, MC – Main Cordillera, PC – Principal Cordillera, SP – Sierras Pampeanas, Pc. – Precordillera, FC – Frontal Cordillera.

In the area of flat-slab, the major morphotectonic provinces are, from west to east, the forearc, the Western Cordillera, the northern part of the Altiplano, the Eastern Cordillera and the Subandes (Fig. 2B). The basement of the Peruvian Central Andes consists of sialic Paleozoic basement exposed in the inner Eastern Cordillera and of Proterozoic to Paleozoic basement exposed in the Arequipa-Antofalla coastal block (Fig. 2B) (Mégard, 1987; Chew et al., 2007). This vast region represents a typical Andean-type orogen whose tectonics have been controlled by long-lived subduction processes, which records a complex tectonic history, including major changes in the Wadati-Benioff geometry that accompanied uplift. The development of the present flat-slab subduction began ~11 Ma (Hampel, 2002) and progressively produced inland migration of magmatism as well as compression that propagated towards the foreland and eventually uplifted the Peruvian Andes (Sebrier and Soler, 1991; Ramos and Folguera, 2009). In contrast with the Mexican flat-slab region, the Peruvian flat-slab segment is characterized by the lack of Plio-Quaternary volcanism. The present intense intra-plate shallow seismicity and high rate of shortening (0.4 cm/yr) recorded in central Peru has been considered the effect of flat-slab subduction (Ramos, 1999; Ramos and Folguera, 2009).

Recent seismic experiments constrained the structure of the upper plate and the flat-slab geometry in great detail. Using ambient noise seismicity and surface wave analysis, Ma and Clayton (2014) imaged the subducting plate dipping at ~30° up to 150 km from the coast and then becoming horizontal up to 350 km at a depth of ~90 km. The mantle above the flat slab shows relatively high velocity, suggesting that it is part of the continental lithosphere (Ma and Clayton, 2014).

2.3. The Pampean flat-slab

Based mainly on the distribution of seismicity and the absence of arc volcanism, the pioneer work of Barazangi and Isacks (1976), Isacks et al. (1982) and Jordan et al. (1983) first identified a flat-slab segment beneath central Chile between ~31° S and 32.5° S. Here, the relatively young Nazca plate (33–38 Ma according to Clouard et al., 2007) subducts beneath the South American continental plate at a present-day convergence rate of ~7.1 cm/yr (O'Neill et al., 2005) (Fig. 1C,D). Like the MAT, the South American Trench (SAT) in the flat-slab area rolls back at a rate of ~0.6 cm/yr. Among the many ridges located on the Nazca plate, the Juan Fernandez Ridge (JFR) is of particular interest for the Pampean flat-slab. The JFR is a ~900km long volcanic hotspot chain that originates from a narrow mantle plume (Kopp et al., 2004, Zhao, 2007). The JFR acts as a barrier in the sediment transportation along the trench (Lowrie and Hey, 1981), and its interaction with the South America plate resulted in several tectonic effects such as shoreline indentation, crustal uplift and thickening on the overriding continental plate (Fromm et al., 2004). Recent regional and local seismicity studies show the subducting Nazca plate descending to ~100–110 km depth, and then flattening out and remaining at a constant depth for ~300 km before plunging into the mantle to a more normal subduction angle (Anderson et al., 2007; Linkimer et al., 2011; Marot et al., 2013). Although not all the aseismic ridges located on the Nazca plate are associated with flat-slab segments, the obvious spatial correlation between the position of the Pampean flat-slab and the intersection of the JFR with the SAT has long been used as an argument for suggesting that its extra buoyancy is the main cause for slab flattening in central Chile (Pilger, 1984; Gutscher et al., 2000; Yáñez et al., 2001; Kay and Mpodozis, 2002).

The magmatic, tectonic and sedimentary processes associated with the Pampean flat-slab have been investigated in many papers (e.g., Jordan et al., 1989, 1993, 1997; Kay et al., 1988, 1991; Kay and Abbruzzi, 1996; Kay and Mpodozis, 2002; Ramos et al., 1991, 2002; Ramos, 1999) and more recently reviewed in Ramos and Folguera (2009). As in the case of the Mexican flat-slab, the continental crust in central Chile is composed by an assemblage of several terranes with different age and thickness, orientated roughly parallel to the trench. The major morphotectonic provinces above the flat-slab are the forearc, the Main Cordillera, which includes the Principal Cordillera, the Frontal Cordillera, the Precordillera, and the Sierras Pampeanas (Fig. 2B). The high Andes are part of the Chilenia terrane, and are separated into two main tectonic units, the Principal and Frontal Cordillera, both of them consisting of thick- and thin-skinned thrust belts covered by old volcanic rocks (Allmendinger et al., 1990). The Principal Cordillera is composed by Mesozoic and Tertiary volcanic and sedimentary basement rocks with a crust thickness up to 55 km. The Frontal Cordillera is characterized by late Paleozoic marine and early Mesozoic igneous rocks with a crust thickness up to 70 km (Allmendinger et al., 1990; Gilbert et al., 2006; Heit et al., 2008; Gans et al., 2011). Farther to the east is the Precordillera, a thin-skinned fold and thrust belt, with a Grenville age basement covered by Paleozoic shelf carbonates (Cuyania terrane, Astini et al., 1995; Thomas and Astini, 2003), that accommodated ~70% of the total regional shortening since 16 Ma (Allmendinger et al., 1990). The most inland tectonic unit is represented by the Sierras Pampeanas that extend from eastern half of the Cuyania terrane across the Pampean terrane up to the edge of the Rio de la Plata craton (Fig. 2B). The Sierras Pampeanas represent a thick skinned block-faulted belt that extends >800 km inland from the trench, and whose style of

deformation is characterized by large basement-cored uplifts separated by sediment-filled basins (Jordan and Allmendinger, 1986; Giménez et al., 2000; Alvarado and Ramos, 2011).

3. Geophysical observations

Due to their unique geophysical and geodynamic signature, flat-slab regions offer a good opportunity to study subduction zones from a different perspective than normal subduction systems. In the last few decades a wealth of geophysical experiments has been carried out in areas of flat-slabs, offering the necessary data to study the intriguing phenomena of flat subduction. In this chapter, we present a review of available geophysical observations of flat subduction regions. We first review seismic observations, such as earthquake distribution, Moho depths, mantle tomography and seismic anisotropy, then we analyze results from magnetotelluric experiments, and finally heat flow observations related with flat subduction in Mexico, Peru and Chile.

3.1. Seismicity and geometry of the flat-slab

To image in detail the flat-slab subduction geometry is essential to understand its long-term geodynamic and tectonic evolution. Starting with the pioneer work of Barazangi and Isacks (1976), who were the first to identify flat-slab segments beneath South America using teleseismic earthquake locations, many seismic studies followed and nowadays the flat-slab geometries in Mexico, Peru and Chile are well known. Recent seismological data provide an improved image of the current geometry of the subducting plate below Mexico and South America (Fig. 1). The subducting slabs along both the Mexican and South American margin show a remarkable variability despite a relatively smooth variation in the incoming plate subduction parameters such as plate age and convergence rates (O'Neill et al., 2005), for example.

While early studies identified that the Mexican subduction zone presents large dip variations along strike (Molnar and Sykes, 1969; Stoiber and Carr, 1973), it was Pardo and Suárez (1995) who, based on relocated hypocenters of local and teleseismic earthquakes, showed for the first time the entire Cocos and Rivera slab geometry along MAT, including the flat-slab segment. This study also revealed that the Mexican flat-slab lacks widespread earthquakes in both the forearc region and within the subducting Cocos slab (Fig. 3A). For this reason, in the flat-slab area the subducting slab could not be accurately mapped for distances beyond 250 km from the MAT due to the lack of intraslab seismicity for depths below 80–100 km. More recently, based on analysis of data provided by an ultra-dense 2D temporary broadband seismic array located above the flat-slab region (Middle America Subduction Experiment or MASE), Pérez-Campos et al. (2008) used both local and teleseismic waves to show that the subducted Cocos plate beneath central Mexico becomes almost perfectly horizontal or flat at a distance of ~75 km from the MAT and at ~50 km depth. The slab runs flat for ~175 km then in plunges steeply at ~75° into the mantle (Fig. 3A).

Although the Mexican flat-slab lacks extensive seismic activity, the observed stress distribution shows a preferred orientation in three principal regions parallel to the trench (Pardo and Suárez, 1995) as following: a shallow (<25 km depth) thrust faulting region which overrides a layer characterized by compressional events (40–50 km), followed by a sparse intra-slab seismicity region with downdip T-axes which ends at ~100 km depth (Pardo and Suárez, 1995). The lateral extent, along the MAT, of the flat-slab in Mexico is still not entirely know, although Pardo and Suárez (1995) suggested that this area is bounded by the Orozco and the O'Gorman fracture zones (Fig. 1A,B). This observation was later reinforced by Manea and Manea (2011a), where they show that a regional thermal anomaly above the flat-slab in Mexico is bounded by the prolongation of the Orozco and the O'Gorman fracture zones. It is worth noting that crustal seismicity in the overriding plate above the flat-slab is quite low and no contractional deformation is observed

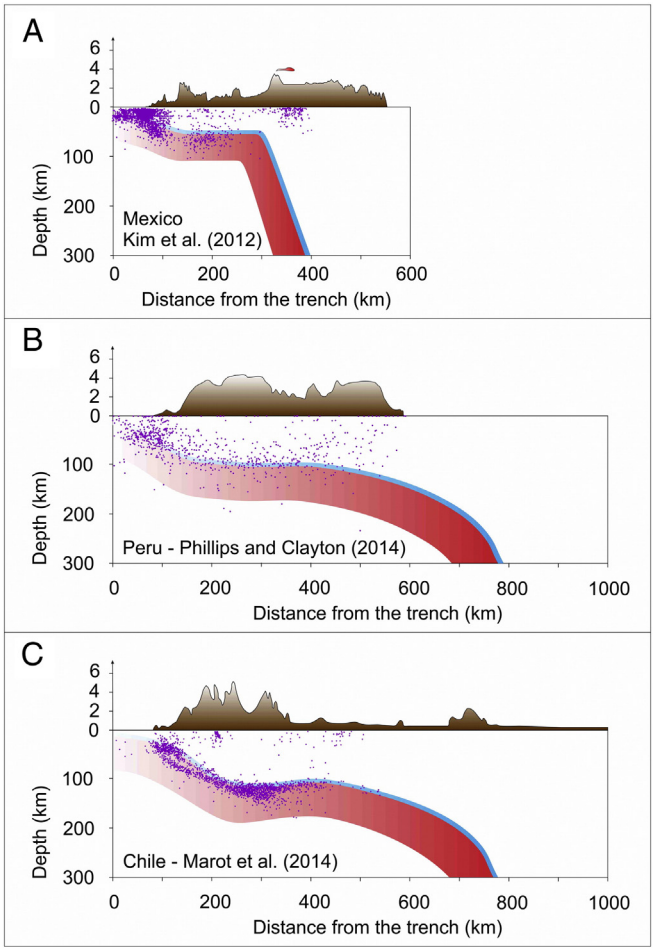

Fig. 3. Vertical cross-sections through the Mexican (earthquakes from SSN (Servicio Sismologico Nacional)), Peruvian and Chilean flat-slabs based on Kim et al. (2012b), Phillips and Clayton (2014) and Marot et al. (2014). Light blue surface depicts the oceanic crust; red surface represents the oceanic lithosphere; purple dots show the earthquakes location.

in the overriding plate unlike other flat subduction systems, like in Peru and Chile. The existence of a thin (~3–5 km thick) ultra slow velocity layer (USVL) located on top of the flat-slab segment revealed by Song et al. (2009), strongly suggests that in Mexico the flat-slab and the overriding plate are essentially decoupled by a mechanically weak layer of serpentine (Manea et al., 2013) or talc (Kim et al., 2012a). The origin of the serpentinized layer is closely related with the presence of fluids. In central Mexico the subducting plate is younger when compared with the slab in Peru and Chile, and most of the fluids are released before the slab reaches 50–70 km depth (Manea and Manea, 2011b). In addition, the long lasting Tertiary magmatic activity in the region above the flat slab (Ferrari et al., 2014) may have created an impermeable lower crust that traps the fluids in the USVL.

Seismicity distribution in Peru has been used in numerous studies aimed at clarifying the Wadati-Benioff geometry and state of stress within the subducting slab (Chandra, 1970; Isacks and Molnar, 1971; Pennington, 1981; Jordan et al., 1983; Bevis and Isacks, 1984; Doser, 1987; Suárez et al., 1990; Norabuena et al., 1994; Tavera and Buforn, 2001). In central Peru, the map distribution of shallow (<60 km) and intermediate depth earthquakes (<350 km) revealed that they are located in the region between the trench and the coast, as well as inland in an area located between the Cordillera Occidental and the Subandean zone (Fig. 3B). A nest of deep seismic hypocenters (> 350 km) shows a distribution subparallel with the trench and is confined to a band with a N-S trend. The cross section location of seismicity shows that the depth of earthquakes increases gradually from west to east at an

angle of ~30° to a depth of ~150 km where it remains constant for several hundreds of km (Fig. 3B). In this area, the Nazca plate is considered to subduct horizontally beneath central Peru. Farther inland, the existence of a deep nest of seismicity at 500–600 km suggests that the slab descends through the upper mantle into the transition zone (Gutscher et al., 2000). Similarly to the Mexican flat-slab, the focal mechanisms associated to the Peruvian flat-slab in each of the three regions mentioned above show different plane orientations and mechanisms. The offshore and onshore shallow seismicity revealed the existence of thrusting faults with planes oriented N-S, parallel to the Cordillera. Tavera and Buforn (2001) suggested that the offshore horizontal compression is due to the positive convergence between the oceanic Nazca and continental South America plates, and the onshore compressional regime may be the consequence of the underthrusting of the Brazilian Shield under the Cordillera Oriental. On the other hand, the intermediate depth as well as deep seismicity shows horizontal tension axes oriented E-W and parallel with the convergence direction, suggesting that the subducting Nazca plate is driven by slab pull forces.

According to the distribution of earthquakes in central Chile (Fig. 3C) the geometry of the Pampean flat-slab shows a remarkable similarity with the flat-slab region of Mexico and Peru: the slab first dip on average at ~30 down to ~100 km depth, where it flattens out underneath the overriding lithosphere for several hundreds of kilometers before sinking into the upper mantle asthenosphere (Fig. 3C). For depths >200 km the seismicity in this region is nearly absent; only one earthquake cluster can be identified at ~200 km depth but separated from the shallower intermediate seismicity by a gap (Gutscher et al., 2000). Although the presence of this aseismic gap is evident, several studies (Isacks and Barazangi, 1973; James and Snoke, 1990, Engdahl et al., 1995, Pardo et al., 2002) have assumed a continuity of the slab based on tomography data (Gutscher et al., 2000). One feature that distinguish the Chilean flat-slab from Mexico and Peru, is the presence of a double seismic zone located within the subducting Nazca slab at intermediate depths (50–200 km) and separated by a 20–25 km thick zone with low seismicity (Marot et al., 2013).

The focal mechanisms of earthquakes in the flat-slab region of central Chile indicate a compressive regime (thrust and reverse faulting) at depths above 70 km, and an extensional regime below (normal faulting) (Pardo et al., 2002; Marot et al., 2013). The seismicity in the overriding plate shows the presence of several clusters located just below the Sierras Pampeanas at a maximum depth of ~50 km and characterized by reverse-faulting events.

3.2. Moho depths above flat-slabs

Crustal thickness variation above flat-slabs plays an important role not only in arc volcanism, petrology and deformation of the upper plate (Carr, 1984; Gómez-Tuena et al., 2007; Wallace and Carmichael, 1999; Ferrari et al., 2012), but also in producing flat-slab (Manea et al., 2012). Recent receiver function studies provided details of the structure of the flat-slab subduction systems in Mexico, Peru and Chile, including Moho depth (Pérez-Campos et al., 2008; Phillips et al., 2012; Phillips and Clayton, 2014; Gans et al., 2011; Perarnau et al., 2012). In Fig. 4 we present a summary of crustal thickness variation above flat-slabs. In Central Mexico, crustal thickness varies from ~35 km in the Guerrero terrane (initially located ~90 km from the MAT) to ~45 km in the area of flat-slab (located at 130–300 km from the MAT), but reaches 50–55 km in the area of the Mixteco-Oaxaca terranes beneath the volcanic arc (Fig. 4A) (Ferrari et al., 2012; Manea et al., 2013).

In Peru, a trench-orthogonal transect passing though Cusco, in the southern part of the flat slab segment, the Moho depth increases from 20 to 40 km in the coastal Cordillera, reaches ~65 km in the Western Cordillera and reaches a maximum depth of ~75 km beneath the Altiplano (Phillips et al., 2012; Phillips and Clayton, 2014) (Fig. 4B).

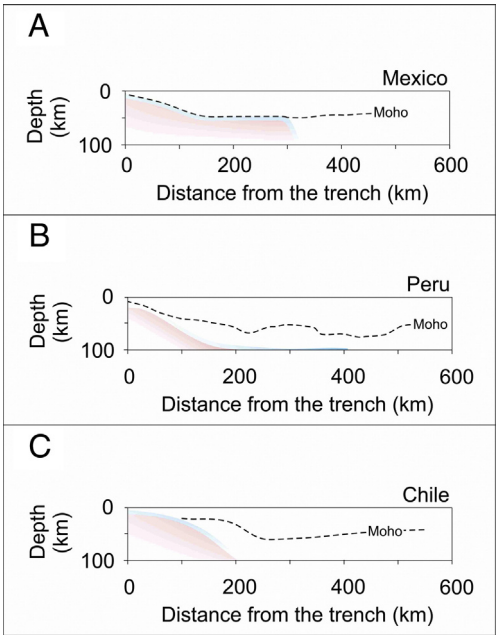

Fig. 4. Moho geometry for Mexico, Peru and Chile flat-slab regions based on seismic experiments of Pérez-Campos et al. (2008), Kim et al. (2012b), Phillips and Clayton (2014), and Marot et al. (2014).

In Chile, recent study of Gans et al. (2011) shows that the continental Moho above the flat slab is rather thick (~70 km), complex and discontinuous in correspondence with the Andean Cordillera. Also a fairly deep Moho (55–60 km) characterizes the continental crust beneath the Precordillera and western Sierra Pampeanas (Regnier et al., 1994; Fromm et al., 2004; Beck et al., 2005; Gilbert et al., 2006; Alvarado et al., 2007; Heit et al., 2008; Ammirati et al., 2013), but reaches only ~35 km in the eastern Sierras Pampeanas (Gilbert et al., 2006; Gans et al., 2011; Perarnau et al., 2012) (Fig. 4C).

3.3. Slow-slip Phenomena

Slow slip phenomena comprises a range of phenomena that include Slow-slip events (SSEs), or slow fault slips that manifest as aseismic deformation, and related seismic phenomena that include tectonic tremors (TTs), low frequency earthquakes (LFE's), and very low frequency earthquakes (LVF's). They represent a valuable piece of information that can provide constraints on the pressure and thermal structure of subduction zones. It is now well established that the location of short term SSE's and NVT's correlate well in Japan and Cascadia and the NVT's are generally accepted to be a manifestation of the slip produced by the SSE's (Shelly et al., 2007; Wech et al., 2009; Obara, 2010; Wech and Bartlow, 2014). Slow slip phenomena are found between 10 and 50 km depth in normal subduction zones (e.g. Beroza and Ide, 2011; Obara et al., 2010; Obara, 2011), nut have not been found in either the Peruvian or Pampean flat slabs where there are only sparse GPS and seismic networks. However, the current understanding of the phenomena suggests that it does not occur at greater depths. It is likely that there is some slow slip phenomena occurring in these regions between 10 and 50 km depth, but its behavior should be like that of a typical subduction zone without interacting with the deeper flat slab sections.

In Mexico, the flat slab is within the 10–50 km depth range for an extended distance and slow slip phenomena are found to stretch out over a greater area than at any other place in the world. The SSEs there have now been precisely recorded for more than a decade, and they include the largest reliably detected events ever (Kostoglodov et al., 2003; Radiguet et al., 2012; Zigone et al., 2012). The SSE's have been found in two regions corresponding to flat slab subduction: 1) the central part in the state of Guerrero where the largest ones occur (Mw ~ 7.5);

and 2) to the east in Oaxaca where they are still quite large (Mw ~ 6.6), but have a smaller recurrence interval (Correa-Mora et al., 2008, 2009). The largest SSE's recorded in the world occur in Guerrero, with an average slip of ~10 cm, produce measurable displacements over an area of ~550 × 250 km^2 every ~4 yrs and last for 6 months–1 yr (Radiguet et al., 2012). The majority of the slip from these SSE's is located between the seismogenic zone and the flat slab region (~15 km–40 km depth range) within the Guerrero Seismic Gap (Radiguet et al., 2012) (Fig. 5). It has been estimated that due to these large SSE's the accumulated slip within the Gap is 1/4 that outside of the Gap. This could be the reason that no large earthquake (M ≥ 7) has occurred in > 100 yrs within the Gap. There are also small, short recurrence interval SSE's located on

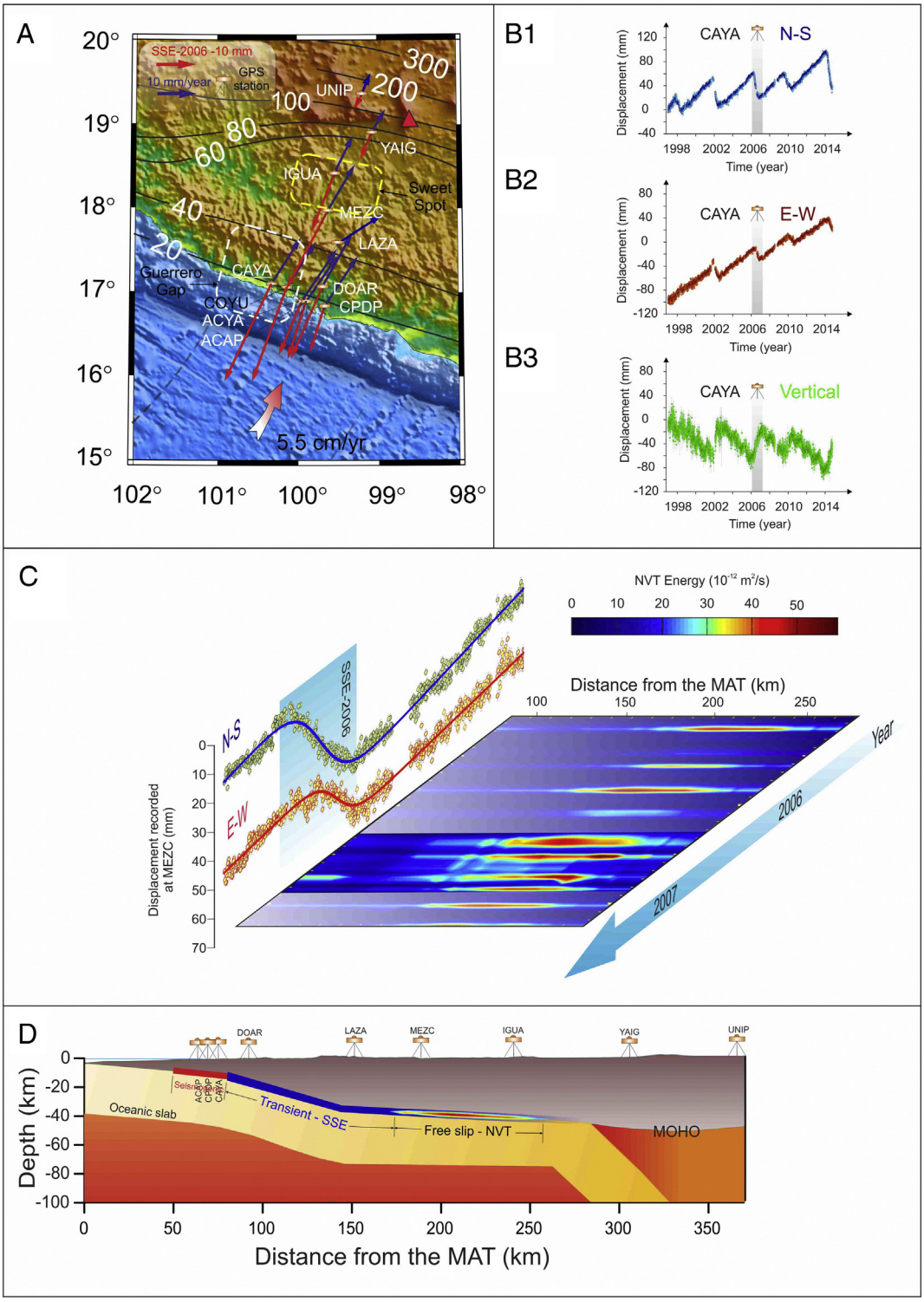

Fig. 5. A. GPS stations and total displacements (red vectors) produced by the 2006 SSE in central Mexico (Kostoglodov et al., 2010); white dashed square represents the Guerrero Seismic Gap, and yellow dashed square represents the Sweet Spot. B. Displacements records at CAYA permanent GPS station in Mexico for a time span of more than 16 yrs. Note the regular recurrence of SSEs in the flat-slab area in central Mexico. Gray band depicts the 2006 SSE shown in A. C. Temporal distribution (mid 2005–2007) of the NVT energy along a profile over the flat-slab in central Mexico and the good correlation with high-NVT energy release during the 2006 SSE. D. Seismogenic, transit-SSEs and NVTs locations along the flat-slab interface in central Mexico.

the flat slab, down dip of the large SSE's (Husker et al., 2012; Frank et al., 2015). Their recurrence interval is 50–90 days and they last for about a week with a moment magnitude equivalent of Mw ≤ 6.4 (Frank et al., 2014, 2015).

The TT's in the flat-slab region in Mexico have a quite complex behavior. All tremors occur close to the plate interface at ~40 km depth. The area of tremor activity has been divided into 3 zones (Fig. 5C). The transient zone located at the corner of the slab when it first bends up at 40 km depth (~130 km–165 km from the trench). Next there is the buffer zone, which has very little TT and is located ~165 km–190 km from the trench. It appears that the small SSE's occur in the buffer zone, but extend into the next region (Frank et al., 2015, 2016). The third region (called a Sweet Spot) concentrates the overwhelming majority of NVT and is located ~190 km–245 km from the trench. To the trenchward side of the Sweet Spot and Transient Zone there are high V_p/V_s values observed in the upper part of the slab (Kim et al., 2010). These are most likely due to high pore fluid pressure that delimits the zones explained above. The high pore fluid pressure regions may exist due to dewatering of the slab as it changes phases from the temperature and pressure gradient within the subduction zone (Manea and Manea, 2011b; Manea et al., 2004).

The flat slab region in Oaxaca (eastern part of the flat slab) does not extend as far as in Guerrero and the region where slow slip phenomena are found is reduced. Only one type of SSE has been found there. It seems to occupy a similar location to the large SSE's in Guerrero on the dipping portion of the slab, but its recurrence interval (~2 yrs), duration (~3 months) and magnitude equivalent (Mw 6.6) are between those of the short term and long term SSE's of Guerrero (Correa-Mora et al., 2008, 2009). TT has been located there, but the studies there have relied on sparse networks and so it does not have information as detailed as in Guerrero. However, it appears to be on the downdip edge of the SSE there as in Guerrero (Brudzinski et al., 2010).

3.4. Seismic tomography

A powerful tool in studying the mantle above subducting slabs, including flat-slabs, is seismic tomography. Apart for permitting illuminating parts of subduction zones where no *in situ* seismicity is available, seismic tomography can be used for determining the composition, state, and temperature of rocks by linking petrology and temperature to elastic properties. Thus, identifying regions with anomalous V_p, V_s and V_p/V_s ratios, offers us a unique opportunity to eventually unravel the hidden structure of subduction zones. Fortunately, in recent years a series of high-density high-quality seismic experiments have been carried out in Mexico, Peru and Chile in the regions of flat-slab subduction (MASE experiment in Mexico (Pérez-Campos et al., 2008); CAUGHT and PULSE experiments in Peru (Ward et al., 2013); OVA99, CHARGE, CHARMSE and CHASE experiments in Chile and Argentina (Alvarado et al., 2009; Anderson et al., 2004; Wagner et al., 2005).

Previous attempts to identify in great detail the flat-slab geometry and structure beneath central Mexico were only partially successful because of scarce and sparse intraslab seismicity. One of the first tomographic images of the flat-slab was produced only a decade ago by Gorbatov and Fukao (2005). Using global P-wave travel times they revealed the velocity structure beneath Mexico, including the flat-slab region. Although the P-wave tomography offered a low-resolution (50x50km) image at that time, the shape of the Cocos plate in the flat-slab region could be clearly identified. One unexpected feature of this study was the very steep inclination of the Cocos slab behind the flat-slab segment. This was later confirmed by Husker and Davis (2009) who show that the subducting slab runs flat from the coast to just south of Mexico City, where it dives sharply into the mantle below the volcanic front of the Trans-Mexican Volcanic Belt with a dip of ~75°, and can be followed up to ~500 km depth where it is truncated. The MASE experiment offered a good opportunity to seismically image in great detail the Cocos plate subduction zone system in central Mexico. Later on, Kim et al. (2012a), took the advantage of the densely spaced station array of MASE, and using an advanced 2-D generalized radon transform-based migration method, produced a clear image of the entire flat-slab subduction system in central Mexico (Fig. 6A). The subducted oceanic crust can be identified as a thin low-velocity layer (7–8 km thick), which dips at 15–20° beneath the coast, then flattens out ~300 km from the MAT where it sharply bends at ~75° degrees underneath the Trans-Mexican Volcanic Belt (TMVB). Also, Kim et al. (2010) revealed a negative discontinuity (fast-to-slow) located at 65–75 km within the lower crust beneath the TMVB, interpreted as a layer characterized by partial melt (Fig. 6A). The magneto-telluric study of Jödicke et al. (2006) along the same trace of the MASE transect imaged a low resistivity layer in the same position that they also interpret as a partially molten lower crust. It is worth mentioning that in Mexico the Cocos flat slab lies only 3–5 km beneath the North American continental Moho, with no, or very little, lithospheric mantle in between. Manea et al. (2013) proposed that part of the low-velocity layer located atop of the flat-slab segment might actually represent a thin layer of trapped lithospheric mantle that underwent serpentinization.

One distinctive characteristic of the Peruvian, and Chilean, flat-slabs when compared with the Mexican flat-slab is the presence of upper mantle above the flat-slab segment. In Peru and Chile, previous regional tomography shows basically fast features corresponding with the seismicity in the subducted slab, but they did not provide a more detailed V_p/V_s tomography for the slab and overlying plate (Gutscher, 2002; Feng et al., 2004). The Peruvian flat-slab, although is the largest zone of present-day horizontal subduction, has not been thoroughly

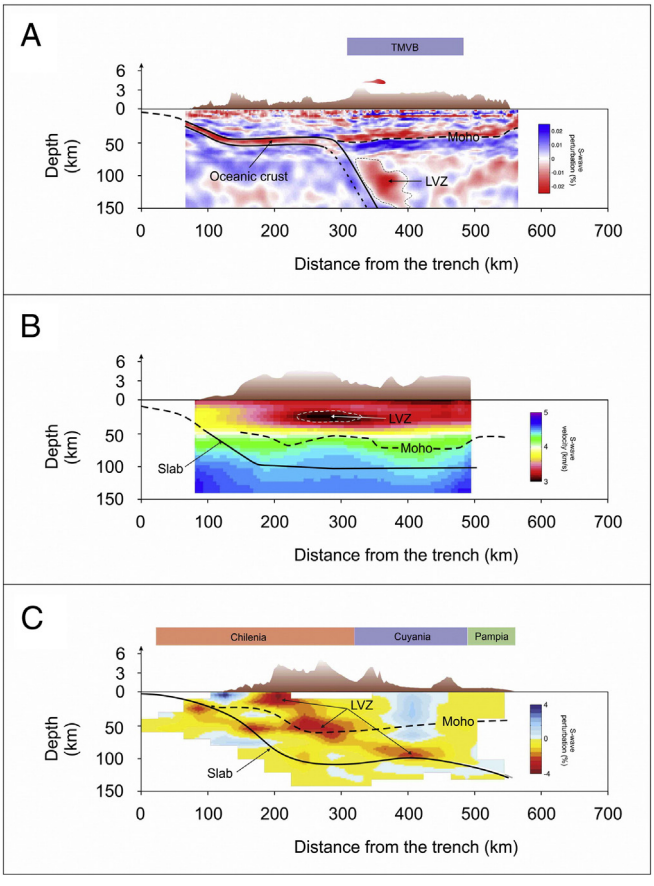

Fig. 6. A. Composite dV_s/V_s image for a 500 km transect across central Mexico from Kim et al. (2010). Note the presence of a low-velocity region beneath the active volcanic arc. B. S-wave velocity structure for the Peruvian flat-slab from Ma and Clayton (2014). Note the clear presence of a mid-crustal low-velocity zone above the flat-slab segment. C. Model perturbations for S-wave through the Chilean flat-slab of Marot et al. (2014). Similarly as for Peru, there are several low velocity anomalies located above the flat-slab segment.

investigated in its entire width, and most studies have focused on the transition from flat-slab to normal dipping slab along its the southern flank. Other recent studies used receiver function in order to better constrain the Moho depth and flat-slab geometry (Phillips et al., 2012; Phillips and Clayton, 2014). Yet, Ma and Clayton (2014) revealed in detail for the first time the velocity structure in the crust and uppermost mantle above the Peruvian flat-slab using surface wave analysis. The shear-wave velocity structure above the flat-slab seems to be fairly simple, with the mantle above the flat-slab segment having a relatively high velocity structure, and a sill-like low-velocity layer, in the mid-crust interpreted as partially melted zone (Fig. 6B).

In central Chile, recent tomographic studies of the upper mantle above the flat-slab revealed that seismic velocity structures are rather different from those observed in normal-dipping subduction zones (i.e. high V_p/V_s ratios) (Wagner et al., 2006), and more heterogeneous when compared with the Peruvian flat-slab. In Chile, a sliver of lithospheric mantle above the horizontal segment of the subducting slab is characterized by low V_p/V_s ratios corresponding to fast S-waves and low P-wave velocities (Wagner et al., 2005, 2006, 2008). It is generally accepted that low temperature coupled with slab dehydration induce mantle serpentinization above the subducting slabs, a process that produce high V_p/V_s ratios in seismic tomography. In central Chile the low V_p/V_s ratio is unusual for active subduction zones, and has been interpreted as an indication of low temperature coupled with the absence of mantle hydration (Wagner et al., 2006), probably indicating the presence of ancient depleted continental cratonic lithosphere. Recently, Porter et al. (2012) combined ambient-noise tomography and earthquake-generated surface wave measurements in order to obtain a more detailed 3D shear velocity regional model for the Pampean flat-slab region in central Chile. One key finding of this study revealed that above the flat slab, the mantle wedge is heterogeneous, with significant horizontal variations in seismic velocities and V_p/V_s ratios (Fig. 6C). Whereas slab velocities increase to the east, velocities in the overlying lithosphere actually decrease, suggesting that progressively slab dewatering increase the quantity of fluids in the overlying mantle. Actually, low shear wave velocities are identified in the upper mantle beneath the Sierras Pampeanas, and are interpreted as hydrated continental lithosphere (Porter et al., 2012; Marot et al., 2014). At the same time the localized low-shear wave velocity zones (or a high V_p/V_s ratio) detected within the subducting Nazca slab can be interpreted as a serpentinized mantle, as is common in other subduction zones.

3.5. Seismic anisotropy

Rocks in the Earth's upper mantle are subject to the long-term deformation caused by convective flow. The stress produces strain that tends to align the mineral crystals within the rocks. This alignment in turn produces seismic anisotropy, whereby waves traveling in different directions propagate at different velocities. Different seismic waves and methods such as phase-delay tomography, shear wave splitting, surface-wave scattering, and *Ps* converted waves have been used to quantify seismic anisotropy (see Park and Levin, 2002 for a review). Shear wave splitting has become a widely used tool to study the flow, deformation and dynamics of the upper mantle anywhere a seismic station can be deployed (Silver and Chan, 1988, 1991; Silver, 1996; Savage, 1999; Park and Levin, 2002; Long and Becker, 2010), including subduction systems (Long and Silver, 2008, 2009; Long, 2013; Long and Wirth, 2013). Anisotropic structures are formed by deformation and reorientation of minerals, known as lattice-preferred orientation (LPO), and are usually parallel with the direction of mantle flow. Field observations and laboratory measurements revealed how the crystallographic axes of olivine align with shear stress (Jung and Karato, 2001). Since olivine, a naturally anisotropic mineral, is the dominant element of the upper mantle and has an elongated crystalline structure, LPO is considered to be the primary cause of anisotropy observations, although there might be some secondary contribution from other factors such as the preferred orientation of partial melt pockets (especially in the mantle wedge below active volcanic arcs) (Zimmerman et al., 1999; Vauchez et al., 2000).

The shear wave splitting technique is commonly applied to teleseismic *SKS* phases (downgoing *S* wave through the mantle on the source side, converted to a *P* wave through the liquid outer core, and converted to an upgoing *S* wave through the mantle and crust on the receiver side) in order to study upper mantle anisotropy. In the case of subduction zones, the anisotropy is accrued from the point where the *P* wave is converted to an *S* wave upon leaving the outer core, thus including contributions from the subslab mantle, the slab itself, the mantle wedge, and the overriding plate (Savage, 1999; Long and Silver, 2008, 2009; Long, 2013; Long and Wirth, 2013). Splitting measurements are often performed using local *S* waves from intraslab earthquakes (Yang et al., 1995; Long and Silver, 2008; Long and Becker, 2010; Long, 2013; Long and Wirth, 2013). These measurements exclude the anisotropic contribution from the subslab mantle. Additionally, source-side anisotropy can be measured using teleseismic *S* waves from intraslab events, provided that anisotropy is well characterized under the station, as is often the case from *SKS* observations (Vinnik and Kind, 1993). This method is very valuable in studies of the subslab mantle (e. g., Russo and Silver, 1994; Foley and Long, 2011; Eakin and Long, 2013; Lynner and Long, 2013, 2014a, 2014b). The method of shear wave splitting simultaneously determines two parameters. The polarization direction of fast shear waves, φ, or fast polarization direction, provides information about the LPO of olivine (or magmatic lenses). The second parameter is the delay time, δt, between the fast and slow arrivals and is an indicator of the extent and strength of anisotropy. There are two main olivine fabric types that are related with the anisotropy patterns observed in subduction zones: A- and B-type fabrics. Additionally, the C-, D-, and E-type olivine fabrics have also been identified in natural rocks and by a series of experimental studies (Tommasi et al., 2006; Katayama and Karato, 2006; Jung et al., 2006; Jung, 2009). However, A-, C- and E-type olivine fabrics show the same shear wave splitting pattern in the case of horizontal shear (Karato et al., 2008), therefore we will focus our review only on A- and B-type olivine fabrics and their signature on seismic anisotropy. A-type olivine fabric (the most commonly observed fabric in anhydrous peridotite) develops an LPO pattern in which the fast axes of individual olivine crystals tend to align in the direction of shear, and consequently the fast axis of anisotropy recorded at the seismic station is oriented in the direction of mantle flow (Karato et al., 2008). This type of olivine fabric can be found in geodynamic settings where a combination of relatively low stresses, high temperatures, and low water contents are characteristic (Karato et al., 2008). Therefore, in subduction systems A-type olivine fabric is often found in the core of the mantle wedge as well as in the subslab mantle (Kneller et al., 2005, 2007; Jung et al., 2006; Long and Silver, 2008). However it has been demonstrated that LPO geometries are affected by stress, temperature, pressure, and especially by the presence of melt and fluid content. Jung and Karato (2001) show that in rock samples with a high fluid content and deformed by simple shear, the olivine fabric is B-type, and so the fast axis of anisotropy observed at the seismic station is perpendicular to the direction of mantle flow. In subduction systems B-type olivine fabric is expected to occur in low temperature areas (below 800 °C), rich in volatiles and characterized by high stress, typical of the cold corner of the mantle wedge (mantle wedge tip) (Kneller et al., 2005, 2007; Jung et al., 2006).

Shear wave splitting measurements in different subduction zones revealed in general a certain preference for trench-parallel fast directions for areas close to the tip of the mantle wedge, and trench-perpendicular fast directions farther away from the trench (Anderson, 2005; Anderson et al. (2005); Nakajima and Hasegawa, 2004; Long and van der Hilst, 2005; Long and Wirth, 2013). Also, in many cases, fast polarizations for shear waves with paths beneath the slab are parallel to the strike of the subduction zone, or trench-parallel (Long and Silver, 2008). This observation has often been interpreted as 3-D return flow

induced by trench migration (see Long and Silver, 2008 for a review). The most notable exception to this rule may be the Cascadia subduction zone, where the fast polarization axes are trench-perpendicular (Currie et al., 2004; Long and Silver, 2008; Eakin et al., 2010). Likewise, in Mexico trench-normal fast polarization directions have been explained either by past (Obrebski et al., 2006; van Benthem et al., 2008) or present subduction (van Benthem, 2005; Stubailo and Davis, 2007, 2012a, 2012b, 2014, 2015; Bernal-Díaz et al., 2008; León Soto et al., 2009; Rojo-Garibaldi, 2011; Rojo-Garibaldi et al., 2011; Ponce-Cortés, 2012; van Benthem et al., 2013; Bernal-López et al., 2014, 2015; Bernal-López, 2015). In both regions the lithospheric plates being subducted are relatively small, young fragments of the Farallon plate. In the case of Cascadia these are the Juan de Fuca and Gorda slabs, while the Cocos and Rivera plates are subducting under Mexico. Proposed explanations for subslab, trench-normal fast polarizations include the absence of a thin decoupling layer under young and hot slabs (Long and Silver, 2009) and the presence of horizontally aligned sheets of melt where the slab dips at angles <25° (Song and Kawakatsu, 2012). Below we will review the anisotropy observations for each of the three flat-slab subduction zones, and propose a series of models that link mantle flow, olivine fabric and observations.

3.5.1. The Mexican flat-slab

In the Mexican subduction zone, several studies now exist of upper mantle shear wave anisotropy using records of teleseismic *SKS* phases (van Benthem, 2005; Stubailo and Davis, 2007, 2012a, 2012b, 2014, 2015; Bernal-Díaz et al., 2008; León Soto et al., 2009; Rojo-Garibaldi, 2011; Rojo-Garibaldi et al., 2011; Ponce-Cortés, 2012; van Benthem et al., 2013; Bernal-López et al., 2014, 2015; Bernal-López, 2015; Stubailo, 2015), using *S* waves recorded locally (León Soto et al., 2009; León Soto and Valenzuela, 2013), and also source-side subslab anisotropy using teleseismic *S* phases (Lynner and Long, 2014a). In the area of flat-slab, all fast polarization directions φ are oriented roughly in the direction perpendicular to the MAT with delay times δt of about 1 s (Rojo-Garibaldi, 2011; Rojo-Garibaldi et al., 2011; Ponce-Cortés, 2012; van Benthem et al., 2013; Bernal-López et al., 2014, 2015; Bernal-López, 2015; Stubailo, 2015). Physical conditions in the subslab mantle are low stress, low water content, and relatively high temperature, so the LPO of olivine is expected to be A-type (Jung et al., 2006; Long and Silver, 2008). Therefore, van Benthem et al. (2013) propose that fast polarization directions in the forearc region under the Cocos slab reflect the subslab flow direction, and are indicative of entrained flow (Fig. 7A). *SKS* observations using a 100-station linear array found that the fast axes for stations in the forearc are oriented NE-SW on average, i.e. approximately trench-perpendicular. However, under the backarc, where the Cocos slab subducts steeply, the fast polarization directions are oriented N-S, i. e. perpendicular to the strike of the slab, and are interpreted as a result of 2-D corner flow within the mantle wedge (Rojo-Garibaldi, 2011; Rojo-Garibaldi et al., 2011; Bernal-López et al., 2014, 2015; Bernal-López, 2015). The differences observed in the orientation of the fast polarization directions between the forearc and the backarc are due to the fact that the volcanic arc is not subparallel to the MAT (Bernal-López et al., 2015). Also, the lack of trench-parallel (or slab strike-parallel) fast polarization directions for stations located in the arc and backarc region (Rojo-Garibaldi, 2011; Ponce-Cortés, 2012; van Benthem et al., 2013; Bernal-López et al., 2015) suggests that B-type olivine fabric is not present. It is commonly accepted that one of the regions that offer proper conditions for B-type olivine fabric is the water-rich, cold nose of the mantle wedge. However, the absence of B-type olivine fabric would imply that the mantle wedge associated with flat-slab subduction in Mexico does not offer all the necessary conditions for this type of fabric to properly develop. Indeed, Manea and Manea (2011b) show that most of the dehydration processes occur along the flat-slab segment before the slab plunges in the asthenosphere. In the mantle wedge, the transition from A-type to B-type olivine fabric is controlled by temperature, and this transition takes place at

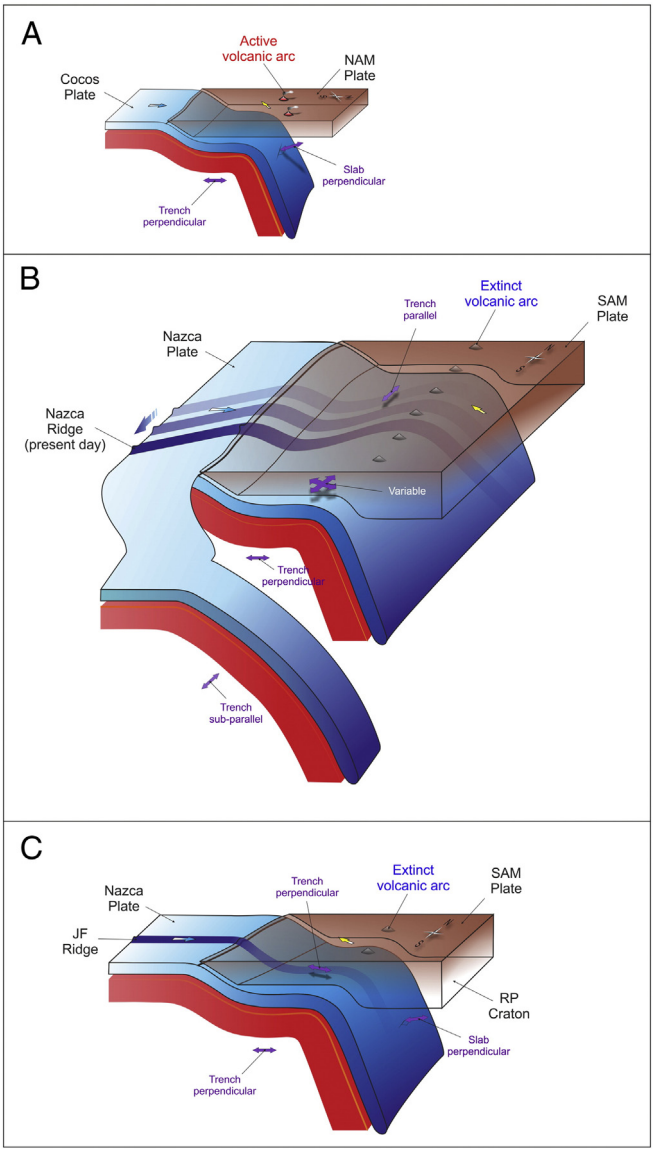

Fig. 7. Schematic views of the flat-slab geometries in central Mexico, Peru and central Chile subduction zones, and the relationship with observed seismic anisotropy (purple arrows). Blue arrows represent the oceanic plates velocities, and yellow arrows show the overriding plates velocities. Note the consistent trench perpendicular sub-slab anisotropy observed for all three flat-slabs. A. Trench-perpendicular shear-wave fast axes are observed in Mexico beneath the slab, and perpendicular to the strike of the slab for the mantle wedge above the slab. Notice that the trench and the volcanic arc are not subparallel. B. In Peru the southward migration of the Nazca ridge (variable blue tone ribbons) through time seems to induce a complicated pattern of mantle anisotropy above the flat-slab segment. To the south, the sub-slab mantle is trench-subparallel. C. In central Chile the mantle anisotropy distribution is comparable with central Mexico. RP – Rio de la Plata craton.

~800 °C (Long, 2013). For the particular geometry of flat-slab subduction in Mexico, thermal models predict high temperature in the mantle wedge beneath the active volcanic arc, without a pronounced cold (<800 °C) mantle wedge (Manea et al., 2005), in agreement with the absence of trench-parallel (or slab strike-parallel) fast axes (Rojo-Garibaldi, 2011; Ponce-Cortés, 2012; van Benthem et al., 2013; Bernal-López et al., 2015).

Other segments of the MAT in Mexico, outside the region of flat slab subduction, also show trench-normal fast polarization directions, including the source-side subslab anisotropy data set of Lynner and Long (2014a). Farther to the northwest, where the Rivera plate subducts under North America, León Soto et al. (2009) used teleseismic *SKS* data and found trench-perpendicular fast axes in the middle of the Rivera

slab, which is an indication that corner flow occurs in the mantle wedge, and also that flow is entrained underneath the slab (similar to Long and Silver (2008) model). Their use of *S* waves from local events, however, measured anisotropy mostly in the continental crust because of the paucity of deep earthquakes, which kept them from thoroughly sampling the mantle wedge. In the segment of the MAT southeast of the flat slab, where the slab dips into the mantle at ~25°, teleseismic observations found trench-perpendicular directions (Bernal-Díaz et al., 2008; Ponce-Cortés, 2012; van Benthem et al., 2013; G. León Soto and R.W. Valenzuela, manuscript in preparation, 2016). Measurements using *S* waves from local, intraplate Cocos earthquakes established the existence of two distinct anisotropy patterns in the mantle wedge, separated by the 100 km isodepth contour (León Soto and Valenzuela, 2013). It should be noted that in this part of Mexico no active volcanic arc exists associated to subduction of the Cocos slab, probably due to a lack of dehydration fluids. For the seismic stations located above the slab with depth > 100 km, the anisotropy measurements show a clear pattern of trench perpendicular fast directions (average $\delta t = 0.36$ s), which is consistent with the existence of A-type olivine and a 2-D corner flow model. On the other hand, for slab depths between 60 and 85 km, the data show some trench-parallel fast axes (average $\delta t = 0.28$ s), but the pattern is complex given that other measurements with their fast axes oriented in different directions are interspersed throughout the same region, where B-type olivine is expected. This complexity likely arises from the fact that for shallow earthquakes, the path through the mantle wedge is shorter, and thus the anisotropy contributions from the continental crust and also from the slab itself become more significant (León Soto and Valenzuela, 2013). Teleseismic measurements farther southeast along the MAT, to the east of the subducted extension of the Tehuantepec Ridge, show small delay times and variable orientations of the fast polarization directions, indicative of little mantle anisotropy (Ponce-Cortés, 2012). These observations may suggest that the pattern of mantle flow driven by trench migration is not coherent (Long and Silver, 2008). Furthermore, these measurements may mark a transition in the mantle flow regime given that trench-parallel fast polarization directions are observed farther east in the MAT in Nicaragua and Costa Rica, both below and above the subducted slab (Abt et al., 2009, 2010). However, the situation in Central America may be more complex. Lynner and Long (2014a) made source-side splitting measurements and found trench-perpendicular subslab fast polarization directions under Nicaragua. Lynner and Long (2014a) suggested that their results differ from those in the work by Abt et al. (2010) because their data sets sample different volumes of the subslab mantle.

3.5.2. The Andean flat-slabs

The pioneering upper mantle anisotropy study of Russo and Silver (1994) along the Andean subduction zone revealed that the mantle flow beneath the subducting Nazca plate, with few exceptions, is actually trench-parallel. This observation led to the conclusion that the subducted lithosphere is mainly decoupled from the underlying asthenosphere, and that trench-parallel mantle flow is a consequence of the retrograde motion (or slab rollback) of the subducting slab, together with a barrier to entrained mantle flow at depth, beneath the slab.

3.5.2.1. The subslab mantle. The above-mentioned exceptions are associated to the regions of flat-slab subduction in Peru and Chile. Russo and Silver (1994) showed that in these two particular areas, subslab φ directions are trench-perpendicular where the dip of the slab changes abruptly, as when going from flat to normal subduction. They further proposed that the change of slab geometry is responsible for local perturbations of the pressure gradients and associated mantle flow. Recently, Eakin and Long (2013) conducted a detailed shear wave splitting analysis of the Peruvian flat-slab subduction system. They used high-quality measurements of *SKS*, *ScS*, and local *S* phases at a single permanent station located just above the central part of the Peruvian flat-slab. They also made source-side splitting measurements using teleseismic *S* phases originating from slab earthquakes in Peru. The anisotropy measurements show that the mantle beneath the flat-slab is characterized by trench-normal fast splitting directions. Eakin and Long (2013) and Eakin et al. (2015) interpret these observations as subslab trench-perpendicular mantle flow characteristic of E- or C-type olivine LPO fabrics (Fig. 7B). Farther south, where the Nazca slab is subducted at a normal dipping angle, the fast anisotropy directions in the subslab mantle show a preferred trench-sub parallel orientation (Eakin and Long, 2013; Eakin et al., 2015).

Anderson et al. (2004) applied the shear wave splitting technique using *SKS*, *SKKS* and *PKS* arrivals in order to obtain fast polarization directions (φ) and splitting delay times between fast and slow shear waves (δt) in the Chilean flat-slab region. They showed that the source of anisotropy in the flat-slab region, as well as the adjacent areas, is found within and below the slab (i. e., a 75–200 km thick layer located below the subducting oceanic crust). In Chile, the shear wave splitting measurements revealed a pattern similar to that found for the Mexican and Peruvian flat-slabs. Within the flat-slab region, the average, subslab φ fast directions are oriented E-W, i. e., perpendicular to the trench, with δt of about 1 s, whereas in adjacent areas located west and southwest of the flat slab the fast axes are oriented N-S, i. e., trench-parallel, and the delay times, δt, are ~0.9 s (Fig. 7C).

3.5.2.2. The mantle wedge. Several studies (Anderson, 2005; Anderson et al., 2005; MacDougall et al., 2012) present the results of shear-wave splitting measurements within the mantle wedge for the Chilean subduction zone in the flat-slab area. They show trench-perpendicular fast polarization directions above the flat-slab segment and a transition to trench-parallel close to the trench for the neighboring regions where the Nazca plate dips at a normal angle into the mantle.

Using data from a temporary array, Eakin et al. (2014, 2015) inferred the existence of a 30-km thick wedge of anisotropic mantle material, located between the Peruvian flat slab and the continental crust. They found a pronounced change in anisotropy along the strike of the trench, with trench-parallel fast directions to the north of the subducted Nazca Ridge and variable orientations to the south. They proposed that southward migration of the subducted Nazca Ridge produces the observed anisotropy pattern.

3.5.3. Comparative analysis of shear-wave splitting of the Mexican, Peruvian and Chilean flat-slabs

Shear wave splitting observations in the mantle wedge above subducting slabs worldwide revealed a rather complex distribution, with a pronounced spatial variability and also significant variations in splitting delay times (Long and Wirth, 2013). Nonetheless, on a global scale, a common first-order splitting observation is the existence of trench-parallel fast directions in the mantle wedge and in the subslab mantle (Long, 2013). In flat-slab regions, however, deviations from this pattern are quite significant and trench-perpendicular fast directions have been reported. A comparative analysis of the Mexican, Peruvian and Chilean flat-slabs is of critical importance in order to interpret the seismic anisotropy observations.

3.5.3.1. The subslab mantle. In all of these three areas the fast directions in the subslab mantle are oriented perpendicular to the trench (Fig. 7). Additionally, in Peru and Chile the trench-perpendicular fast axes stand in clear contrast with adjacent regions where the fast directions are trench-parallel. Russo and Silver (1994) were among the first ones to suggest that slab geometry has a local effect on subslab mantle flow. Later on, Anderson et al. (2004) proposed that subslab mantle flow in the Chilean subduction zone is locally controlled by the geometry of the subducting lithosphere. The model of Anderson et al. (2004) explains the E-W (trench-perpendicular) fast directions observed beneath Central Chile in the flat-slab area as a consequence of the active flattening process and the formation of a slab space that allows for the accommodation of the general eastward mantle flow. Closer to the trench, in

the regions to the west and southwest of the flat slab, however, the subslab mantle flows N-S and is consistent with the general, trench-parallel trend for South America (Russo and Silver, 1994; Anderson et al., 2004). Furthermore, Anderson et al. (2004) take the point of view that the slab is not torn in its transition from flat to normal subduction because flow is oriented parallel to the contours of the subducting slab. In the case of Peru, source-side splitting measurements reveal trench-perpendicular fast axes beneath the flat-slab (Eakin and Long, 2013; Eakin et al., 2015). The fast directions become trench-oblique to subparallel to the southeast of the flat slab, where the dip angle steepens again (Eakin and Long, 2013; Eakin et al., 2015), which is broadly consistent with the trench-parallel trend for South America (Russo and Silver, 1994). Unlike the regions of normal-dipping subduction adjacent to the flat slabs in South America, no trench-parallel fast axes are observed in Mexico. The region of flat slab subduction in Mexico runs between 96 and 101°W and shows consistently trench-perpendicular fast polarization directions (van Benthem, 2005; Rojo-Garibaldi, 2011; Ponce-Cortés, 2012; van Benthem et al., 2013; Bernal-López, 2015; Bernal-López et al., 2015; Stubailo, 2015). East of 96°W the MAT makes a bend and changes its trend from WNW-ESE to NW-SE. Likewise, the flat slab ends and dips at an angle of ~25° (Pardo and Suárez, 1995; Rodríguez-Pérez, 2007; Melgar and Pérez-Campos, 2011; Kim et al., 2011). The fast polarization directions in this region are rotated ~25° clockwise relative to the stations located over the flat slab to the west, but they are still generally trench-perpendicular (Bernal-Díaz et al., 2008; Ponce-Cortés, 2012; van Benthem et al., 2013; G. León Soto and R.W. Valenzuela, manuscript in preparation, 2016). The rotation of the fast axes may be related to the change in the trend of the MAT. In stations located still farther east, across the projected extension of the Tehuantepec Ridge, delay times are short ($\delta t \approx 0.5$ s) and suggest that there is little anisotropy (Ponce-Cortés, 2012). On the other hand, to the west of the flat slab, i. e. west of 101°W, few splitting measurements are available over the Cocos slab, but these are generally, trench-oblique (León Soto et al., 2009; Ponce-Cortés, 2012). Farther west, the Rivera slab dips more steeply than the adjacent Cocos slab (Pardo and Suárez, 1995), and a tear between the two has been tomographically imaged (Yang et al., 2009). In the central part of the Rivera slab, trench-perpendicular fast axes are observed and are consistent with both 2-D entrained flow beneath the slab and with corner flow in the mantle wedge (León Soto et al., 2009). The orientation of the fast axes, however, is consistent with 3-D toroidal flow around the western edge of the Rivera slab, and with flow through the tear between the Rivera and Cocos slabs (León Soto et al., 2009).

3.5.3.2. The mantle wedge. Usually, the best way to quantify mantle anisotropy above the slab with the shear wave splitting technique is by using *S* waves from local, intraslab events. Several studies (Anderson, 2005; Anderson et al., 2005; MacDougall et al., 2012) show that mantle wedge fast directions in Chile are trench-perpendicular above the flat slab and trench-parallel in neighboring regions to the south, where the slab dips more steeply into the mantle. In Peru the southward migration of the subducted Nazca Ridge controls the anisotropy pattern within a mantle layer sandwiched between the flat slab and the continental crust. To the north of the subducted Nazca Ridge the fast axes are trench-parallel, whereas to the south the fast axes show variable orientations (Eakin et al., 2014, 2015). In spite of the occurrence of intraslab earthquakes within the flat slab segment in Mexico (Pardo and Suárez, 1995; Pacheco and Singh, 2010; Singh et al., 2014), no shear wave splitting studies have been conducted using local *S* waves. Constraints on the anisotropy structure are available, however, from other techniques. Several studies have reported the existence of a thin (<10 km) low velocity zone (LVZ) between the continental crust and the subducted oceanic mantle. This LVZ has been interpreted as a low velocity mantle "wedge" (Pérez-Campos et al., 2008) and/or as low velocity subducted oceanic crust (Pérez-Campos et al., 2008; Song et al., 2009; Kim et al., 2010, 2012b, 2013; Song and Kim, 2012b). Furthermore, it has been suggested that this low velocity layer decouples the slab from the overriding plate (Kim et al., 2010). Song and Kim (2012b) found that the upper oceanic crust of the subducting Cocos slab is a 3 to 5 km thick ultraslow-velocity layer showing anisotropy >5%. Song and Kim (2012a) concluded that the topmost 2 to 6 km of the Cocos subducted oceanic mantle is an anisotropic high-velocity lid. It has fast polarization axes oriented in the direction of plate convergence and an anisotropic strength of about 7%. It was further suggested that anisotropy was frozen in at the time the plate formed at the Pacific-Cocos ridge spreading center (Song and Kim, 2012a; Audet, 2013). Work using receiver functions determined the anisotropy in the continental crust, and both the upper and lower oceanic crust (Castillo et al., 2014; Castillo-Castellanos, 2015; J. Castillo et al., "Crust and upper mantle seismic anisotropy variations from the coast to inland in central and southern Mexico", submitted to the Geophysical Journal International, 2016), and subtracted these values from the *SKS* shear wave splitting study by Rojo-Garibaldi (2011). Lastly, Huesca-Pérez et al. (2016) determined continental crust seismic anisotropy from tectonic tremor and suggested that a highly foliated system of folds-and-thrusts is the most likely cause of the observed anisotropy.

3.6. Heat flow associated with flat-slabs

Another geophysical observation that improves our understanding of subduction zone processes in general, and flat-slab subduction in particular, is represented by regional heat flow. Surface heat flow in the continents comes from two main sources: radioactive decay mainly from U, Th and K isotopes and from the mantle. According to Smithson and Decker (1974), Smithson and Brown (1977), and Allis (1979) ~40% (or ~25 mW/m^2) of the average continental heat flow is generated from radioactivity whereas the remaining ~60% comes from the mantle. According to Pollack (1980), the heat flow from the continents is lower than that from the ocean basins, and, as we discuss in this section, flat-slab areas show ever-lower values of heat flow. At a global scale, regions with surface heat flow greater than ~70 mW/m^2 and lower than ~40 mW/m^2 are considered above and below normal values (Blackwell, 1969, 1971, Roy et al., 1972). Due to the cooling effect of descending slabs fore arc areas are characterized by low heat flow (30–40 mW/m^2), whereas regional surface heat flow above 100 mW/m^2 is common in volcanic arcs, and values of ~70 mW/m^2 are reported in back arc areas.

Recent increase in heat-flow data measurements, coupled with significant improvements in digital geology maps and maps of ocean crustal age permitted the creation of high-resolution global maps of surface heat flow (e.g. Davies, 2013). A preliminary analysis of heat flow distribution over flat-slab areas in Mexico, Peru and Chile show that these regions can be easily identified because of their low heat flow (Fig. 8A, B). Low heat flow flat slab areas can be observed also in global heat flow maps indirectly derived from seismic models based on surface waves (Shapiro and Ritzwoller, 2004).

In central Mexico, direct heat flow measurements of Ziagos et al. (1985) show that the flat-slab fore arc region is characterized by below-normal heat flow values of only 13–22 mW/m^2, suggesting low temperatures at the flat-slab interface (~45 km). Indeed, Currie et al. (2004), and Manea et al. (2004, 2005) show that just a small amount of shear heating along the flat-slab interface is necessary in order to fit the modeled heat flow. Such low heat flow records are more common for shield and cratonic areas (12–14 mW/m^2), such as the Grenville Province of the Canadian Shield and the Appalachians (Lenardic et al., 2000). However, in central Mexico, low heat flow values above the flat-slab may actually indicate that the contribution from the mantle is lacking. This can happen when there is no mantle between the slab and the crust and the continental crust is actually shielded from the mantle by the flat-slab immediately below. A clearer picture of the heat-flow distribution and extension above flat-slab in Mexico is

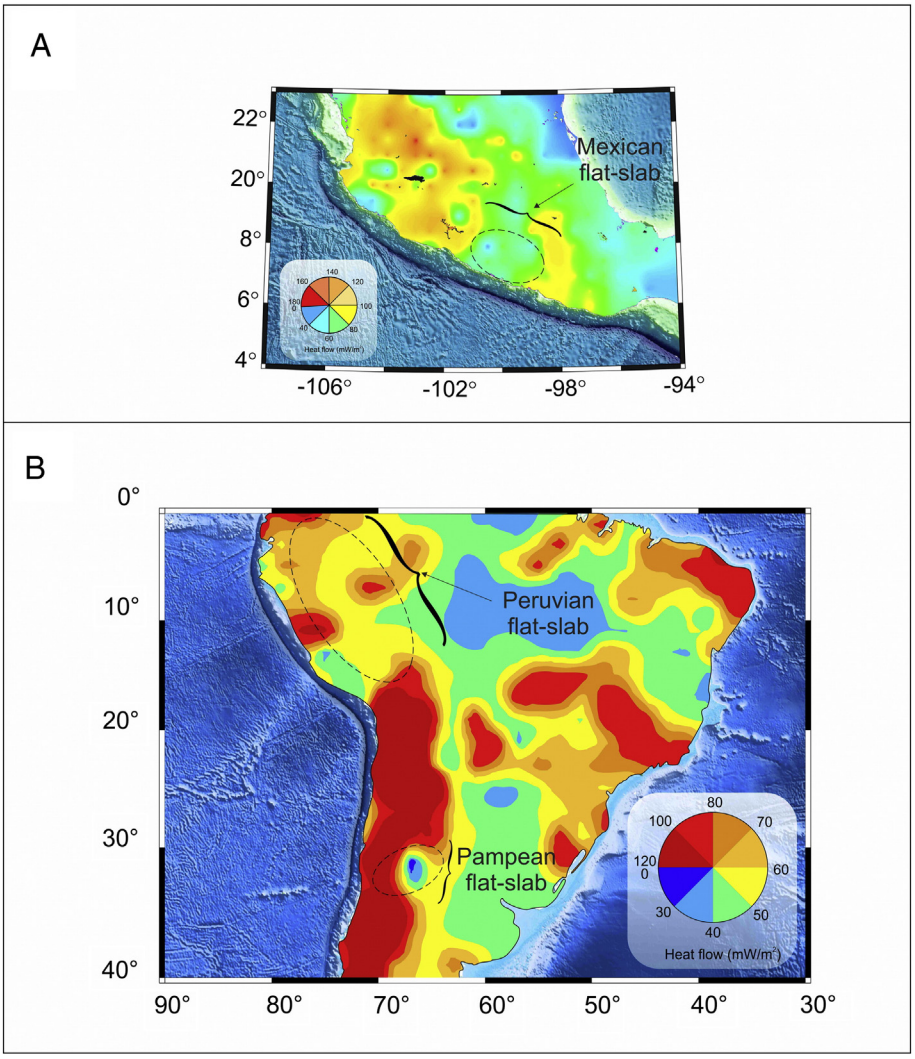

Fig. 8. A. Heat flow map of central Mexico based on spectral analysis of aeromagnetic anomalies (Manea and Manea, 2011a). B. Heat flow map of South America based on spherical harmonic expansion to degree 36 of the global heat flow (Hamza et al., 2005; Cardoso et al., 2010). Note the reduced heat flow values for all three regions located above the flat-slabs.

provided by Manea and Manea (2011a). Using spectral techniques applied to aeromagnetic anomalies they estimated the depths to the Curie isotherm (~600 °C), which in turn are used to estimate the heat flow. The resulting heat flow map of southern Mexico agrees well with the locations of the main tectonic provinces but also with the flat-slab area (Fig. 8A). According to the Manea and Manea (2011a), low values of heat flow above the flat-slab extend over an area of ~230 km along the Pacific coast, and bounded laterally by the prolongation of the Orozco and O'Gorman oceanic fracture zones (Fig. 1A). The Trans Mexican Volcanic Belt is characterized by high heat flow records above 100 mW/m^2 (Ziagos et al., 1985), and locally even higher near active volcanic centers, suggesting the occurrence of temperatures in excess of 1000 °C below the volcanic arc at Moho depths. Farther in the back-arc region, surface heat flow decreases to ~70 mW/m^2 still significantly higher than the average heat flow (~40 mW/m^2) measured in regions characterized by thickened lithosphere or cratons (Chapman and Furlong, 1992; Vitorello et al., 1980).

In the Andes, compared with the adjacent regions where the slab is steep, the flat-slab regions are also distinguishable due to low heat flow (Fig. 8B). For example, in central Peru low surface heat flow (~30 mW/m^2) have been attributed to the absence of asthenospheric mantle wedge above the flat-slab region (Muñoz, 2005). In central Chile, according to Hamza and Muñoz (1996), Hamza et al. (2005) and Cardoso et al. (2010), heat flow above the flat-slab region is ~40 mW/m^2 and increases to only ~60 mW/m^2 inland. Although there is relatively little variation of heat flow across the flat-slab area, the values are well above typical heat flow recorded in continental areas (~25 mW/m^2) and likely reflect additional processes such as radioactive heat production within the overthickened crust, friction along the contact between the subducting Nazca plate and the overriding South American plate, and the presence of lithospheric mantle between the flat-slab and the crust.

3.7. Magnetotellurics

Electrical resistivity determined from magnetotellurics (MT) surveys are naturally sensitive to the presence of fluids, whether they are aqueous of partial melts, the more fluids are present the lower the rock resistivity (Unsworth and Rondenay, 2013). It is known that subducting slabs, including flat-slabs, play a central role in transporting fluids into the overlying mantle and crust where they control the chemical properties of the rocks (Rüpke et al., 2004; Soyer and Unsworth, 2006). At shallow depths (<15 km), fluids stored in the oceanic crust and sediments are released by compaction of the pore space, while at greater depths, they are discharged gradually (at different P-T conditions) by metamorphic dehydration reactions of a series of hydrous minerals (Hacker, 2008). Additionally, slab-derived fluids trigger partial melting of the mantle wedge that generate arc magmatism.

Since electrical resistivity of rocks is quite sensitive to the presence of fluids, MT surveys can illuminate zones with highly conductive fluids (water or melt), and effectively broad the image of deep structure of subduction zones.

There are several MT studies related with flat-slab subduction in particular, the MT study of Jödicke et al. (2006) for the Mexican flat slab and Booker et al. (2004), Burd et al. (2013), and Orozco et al. (2013) for the Chilean flat slab. The MT study across the flat-slab region in Mexico carried out by Jödicke et al. (2006) revealed several high conductivity anomalies: an elongated conductive zone extending >250 km in the lower crust below the Trans-Mexican Volcanic Belt (TMVB) and two highly conductive isolated anomalies located above the slab interface between the trench and the volcanic front (Fig. 9A). The elongated highly conductive zone below the TMVB was interpreted as the presence of partial melts and fluids in the continental crust. By contrast the two isolated highly conductive spots were interpreted as regions of fluids release due to the progressive metamorphic dehydration of the basaltic oceanic crust and uppermost mantle (Jödicke et al., 2006; Manea and Manea, 2011b). On the other hand, the Cocos slab is imaged as a resistive zone, with decreasing resistivity along the flat slab portion, probably due to the increase in slab temperature.

For the Chilean flat-slab, the two-dimensional electrical resistivity model of Booker et al. (2004) reveals a couple of highly resistive areas separated by a vertical conductor or plume (Fig. 9B). The high resistive regions correspond to a segment of the Nazca flat-slab, the crystalline basement exposed at surface in the Sierras Pampeanas and the Rio de la Plata craton. According to Booker et al. (2004) the high resistivity region attributed to the Rio de la Plata craton extends down to 200–300 km, and its presence at such depth suggests that the further advance of the Nazca flat-slab was blocked by the collision with the craton. This process would also prevent the development of a normal hot asthenospheric wedge, consistent with the lack of volcanism in this region. Also, a 100-km-thick electrically resistive region located between the craton and the Andes characterize the Sierras Pampeanas lithosphere (Fig. 9). The origin of this highly conductive zone, or plume, rising from deeper mantle to about 100 km and squeezed between the Nazca slab and the Rio de la Plata craton is apparently related to partial melts and hydrous fluids released from the Nazca slab (Booker et al., 2004). However, the recent MT study of Burd et al. (2013) proposed that a wedge-shaped slab window into the subducting Nazca plate allows the conductive plume to rise through the mantle up to the base of the lithosphere. Somehow similar with the Mexican flat-slab, low resistivity is also found in the lower continental crust beneath the highest elevation of the Sierras de Cordoba (Fig. 9B). Interestingly, the location of crustal electrical conductor corresponds with the edge of the Rio de la Plata craton and the eastern extent of the Nazca flat-slab, that could be explained by fluids released from the bending subducting slab (Booker et al., 2004).

In general, flat-slab regions in Mexico and Chile show several similarities, as highly resistive slabs and highly conductive regions located in the overriding crust, however, there are also significant differences. The overriding crust below the volcanic belt shows the presence of a ~250 km long MT low-resistivity anomaly possibly related with the presence of fluids and partial melts in the lower crust as a result of trenchward migration of volcanism in the last 10 Myr. Compared with the observed average trench migration rate of 1.7 cm/yr (Schellart et al., 2011), in Mexico the flat-slab rolled back at a higher rate of ~2.5 cm/yr. This might indicate a higher rate of trench erosion along the MAT in the past of ~0.8 cm/yr, which is considerably higher than the present-day assumed erosion rate of ~0.1 cm/yr (Mercier de Lépinay et al., 1997; Vannucchi et al., 2013). On the other hand, in Chile, there is only one low-resistivity spot 100 km long located in the crust beneath the Sierras de Cordoba. This likely reflects the absence of volcanism related with flat-slab subduction in Chile. Although the maximum depth of MT survey in Mexico is limited to 100 km only, there are other major differences between the two flat-slab subduction zones such as the presence of a 200–300 km thick resistive Rio de la Plata craton in Chile and a vertical conductor located above the sinking Nazca slab.

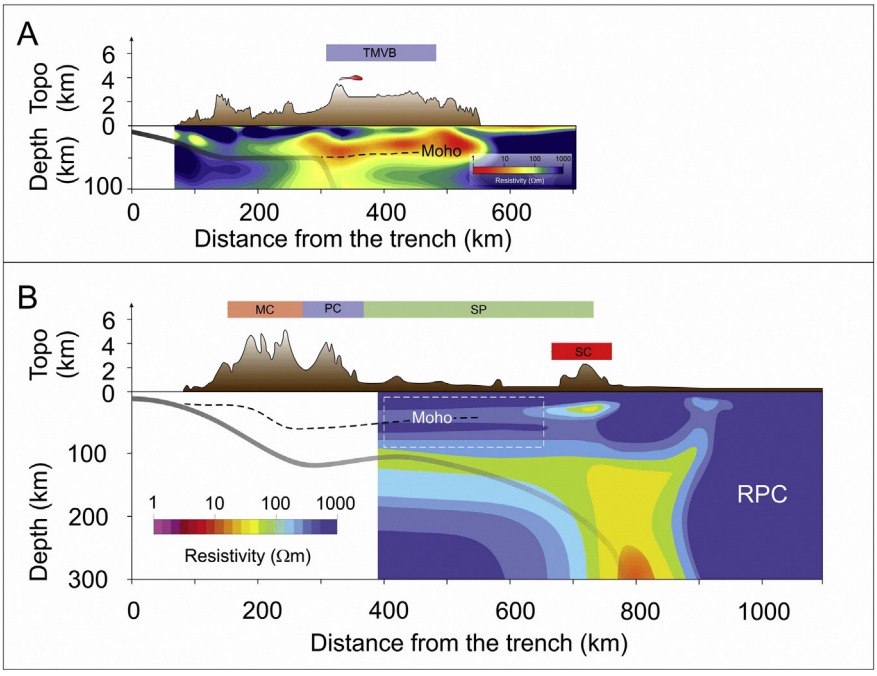

Fig. 9. A. Magnetotelluric profile above the Mexican flat-slab from Jödicke et al. (2006). Note the presence of a large conductive region beneath the TMVB and above Moho. B. Magnetotelluric profile across the eastern edge of the Sierras Pampeanas above the Chilean flat-slab from Booker et al. (2004). Note the presence of a lower crust conductor beneath the Sierras de Cordoba (SC), and also of a large vertical conductor at mantle depths above the slab. Semitransparent thin gray band represents the slab surface. White dashed square marks the high resistivity region located between the Andes and the Sierras Pampeanas. Other notations are like in Fig. 2.

4. Cocos and Nazca Plates tectonic history from Miocene to Present-day

Another parameter that control slab geometry evolution in time is the convergence rate. According to Turcotte and Schubert (2014), pressure forces induced by the mantle flow around subducting slabs contrabalance slab pull forces. The net flow pressure acting on a descending slab is negative, producing suction forces able to lift the slab against gravity. Suction force is directly proportional with convergence rates and mantle wedge viscosity, the higher the convergence rate and mantle wedge viscosity, the higher the suction force. Present day convergence rates show some modest variability, from 5.5 cm/yr in central Mexico to 6 cm/yr in Peru and 7 cm/yr in central Chile, however since mid-Miocene subducting plates in these flat slab regions experienced significant variations. For example, in central Mexico, Cocos plate experienced a substantial spike in velocity since mid-Miocene from ~6 cm/yr to ~14 cm/yr in a relatively short time span of ~5 Ma (Fig. 10). Interestingly, the interval from 16 Ma to 9 Ma is thought to be the period of the flat-slab onset in central Mexico. On the other hand, in Peru and Central Chile, we observe only a steady decrease in convergence rates (Norabuena et al., 1999; Sdrolias and Muller, 2006) since mid-Miocene from ~14 cm/yr to present day values (Fig. 10). Although in central Mexico the Cocos plate acceleration during the 17–12 Ma period agrees with the onset of flat-slab, in Peru and central Chile such a correlation is not observed (Fig. 10B). However, there is an interesting correlation between the onset of flat-slab in Mexico and Peru (and in Chile but for a less extent) and the decreasing age of the incoming plate (Fig. 10B). When comparing the plate age evolution in all three flat-slab areas we can observe that the onset of flat-slab subduction took place on the descending plate age and velocity slope, or in the vicinity when the plate age at the trench is at its minimum. The plots shown in Fig. 10B suggest that the incoming plate age should be ~35 Ma or less in order to induce flat-slab subduction. This might be an important constraint for future studies related with the origin of horizontal subduction.

5. Present-day thermal structure of flat-slabs

It is known that subduction of oceanic lithosphere beneath continents controls the regional thermal structure (Oxburgh and Turcotte, 1970; Anderson et al., 1978; Honda and Uyeda, 1983; Molnar and England, 1990; Peacock, 1996, 2003; Davies, 1999), which in turn has key implications for seismogenic zones, development of slow slip events and non-volcanic tremors (NVTs), and ultimately arc volcanism. Present-day thermal structure in subduction zones is commonly investigated numerically using based on kinematic 2D heat-transfer models that use a fixed slab geometry and time-independent parameters. These are forced convection models where flow in the mantle wedge is driven only by mechanical coupling with the subducting slab. However, despite such limitations, these models are well constrained by geological and geophysical observations, and provide a valuable framework for investigating processes that occur in subducting slabs, overriding plates and mantle-wedges. Although thermal models for normal dipping subduction zones have been developed for long time (i.e. Oxburgh and Turcotte, 1970; Toksöz et al., 1971; Turcotte and Schubert, 1973; Anderson et al., 1978; Honda and Uyeda, 1983; Cloos, 1985; van den Beukel and Wortel, 1988), models tailored to present-day flat-slab regions as in Mexico and Chile, have been published relatively recently (Gutscher, 2002; Currie et al., 2004; Manea et al., 2003, 2004). Here we will evaluate comparatively the most recent present-day thermal models for these three flat-slab regions. In Fig. 11A and B we compare thermal models for central Mexico and central Chile by Manea and Manea (2011B) and Marot et al. (2014). P-T conditions derived from these thermal models are used in order to investigate stability of hydrous phases and estimate dehydration processes along flat-slab interface, as well as within the slab (Fig. 11C, D).

In central Mexico most of the oceanic crust and sediments dehydrate in the flat-slab segment at distances up to ~250 km from the trench (Fig. 11C, D). The oceanic sediments and crust dehydration pattern show that fluids are released in two separate clusters, one located at ~150 km from the trench, and the second one located at ~200–250 km from the trench. The location of these two dehydration clusters correlate remarkably well with the place where NVTs have been recorded (Fig. 5) suggesting a direct causal relationship. As discussed in the previous chapters, one of the peculiarities of southern Mexico is the absence of contractional deformation in the overriding plate as observed in other flat-slab subduction zones. This has been attributed to a low viscosity layer (Manea and Gurnis, 2007) located atop of the flat-slab segment, that later was confirmed by seismic studies of Song et al. (2009)

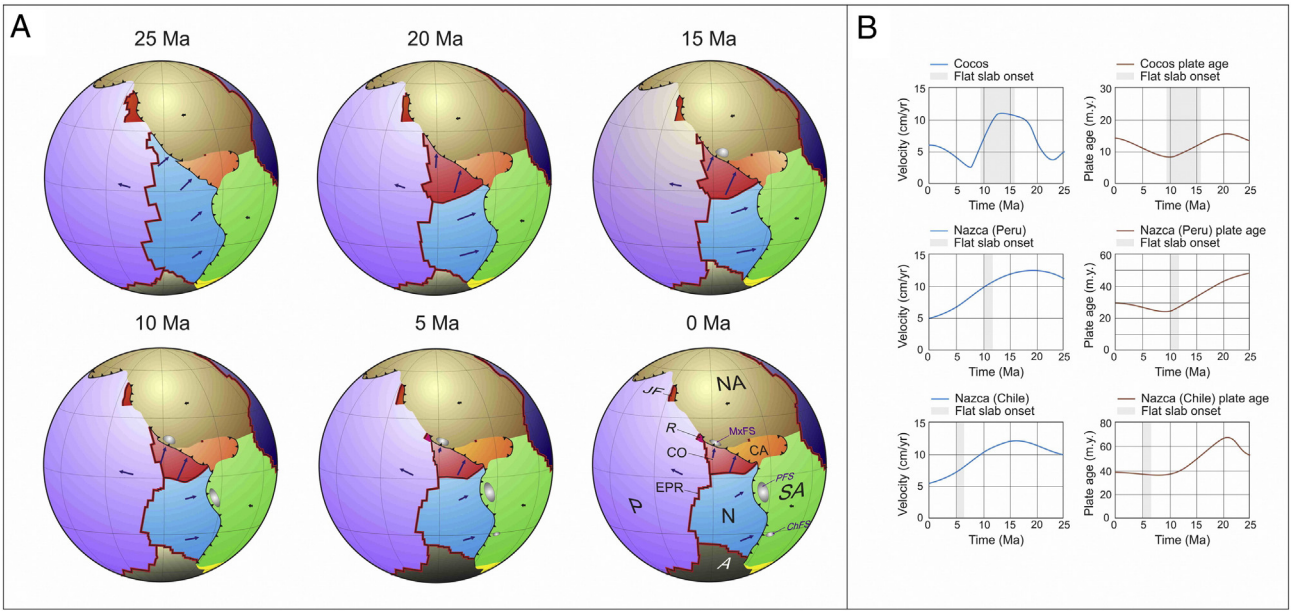

Fig. 10. A. Global paleoreconstructions models based on G-Plates (Gurnis et al., 2012) and the location and evolution of flat-slab areas in Mexico, Peru and Chile (gray ovals). Plate notations are as in Fig. 1-inset. MxFS – Mexican flat-slab, PFS – Peruvian flat-slab, ChFS – Chilean flat-slab. B. Cocos and Nazca incoming plate age and velocity development at flat-slab latitudes. Gray band represents the onset of flat-slab.

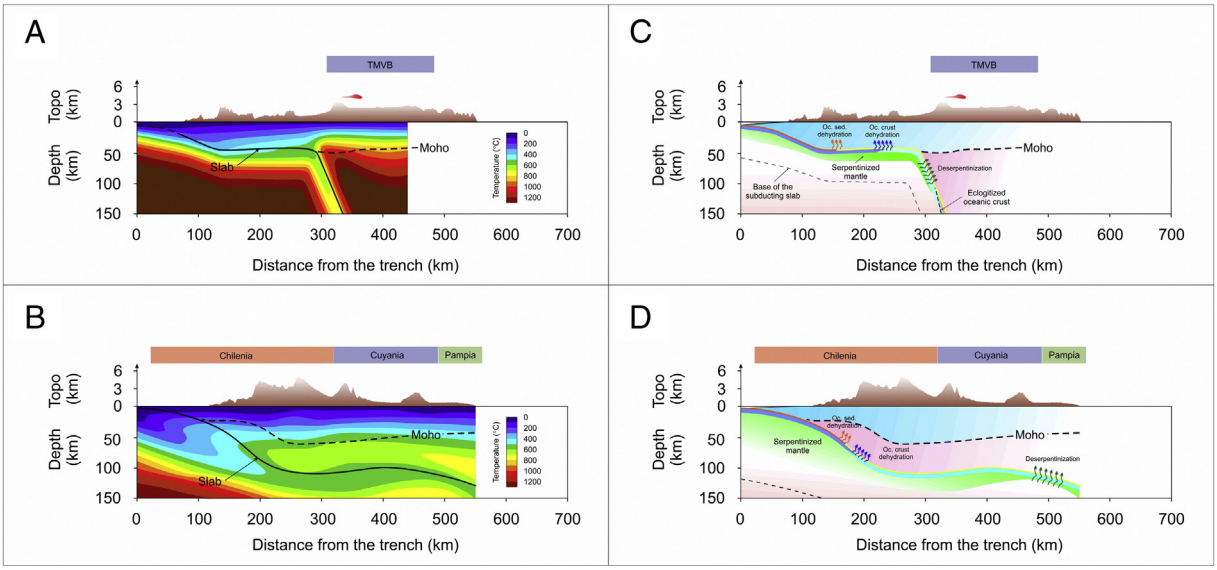

Fig. 11. Present-day thermal structure of flat-slabs in central Mexico (A) (Manea and Manea, 2011b) and Chile (B) (Marot et al., 2014). C, D – Dehydration models along the slab interface.

and Kim et al. (2013). The ~4 km thick ultra-slow velocity layer observed on top the flat-slab interface was interpreted by Song et al. (2009) and Kim et al. (2013) to hydrated minerals as serpentine and talc, formed probable during slab flattening. Thermal models (Fig. 11A) are consistent with these observations and predict P-T conditions of 400–550 °C along the flat-slab interface at 45 km depth, where serpentine and talc are stable.

In terms of fluids released into the mantle wedge, only a small quantity (<0.5 wt% H_2O) comes from the oceanic crust when it transforms into anhydrous eclogite at depths of 100–150 km. This would not be enough to produce the abundant arc volcanism located above the steeply dipping slab behind the flat slab segment. However, if we assume that the oceanic lithosphere below the oceanic crust retains fluids in form of serpentinization, most of the fluids are released into the overlying mantle wedge. This hypothesis strongly suggests that the flat-slab oceanic lithosphere beneath central Mexico retains fluids in form of total or partial serpentinized rocks. Actually, the flat-slab in Mexico seems to be sandwiched between two serpentinzed layers, and this might represent key information to unlock the cause of slab flattening in Mexico (Manea and Manea, 2011b).

In Fig. 11b we present the thermo-mechanical model for central Chile flat slab region of Marot et al. (2014). The continental mantle both above the normal dipping slab as well as above the flat-slab segment down to a depth of ~80 km shows temperature ≤600 °C, potentially permitting mantle rocks to retain fluids in form of partially serpentinized rocks. However, low V_p and V_s seismic velocities (typical for fluid bearing mantle rocks) are recorded above the normal dipping slab, but not above the flat-slab segment. Here the V_p and V_s are higher (Marot et al., 2014), typical for dry mantle rocks. Although numeric modeling shows P-T conditions that allow the mantle to be hydrated, the presence of cold and dry rocks above the flat-slab segment suggest that the subducting slab in this region does not undergo dehydration reactions. It is quite possible that most of the fluids are released into the overriding mantle before the slab reaching 100–120 km depth, consistent with progressive increasing of P-T conditions in the slab and slow V_p and V_s recorded for this region.

Modeling results (Fig. 11D) show P-T conditions within the slab of ~600 °C, temperature that potentially will allow the mantle, but not the oceanic crust, to retain fluids. The nearly anhydrous character of the oceanic crust corresponding to the flat-slab segment is also confirmed by the observed fast seismic velocities that agree with dense and anhydrous eclogites (Marot et al., 2014). It is worth mentioning that this observation runs contrary to the still common acceptance that flat-slab in central Chile is caused by the positively buoyant JFR. However P-T conditions (500– 600 °C at ~120 km depth) within the subducting slab indicate that fluids can be retained within the flat-slab lithospheric segment. Indeed, Marot et al. (2014) show that the subducting Nazca slab may be actually dehydrating but only at the eastern tip of the flat-slab segment, and the positive buoyancy created by the partially serpentinized lithospheric mantle in the flat-slab segment may compensate for negatively buoyant eclogitized oceanic crust.

6. Geochemical signatures of flat-slab subduction

Although magmatism is absent in regions overlying flat slab segments, the age and location of magmatism, and the composition of magmas emplaced during the process of slab flattening provide insights into the timing, evolution, and magma sources in such settings. In the Andean (Chilean) and Mexican flat slab regions, the migration and broadening of the magmatic arc associated to slab flattening was accompanied by changes in magma composition as slab flattening progressed, but with significant differences between these areas.

Volcanic rocks emplaced in the central Trans-Mexican Volcanic Belt (99–101°W) during the progression of slab flattening have subalkaline, medium-K compositions (Fig. 12A) (Gómez-Tuena et al., 2007; Ferrari et al., 2012). As the arc migrated, the composition of the volcanic products became more differentiated from basaltic andesitic to andesitic in positions close to the present volcanic front, to andesitic at 65–100 km from the front, and to andesitic to dacitic at larger distances (Fig. 12A); compositions also show a poorly developed trend to increasing K_2O contents with time. The composition of late Miocene (~9–6 Ma) plateau-forming mafic rocks associated to slab detachment that followed slab flattening is also included for comparison. Volcanic rocks also display a trend to lower epsilon Nd and higher $^{87}Sr/^{86}Sr$ values with time for rocks emplaced between ca. 18 and 11 Ma at increasing distance from the modern volcanic front, which reflects an increasing contribution of crustal materials. The youngest of these samples, with the lowest epsilon Nd values, have also the lowest Ni and Cr abundances at SiO_2 contents similar to those of older rocks, which point to a diminishing role for mantle melts or a lack of equilibration of crustal melts with peridotitic mantle, suggesting thus melting in the lower crust. The previous isotopic trend changed to less isotopically enriched compositions (epsilon Nd between +3.8 and +6.8) in andesite and dacite emplaced at the largest distance to the actual volcanic front at the end of the slab flattening process (ca. 11–9 Ma). The latter volcanic rocks have the geochemical features of adakitic rocks, which reflect a

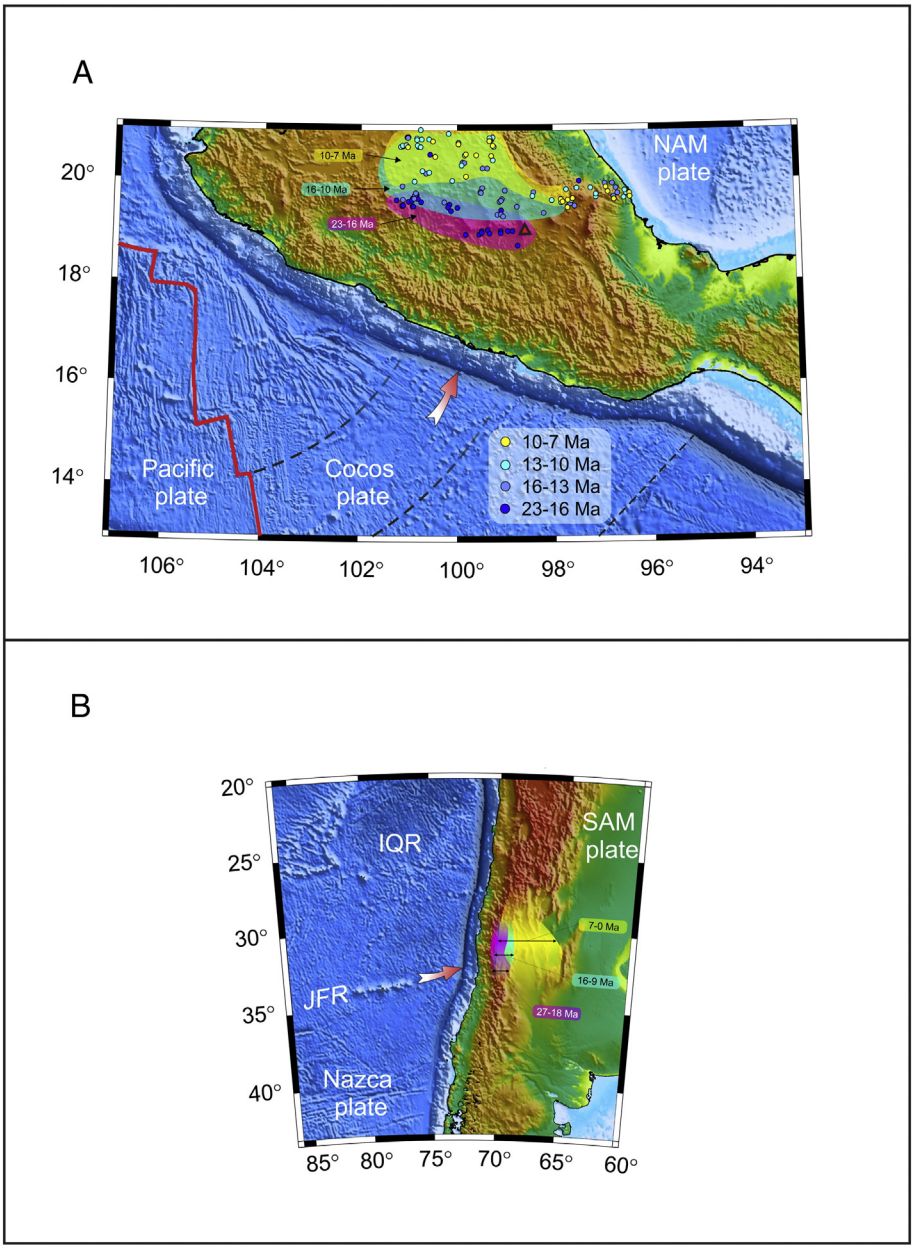

Fig. 12. A. Migration of the Miocene magmatic arc during slab flattening in the Mexican subduction zone. Locus of volcanism migrated ca. 220 km between early and late Miocene to distances of about 480 km from the trench. B. Migration of the magmatic arc in the Pampean flat segment from Oligocene to present. Locus of magmatism reached a distance of ca. 750 km from the trench in the late Miocene to Pliocene. Based on Kay and Mpodozis (2002).

garnet-bearing and plagioclase-free, high-pressure residual source mineralogy or fractionating mineral assemblage (e.g., low Y and heavy rare earth elements, $Sm/Y_b > 4$, $S_r > 890$ ppm; Fig. 12). Late Miocene adakitic rocks in the Trans-Mexican volcanic belt have the geochemical and isotopic features of slab melts and have been interpreted as the product of melting of subducted oceanic crust after prolonged flat subduction (Gómez-Tuena et al., 2003; Mori et al., 2007).

For the Andean flat slab segments, where the flat slab reaches a length of ~750 km form the trench, melting of the slab after prolonged flat subduction has been dismissed as a mechanism for the generation of adakitic rocks, on the basis of thermal and isotopic considerations (e.g., Kay and Mpodozis, 2002). Similar thermal considerations apply to the Mexican flat slab segment, where the relatively old (ca. 30 Ma) oceanic plate that was subducting in the late Miocene reached only 480 km from the trench. Alternatively, we suggest slab detachment and associated asthenospheric mantle flow around the slab edges as a more likely mechanism of slab melting to generate these adakitic rocks.

The Peruvian and Pampean flat slab segments share many common features in their magmatic and tectonic evolution (Ramos and Folguera, 2009). Given the scarcity of geochemical data for the Peruvian area, the following discussion is mainly based on information available for the Pampean flat slab segment. In this area, magmatism associated to slab flattening also evolved with time to SiO_2- and K_2O-richer compositions (e.g., Kay et al., 1988, 1991; Kay and Mpodozis, 2002;), but with much wider variations in both parameters (Fig. 12B), toward andesite, dacite and rhyolite, with high-K or even shoshonitic compositions in some of the youngest volcanic areas (e.g., Kay and Gordillo, 1994; Kay and Mpodozis, 2002). These rocks also display a trend to increasing crustal contributions with time, indicated by lower epsilon Nd and higher $^{87}Sr/^{86}Sr$ values (e.g., Kay et al., 1991; Goss et al., 2013). In the Peruvian and Pampean flat slab segments, rocks with adakitic geochemical features have been also reported (e.g., Kay et al., 1988, 1991; Petford and Atherton, 1996; Kay and Mpodozis, 2002; Coldwell et al., 2011), but unlike the adakites generated at the end of slab flattening in the Mexican

flat slab area, the isotopic signatures of the adakitic rocks from the Peruvian and Pampean segments indicate a dominant contribution of high-pressure continental crust lithologies. Two main models have been considered to account for the high-pressure, garnet signature in these adakite-like rocks: (1) melting at the base of a thickened crust where garnet is stable (>40–45 km) or mixing of mantle mafic magmas with lower crust materials (e.g., Hildreth and Moorbath, 1988; Kay et al., 1988, 1991; Haschke et al., 2002; Kay and Mpodozis, 2002; Goss and Kay, 2009; Coldwell et al., 2011; Mamani et al., 2010); and (2) contamination of the mantle source with fore-arc crustal rocks as result of subduction erosion (e.g., Stern, 1991, 2011; Kay et al., 1991; Kay and Mpodozis, 2002; Litvak et al., 2007; Goss and Kay, 2009; Goss et al., 2013). In the latter model, melting of garnet-bearing lithologies at high pressure and equilibration with the ambient peridotitic mantle would explain the high Mg and Cr and Ni abundances in some of the adakitic rocks (Goss and Kay, 2009; Goss et al., 2013). A further argument given as support for the source contamination model is the transient nature of adakite volcanism coinciding with the migration of the volcanic arc, which is at odds with crustal thickening processes occurring over long time periods (Kay and Mpodozis, 2002).

Geochemical data suggest that a characteristic feature of volcanism in both the Mexican and Andean flat slab segments is the trend to increasing contributions of continental crust materials to the magmas as slab flattening progressed. Nevertheless, crustal thickening and subduction erosion in the Peruvian and Pampean flat slab segments played a central role in determining the composition of the magmas generated during slab flattening, as melting occurred at increasing depths in the crust or mantle, reaching the stability field of garnet. Such crustal thickening processes apparently did not take place in the Mexican segment, which suggest decoupling of the converging plates during the slab flattening phase, as observed in the modern subduction system. On the other hand, slab detachment at the end of slab flattening in the Mexican segment led to adakitic volcanism associated to slab melting followed shortly after by mafic volcanism related to asthenospheric upwelling and decompression. Serpentinization of the oceanic mantle in the bending region behind the trench is a common process in subduction zones. Deserpentinization of these rocks occurs later once they are brought at higher depth and temperature. In flat slab areas this process is retarded but not prevented and if the water is released after the slab plunge again onto the mantle it may produce partial melting and volcanism. Thermal modelling of the flat slab in Mexico (Ferrari et al., 2012) indicate that this process may be an important contribution to the volcanism of the volcanic front.

7. Numeric modeling of flat-slabs formation

Over the last decade or so, numeric modeling has been employed in order to investigate the first order controlling factors causing flat lying subduction. In this chapter we will review, in chronological order, numeric and analog modeling studies dedicated to investigate mechanisms able to induce flat-slab subduction.

One of the first studies dedicated to flat-slab formation was carried out by van Hunen et al. (2000). They performed 2D Cartesian numerical model experiments for a passive oceanic lithosphere that is overridden by a continental plate, and investigated in a systematic manner several major factors that might influence the slab geometry in time and space. The numeric technique used an incompressible medium with infinite Prandtl number and assumed the extended Boussinesq approximation (it uses a constant density, except in buoyancy term). The mantle rheology used was based on a realistic composite rheological model combining Newtonian and non-Newtonian low, corresponding to diffusion and dislocation creep. Five distinct parameters were thoroughly investigated, namely: the depth at which the subduction fault locks, the viscosity of the basaltic crust, the mechanical strength of the mantle, viscous dissipation, and the overriding plate velocity. The study revealed that the only parameter that plays a key role in slab flattening is the overriding plate velocity (Fig. 13A). This study was followed by another work where the effect of buoyant oceanic plateaus in the development of flat-slab subduction (van Hunen et al., 2002) was analyzed. This was motivated by the observed correlation between the location of overthickened oceanic crust regions (Fig. 1) and flat-slab areas in Peru and central Chile. Although these models are 2D, in nature, they can be applied equally to both buoyant ridges and plateaus. Since during subduction the basaltic oceanic crust metamorphoses into the heavier eclogite, one of the main issues related with the overthickened buoyant oceanic crust is the ability to maintain its buoyancy at high pressure and temperature. van Hunen et al. (2002) numeric models revealed that, even in that case of a kinetic delay of eclogitisation of the oceanic crust, flat slabs as those observed in Peru and central Chile cannot be obtained without additional mechanisms involved (Fig. 13A). Furthermore, these models are in 2D, therefore they do not incorporate lateral pulling contribution from steep slabs that bound the flat slab segment on the sides, which will actually decrease even further the positive buoyancy of the ridge or plateau. This conclusion led to another work of van Hunen et al. (2004), where they investigate the effects of overthrusting of the subducting plate, subduction buoyant oceanic plateau, and slab suction forces, using similar 2D Cartesian numeric models employed in the two previous studies. The results show that the minimum condition for slab flattening to occur is the presence of an overthrusting continental plate, where the length of the flat-slab segment is primarily controlled by the slab age, overriding plate motion and mantle viscosity (Fig. 13A). Also, based on Fig. 10B we suggest that the incoming plate age at the trench should be 35 Ma or less in order to facilitate slab flattening. The role of plate suction forces might also be significant, however they were not toughly investigated at that time. Interestingly, the presence of a buoyant oceanic plateau is much less likely to cause flat subduction; eventually it plays a significant role but just after the plateau initiates flattening by other mechanism. Although this chapter is dedicated to numeric modeling of slab flattening, it is worth mentioning that Martinod et al. (2005) uses 3D analog models to investigate the dynamical effects of buoyant ridges and plateaus of the slab dip evolution. These experiments showed that buoyant oceanic features must be quite large enough to alter the dynamics of subduction, however they were not able to reproduce flat slabs similar with those observed today. Buoyant ridges that subduct perpendicular to the trench and similar in size with present-day ridges as Juan Fernandez ridge are not able to lift up the slab and provoke slab flattening. The role of suction forces on slab dynamics was studied by Manea and Gurnis (2007) where the key parameter investigated was the mantle wedge viscosity and distribution. The calculations were performed in a 2-D cut through a sphere on a non-deforming grid, by solving the conservation equations of mass, momentum and energy while making the Boussinesq approximation (Tan et al., 2006). The mantle rheology used was based on a Newtonian rheological model, where mantle wedge viscosity depends on temperature and pressure. This study demonstrated the importance of suction forces in controlling the slab geometry, the transition of a subduction zone into the flat-lying regime being achieved when the mantle wedge viscosity is lower than the surrounding asthenosphere to a depth of ~200 km and within the range of 5 to10×10^{19} Pa s. The shallower the low viscosity wedge and the smaller the viscosity reduction, the higher the negative pressure in the wedge above the slab and therefore the shallower the slab dip. This study showed that the slab flattening process is greatly enhanced when the continental plate overthrusts the subducting oceanic plate, in agreement with the previous studies mentioned above (Fig. 13B). On the other hand, trench roll-forward can only produce steep slabs (Fig. 13B).

Arcay et al. (2008) used for the first time a thermochemical code of convection (Christensen, 1992) in order to study the influence of subducting and overriding plate velocities on slab dip evolution. The calculations are performed in a 2D Cartesian domain, where rocks are assumed to be incompressible, except for the thermal buoyancy term in the momentum equation, and the adiabatic heating term in the energy

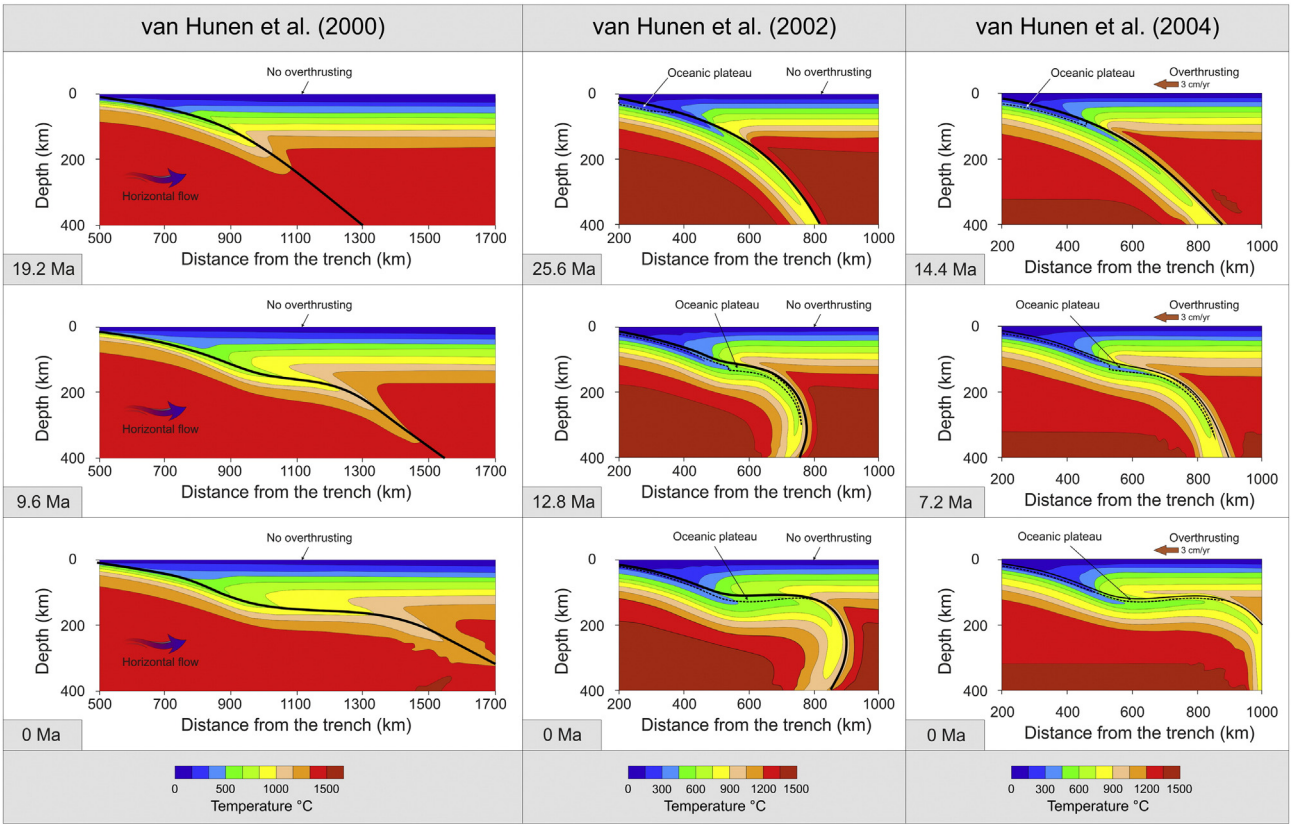

Fig. 13. A. Comparative view of 2D numeric dynamic models of subduction that produce flat slabs (adapted from van Hunen et al. (2000, 2002, 2004)). Horizontal eastward mantle flow, buoyant oceanic plateaus and overthrusting facilitate slab flattening. Note how overthrusting (or trench roll-back) is one of the most efficient ways to promote flat-slabs. B. The strong effect of trench dynamics (rollback or rollforward) on slab geometry is also demonstrated by Manea and Gurnis (2007). Advanced 3D thermo-mechanical numeric models petrologically show that buoyant ridges (as Nazca ridge) alone are not able to induce slab flattening (Gerya et al., 2009). Gerbault et al. (2009) demonstrate that slab flattening is produced when rheological properties of the subducting oceanic plate and the overriding continental plate are interchanged. C. The effect of overriding plate structure (i.e. thickness) on slab geometry evolution is demonstrated by Manea et al. (2012), Rodriguez-Gonzales et al. (2012) (2D models) and confirmed recently by 3D models of Taramon et al. (2015).

equation (extended Boussineq approximation). The mantle rheology used was based on two types of rocks, oceanic crust and mantle, and the rheological model is based on a non-Newtonian law. Additionally, the models incorporate water transport (using particles or tracers) and rock weakening by diminishing viscosity in the non-Newtonian domain by decreasing the pre-exponential constant. This study focused on the thermal and mechanical evolution of the arc lithosphere, and its influence on the slab dip evolution. Modeling results show that when the overriding plate yields under high stress it shortens and becomes thicker in regions located above the mantle wedge. In agreement with previous studies, modeling results incorporating upper plate trenchward advance, revealed extremely high compressive stresses that lead to subducting plate flattening. The progressive mantle wedge closing actually impedes thermal convection and asthenospheric corner flow, resulting in dip angle decrease and triggering slab flattening. This study pointed out for the first time that overriding plate evolution and morphology (i.e. thickening) in the vicinity of mantle wedge can produce quite efficiently slab flattening.

Another attempt to reveal the cause of flat-slab subduction was done by Espurt et al. (2008), where large-scale analog experiments were performed. These experiments showed that flat-slab subduction occur only in a special condition where a large amount of a buoyant slab segment,

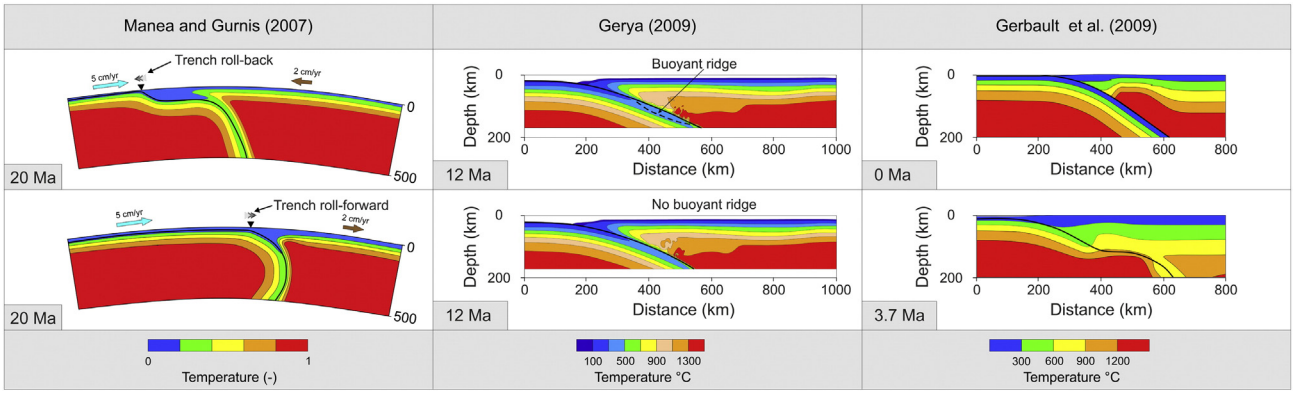

Fig. 13 (*continued*).

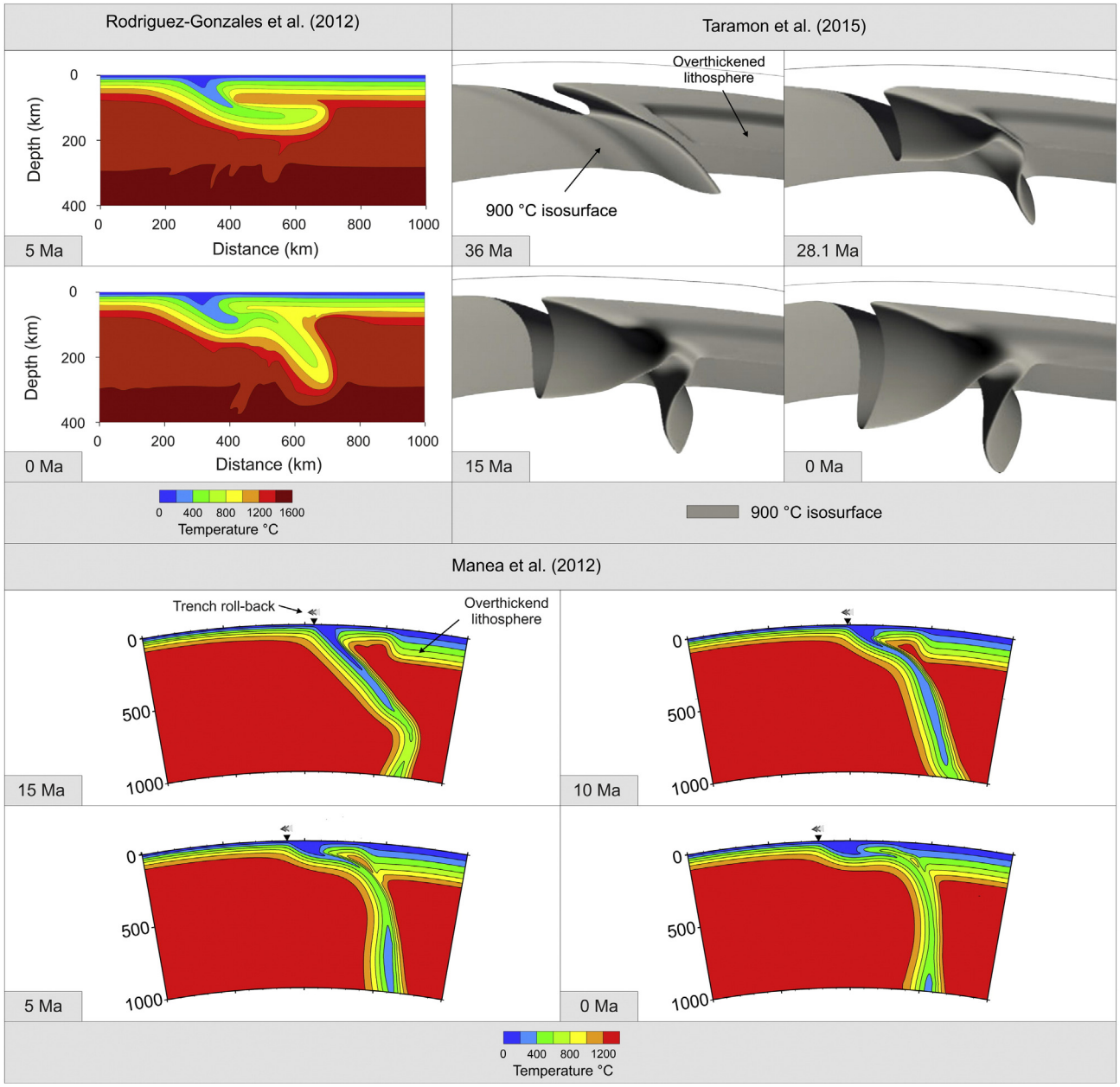

Fig. 13 (*continued*).

or plateau, enters into subduction and actually balances the negative buoyancy of the dense oceanic slab. However, nowadays flat-slab subduction correlates spatially with buoyant oceanic ridges small in size, rather than large oceanic plateaus. Because of this clear spatial correlation between oceanic buoyant features and flat slabs location (Fig. 1), dynamic effects of aseismic ridge subduction has been also investigated using advanced and complex numeric codes, that take into account realistic rheology (i.e. visco-elasto-plastic), phase changes reactions as well as fluid propagation and partial melting (Gerya et al., 2009). The momentum, continuity, and heat conservation equations takes into account thermal and chemical buoyancy, and are solved using the I2ELVIS code (Gerya and Yuen, 2003) based on conservative finite differences and a non-diffusive-marker-in-cell technique to track chemical composition. The numeric model incorporates an oceanic ridge corresponding in size to that of the Nazca ridge (~18 km thick) in the direction orthogonal to the trench. The main conclusion of this study was consistent with previous findings, namely that subduction of realistic buoyant oceanic ridges does not result in strong slab flattening and related decrease of magmatic activity (Fig. 13B). Thermomechanical numeric models were also performed in order to study margin deformation processes along the Andean subduction zone, including flat slab regions (Gerbault et al., 2009). They used a 2D Lagrangian approach (with large-strain Lagrangian formulation) that accounts for elastic-viscous-brittle behavior and the model setup included initial thermal and rheological structures, close to the generic present-day Chilean margin conditions. Modeling results showed that slab flattening is obtained only in the particular case of young and hydrated oceanic plate forced by the slab-pull to subduct under a resistant continent, and more important, when rheological properties of the oceanic and continental mantle are switched. However the length of the flat-slab segment obtained was relatively small (~100 km), whereas intraslab seismicity associated with flat-slab subduction in Peru and central Chile show larger flat-slab segments up to 300 km or more (Fig. 13B).

The role of the overriding plate thermal state on slab geometry was investigated numerically by Manea et al. (2012) and Rodriguez-Gonzales et al. (2012). Both studies used a similar approach where

Table 1
Comparative table of the observed physical parameters specific for flat-slab subduction regions in Mexico, Peru and Chile. Among them, trench rollback, subducting plate structure and tectonic evolution, as well as strong discontinuities in the overriding plate structure are the most important in facilitating slab flattening.

		Mexico flat-slab	Peru flat-slab	Chile flat-slab
Oceanic domain	Oceanic plate age (0 Ma)	~15 Ma	35-45 Ma	~40 Ma
	Convergence rate (0 Ma)	~5.5 cm/yr	~6.0 cm/yr	~7.0 cm/yr
	Youngest oceanic plate age (25-0 Ma)	~9 Ma	~25 Ma	~38 Ma
	Fastest convergence rate (25-0 Ma)	~11 cm/yr	~12 cm/yr	~12 cm/yr
	Buoyant impactor	No	Yes	Yes
	Trench rollback	Yes	Yes	Yes
	Trench erosion	Yes	Yes	Yes
Continental domain	Flat-slab onset	~16-9 Ma	~10 Ma	~5 Ma
	Flat-slab depth	~50 Km	~120 Km	~120 Km
	Flat-slab width	~400 Km	~1000 Km	~200 Km
	Flat-slab segment length	~150 Km	~300 Km	~300 Km
	Estimated temperature along the flat-slab surface (0 Ma)	350-500°C	N/A	550-600°C
	Intraslab seismicity	Low	High	High
	Seismic anisotropy beneath flat-slab	Trench ⊥	Trench ⊥	Trench ⊥
	Seismic anisotropy above/in front of flat-slab	Trench ⊥	Variable	Trench ⊥
	Volcanism (present day)	Present	Absent	Absent
	Presence of overthickened lithosphere (craton)	No	Yes	Yes
	Heat flow above flat-slab	Low	Low	Low
	Mantle lithosphere above	Not present	~50 km thick	~50 km thick
	Weak layer atop of flat-slab	Yes	Not observed	Not observed
	Overriding plate deformation	No	Yes	Yes
	SSEs and NVTs	Yes	Not observed	Not observed
	Low-resistivity above flat-slab	Yes	N/A	Yes

equations of conservation of mass, momentum and energy were solved for an incompressible 2D fluid domain with high Prandtl number, which allows us to neglect inertial forces on the momentum equation. Also, these time-dependent 2D numeric models are similar in terms of boundary conditions, where free slip boundary conditions were applied to the bottom and side boundaries of the model domain, while the top of the models used prescribed velocities. In terms of rheology, Manea et al. (2012) used a simple Newtonian rheology coupled with a low viscosity wedge and channel, whereas Rodriguez-Gonzales et al. (2012) employed a composite rheology based on both diffusion and dislocation creep viscosities. Both studies provided the same main conclusion, where flat-slab subduction is obtained as a result of the increased suction force in the mantle wedge when an overthickened and colder continental lithosphere is located in the vicinity of the subduction system (Fig. 13C).

Flat-slab geometries similar with those observed in central Chile were obtained when a cratonic lithosphere (200 km or more) is actually combined with trench roll-back (Manea et al., 2012). This was later confirmed by Taramon et al. (2015) study, where the influence of cratonic lithosphere on the formation and evolution of flat slabs was carried out using advanced 3-D time-dependent numeric models (Fig. 13C). In a recent study of Antonijevic et al. (2015), based on a detailed three-dimensional model of the structure of shear-wave velocities for the Peruvian flat-slab region, slab flattening is proposed to be the result of the combined effects of trench retreat, suction, and ridge subduction. This study proposed that the buoyant Nazca ridge plays rather a secondary role in flat-slab formation, but eventually could support maintaining flat-slab regimes for longer periods of time.

Although slab flattening seems to occur preferentially in the vicinity of cold and thick cratons and correlate spatially with buoyant oceanic impactors, as is the case of Peru and central Chile, in central Mexico the continental lithosphere is very thin or even missing, and the oceanic Cocos plate lacks large buoyant features. Still flat-slab subduction has been occurring since middle Miocene. The above-mentioned modeling studies indicate that whereas buoyant ridges alone are not sufficient for the formation of flat slabs, the ultimate cause of slab flattening is yet to be found.

8. Concluding remark

As a result of this review we present a comprehensive table (Table 1) comparing a variety of observations of the three flat-slab subduction regions discussed in this work. Among the different parameters analyzed we concluded that trench dynamics (i.e. roll-back) and subducting plate tectonic evolution (i.e. super-fast subduction episodes and/or young incoming oceanic plates), as well as strong discontinuities in the oceanic and overriding plates structure are the most important in facilitating slab flattening. However, we were unable to find a unique set of conditions that provide an explanation for the formation of flat slabs in all three subduction zones. In this respect we think that the ultimate cause of slab flattening is yet to be found. Although at a first sight flat-slab subduction zones do not easily fit into the plate tectonics paradigm, discovering the real cause of slab flattening offer a great opportunity to better understand subduction zones and to unravel the complexity of mechanism that drive plate tectonics.

Acknowledgements

We thank Rafael Bartolome and an anonymous reviewer for comments that improved the paper. We also would like to thank Marianne Marot and Juan Rodriguez Gonzales for generously sharing high quality figures of numeric models. This research has been conducted through the CYBERDYN project (POS CCE O212_ID 593).

References

Abt, D.L., Fischer, K.M., Abers, G.A., Strauch, W., Protti, J.M., González, V., 2009. Shear wave anisotropy beneath Nicaragua and Costa Rica: implications for flow in the mantle wedge. Geochem. Geophys. Geosyst. 10, Q05S15. http://dx.doi.org/10.1029/2009GC002375.

Abt, D.L., Fischer, K.M., Abers, G.A., Protti, M., González, V., Strauch, W., 2010. Constraints on upper mantle anisotropy surrounding the Cocos slab from SK(K)S splitting. J. Geophys. Res. 115, B06316. http://dx.doi.org/10.1029/2009JB006710.

Allis, R.G., 1979. A heat production model for the stable continental crust. Tectonophysics 57, 151–165.

Allmendinger, R.W., Figueroa, D., Snyder, D., Beer, J., Mpodozis, C., Isacks, B.L., 1990. Foreland shortening and crustal balancing in the Andes at 30°S latitude. Tectonics 9, 789–809.

Alvarado, P., Ramos, V., 2011. Earthquake deformation in the northwestern Sierras Pampeanas of Argentina based on seismic waveform modeling. J. Geodyn. 51, 205–218.

Alvarado, P., Beck, S., Zandt, G., 2007. Crustal structure of the south-central Andes Cordillera and backarc region from regional waveform modeling. Geophys. J. Int. 121 (170(2)), 858–875.

Alvarado, P., Pardo, M., Gilbert, H., Miranda, S., Anderson, M., Saez, M., Beck, S.L., 2009. Flat-slab subduction and crustal models for the seismically active Sierras Pampeanas Region of Argentina. MWR204: Backbone of the Americas: Shallow Subduction, Plateau Uplift, and Ridge and Terrane Collision. GSA, Boulder, Colorado, USA, pp. 261–278 (doi: 10.1130/2009.1204(12)).

Ammirati, J.-B., Alvarado, P., Perarnau, M., Saez, M., Monsalvo, G., 2013. Crustal structure of the Central Precordillera of San Juan, Argentina (31°S) using teleseismic receiver functions. J. S. Am. Earth Sci. 46, 100–109.

Anderson, M.L., 2005. Seismic Anisotropy, Intermediate-depth Earthquakes, and Mantle Flow in the Chile-Argentina Flat-slab Subduction Zone. (Ph. D. thesis, 280 pp.). University of Arizona, USA.

Anderson, R.N., DeLong, S.E., Schwarz, W.M., 1978. Thermal model for subduction with dehydration in the downgoing slab. J. Geol. 86 (6), 731–739.

Anderson, M.L., Zandt, G., Triep, E., Fouch, M., Beck, S., 2004. Anisotropy and mantle flow in the Chile-Argentina subduction zone from shear wave splitting analysis. Geophys. Res. Lett. 31, L23608. http://dx.doi.org/10.1029/2004GL020906.

Anderson, M.L., Wagner, L., Gilbert, H., Alvarado, P., Zandt, G., Beck, S., Triep, E., 2005. Constraints on Mantle Kinematics Influenced by a Changing Slab Geometry: Results from the CHARGE Project, South America. Abstract 1000 Presented at the IASPEI General Assembly, Santiago, Chile, October.

Anderson, M., Alvarado, P., Zandt, G., Beck, S., 2007. Geometry and brittle deformation of the subducting Nazca plate, central Chile and Argentina. Geophys. J. Int. 171, 419–434.

Antonijevic, S.K., Wagner, L.S., Kumar, A., Beck, S.L., Long, M.D., Zandt, G., Tavera, H., Condori, C., 2015. The role of ridges in the formation and longevity of flat slabs. Nature 524:212–215. http://dx.doi.org/10.1038/nature14648.

Arcay, D., Lallemand, S., Doin, M.-P., 2008. Back-arc strain in subduction zones: Statistical observations versus numerical modeling. Geochem. Geophys. Geosyst. http://dx.doi.org/10.1029/2007GC001875.

Astini, R.A., Benedetto, J.L., Vaccari, N.E., 1995. The early Paleozoic evolution of the Argentine Precordillera as a Laurentian rifted, drifted and collided terrain: a geodynamical model. Geol. Soc. Am. Bull. 107, 253–273.

Atwater, T., Stock, J., 1998. Pacific-North America Plate tectonics of the Neogene Southwestern United States – an update. Int. Geol. Rev. 40, 375–402.

Audet, P., 2013. Seismic anisotropy of subducting oceanic uppermost mantle from fossil spreading. Geophys. Res. Lett. 40:173–177. http://dx.doi.org/10.1029/2012GL054328.

Barazangi, M., Isacks, B.L., 1976. Spatial distribution of earthquakes and subduction of the Nazca plate beneath South America. Geology 4, 686–692.

Beck, S.L., Hersh, G., Wagner, L., Alvarado, L., Anderson, M., Zandt, G., Araujo, M., Triep, E., 2005. The lithosfera structure of the Sierras Pampeanas region of Argentina. 2005 Salt Lake City GSA Annual Meeting, Session no. 253, Paper No: 253-5.

Bernal-Díaz, A., Valenzuela-Wong, R., Pérez-Campos, X., Iglesias, A., Clayton, R.W., 2008. Anisotropía de la onda SKS en el manto superior debajo del arreglo VEOX (abstract). Geos Bol. Inf. Unión Geofís. Mex. 28 (2), 199–200.

Bernal-López, L.A., 2015. Anisotropía sísmica y flujo del manto producidos por la placa de Cocos subducida en el sur de México. (M. Sc. thesis, 65 pp.). Centro de Sismología y Volcanología de Occidente, Universidad de Guadalajara, Puerto Vallarta, Jalisco, Mexico.

Bernal-López, L.A., León Soto, G., Valenzuela Wong, R., Núñez Cornú, F.J., 2014. Anisotropía sísmica y flujo del manto producidos por la placa de Cocos subducida en el sur de México (abstract). Geos Bol. Inf. Unión Geofís. Mex. 34 (1), 227.

Bernal-López, L.A., Garibaldi, B.R., León Soto, G., Valenzuela, R.W., Escudero, C.R., 2015. Seismic anisotropy and mantle flow driven by the Cocos slab under southern Mexico. Pure Appl. Geophys. http://dx.doi.org/10.1007/s00024-015-1214-7.

Beroza, G.C., Ide, S., 2011. Slow earthquakes and nonvolcanic tremor. Annu. Rev. Earth Planet. Sci. 39, 271–296.

Bevis, M., Isacks, B.L., 1984. Hypocentral trend surface analysis: probing the geometry of Benioff Zones. J. Geophys. Res. 89, 6153–6170.

Blackwell, D.D., 1969. Heat flow in the northwestern United States. J. Geophys. Res. 74, 992–1077.

Blackwell, D.D., 1971. Thermal structure of the continental crust, in Heacock, J.G., ed., "The structure and physical properties of the Earth's crust", Washington, D.C. Am. Geophys. Union Monogr. 14, 169–184.

Booker, J., Favetto, A., Pomposiello, C., 2004. Low electrical resistivity associated with plunging of the Nazca flat slab beneath Argentina. Nature 429, 399–403.

Brudzinski, M.R., Hinojosa-Prieto, H.R., Schlanser, K.M., Cabral-Cano, E., Arciniega-Ceballos, A., Diaz-Molina, O., DeMets, C., 2010. Nonvolcanic tremor along the Oaxaca segment of the Middle America subduction zone. J. Geophys. Res. 115. http://dx.doi.org/10.1029/2008JB006061 (ISSN 0148–0227, eISSN 2156–2202). (B00A23).

Burd, A.I., Booker, J.R., Mackie, R., Pomposiello, M.C., Favetto, A., 2013. Electrical conductivity of the Pampean shallow subduction region of Argentina near 33°S: evidence for a slab window. Geochem. Geophys. Geosyst. 14:3192–3209. http://dx.doi.org/10.1002/ggge.20213.

Cahill, T., Isacks, B.L., 1992. Seismicity and shape of the subducted Nazca plate. J. Geophys. Res. 97, 17503–17529.

Cardoso, R.R., Hamza, V.M., Alfaro, C., 2010. Geothermal Resource Base for South America: A Continental Perspective. Proceedings World Geothermal Congress 2010, Bali, Indonesia, 25–29 April 2010.

Carr, M.J., 1984. Symmetrical and segments variation of physical and geochemical characteristics of the Central American volcanic front. J. Volcanol. Geotherm. Res. 20, 231–252.

Castillo, J.A., Pérez-Campos, X., Husker, A.L., Valenzuela-Wong, R., 2014. Crust and Mantle Anisotropy Variations from the Coast to Inland in Central and Southern Mexico, Abstract DI33A-4303 Presented at 2014 Fall Meeting, American Geophysical Union, San Francisco, CA, 15–19 December.

Castillo-Castellanos, J.A., 2015. Variaciones de la anisotropía sísmica en la corteza y manto superior en el centro-sur de México. (M.Sc. thesis, 147 pp.). Instituto de Geofísica, Universidad Nacional Autónoma de México, Mexico City, Mexico.

Chandra, U., 1970. The Peru-Bolivia border earthquake of August 15, 1963. Bull. Seismol. Soc. Am. 60, 639–646.

Chapman, D.S., Furlong, K.P., 1992. Thermal state of the continental lower crust. In: Fountain, D.M., Arculus, R.J., Kay, R.W. (Eds.), Continental Lower Crust. Elsevier, Amsterdam, pp. 179–199.

Chew, D.M., Schaltegger, U., Košler, J., Whitehouse, M.J., Gutjahr, M., Spikings, R.A., Miškovic, A., 2007. U-Pb geochronologic evidence for the evolution of the gondwanan margin of the north-central Andes. Geol. Soc. Am. Bull. 119 (5/6), 697–711.

Christensen, U.R., 1992. An Eulerian technique for thermomechanical modeling of lithospheric extension. J. Geophys. Res. 97 (B2), 2015–2036.

Cloos, M., 1985. Thermal evolution of convergent plate margins: thermal modeling and reevaluation of isotopic AR-ages for Blueschists in the Franciscan Complex of California. Tectonics 4 (5), 421–433.

Clouard, V., Campos, J., Lemoine, A., Perez, A., Kausel, E., 2007. Outer rise stress changes related to the subduction of the Juan Fernandez Ridge, central Chile. J. Geophys. Res. 112. http://dx.doi.org/10.1029/2005JB003999 (issn: 0148-0227).

Coldwell, B., Clemens, J., Petford, N., 2011. Deep crustal melting in the Peruvian Andes: felsic magma generation during delamination and uplift. Lithos 125, 272–286.

Correa-Mora, F., DeMets, C., Cabral-Cano, E., Marquez-Azua, B., Diaz-Molina, O., 2008. Interplate coupling and transient slip along the subduction interface beneath Oaxaca, Mexico. Geophys. J. Int. 175, 269–290 (doi:10.1111.j.1365-246X.2008.03910.x).

Correa-Mora, F., DeMets, C., Cabral-Cano, E., Diaz-Molina, O., Marquez-Azua, B., 2009. Transient deformation in southern Mexico in 2006 and 2007: evidence for distinct deep-slip patches beneath Guerrero and Oaxaca. Geochem. Geophys. Geosyst. 10, 1–12.

Cross, T., Pilger, R., 1982. Control of subduction geometry, location of magmatic arcs and tectonics of arc and back-arc regions. Geol. Soc. Am. Bull. 93, 545–562.

Currie, C.A., Cassidy, J.F., Hyndman, R.D., Bostock, M.G., 2004. Shear wave anisotropy beneath the Cascadia subduction zone and western North American craton. Geophys. J. Int. 157, 341–353.

Davies, J.H., 1999. The role of hydraulic fractures and intermediate-depth earthquakes in generating subduction-zone magmatism. Nature 398, 142–145.

Davies, J.H., 2013. Global map of solid Earth surface heat flow. Geochem. Geophys. Geosyst. http://dx.doi.org/10.1002/ggge.20271.

DeMets, C., Traylen, S., 2000. Motion of the Rivera plate since 10 Ma relative to the Pacific and North American and the mantle. Tectonophysics 318:119–159. http://dx.doi.org/10.1016/S0040-1951(99)00309-1.

Dorbath, L., Dorbath, C., Jimenez, E., Rivera, L., 1991. Seismicity and tectonic deformation in the Eastern Cordillera and the sub-Andean zone of central Peru. J. S. Am. Earth Sci. 4 (1/2), 13–24.

Doser, D.I., 1987. The Ancash, Peru, earthquake of 1946 November 10: evidence for low-angle normal faulting in the high Andes of northern Peru. Geophys. J. Int. 91 (1), 57–71.

Ducea, M., Valencia, V.A., Shoemaker, S., Reiners, P.W., DeCelles, P.G., Campa, M.F., 2004. Rates of sediment recycling beneath the Acapulco trench: constraints from (U-Th)/He thermochronology. J. Geophys. Res. Solid Earth (1978–2012) 109 (B9).

Eakin, C.M., Long, M.D., 2013. Complex anisotropy beneath the Peruvian flat slab from frequency-dependent, multiple-phase shear wave splitting analysis. J. Geophys. Res. 118:4794–4813. http://dx.doi.org/10.1002/jgrb50349.

Eakin, C.M., Obrebski, M., Allen, R.M., Boyarko, D.C., Brudzinski, M.R., Porritt, R., 2010. Seismic anisotropy beneath Cascadia and the Mendocino triple junction: Interaction of the subducting slab with mantle flow. Earth Planet. Sci. Lett. 297, 627–632.

Eakin, C.M., Long, M.D., Beck, S.L., Wagner, L.S., Tavera, H., Condori, C., 2014. Response of the mantle to flat slab evolution: insights from local S splitting beneath Peru. Geophys. Res. Lett. 41:3438–3446. http://dx.doi.org/10.1002/2014GL059943.

Eakin, C.M., Long, M.D., Wagner, L.S., Beck, S.L., Tavera, H., 2015. Upper mantle anisotropy beneath Peru from *SKS* splitting: Constraints on flat slab dynamics and interaction with the Nazca Ridge. Earth Planet. Sci. Lett. 412:152–162. http://dx.doi.org/10.1016/j.epsl.2014.12.015.

Engdahl, E.R., van der Hilst, R.D., Berrocal, J., 1995. Imaging of subducted lithosphere beneath South America. Geophys. Res. Lett. 22 (16):2317–2320. http://dx.doi.org/10.1029/95GL02013.

Espurt, N., Funiciello, F., Martinod, J., Buillaume, B., Regard, V., Faccenna, C., Brusset, S., 2008. Flat subduction dynamics and deformation of the South American plate: insights from analog modeling. Tectonics 27, TC3011. http://dx.doi.org/10.1029/2007TC002175.

Feng, M., Assumpção, M., Van der Lee, S., 2004. Group-velocity tomography and lithospheric structure of the South American continent. Phys. Earth Planet. Inter. 147, 315–331.

Ferrari, L., Orozco-Esquivel, T., Manea, V.C., Manea, M., 2012. Review article: the dynamic history of the Trans-Mexican Volcanic Belt and the Mexico subduction zone. Tectonophysics 522-523, 122–149.

Ferrari, L., Bergomi, M., Martini, M., Tunesi, A., Orozco- Esquivel, M., López-Martínez, M., 2014. Late Cretaceous-Oligocene magmatic record in southern Mexico: the case for a temporal slab window along the evolving Caribbean-North America-Farallon triple boundary. Tectonics 33:1738–1765. http://dx.doi.org/10.1002/2014TC003525.

Foley, B.J., Long, M.D., 2011. Upper and mid-mantle anisotropy beneath the Tonga slab. Geophys. Res. Lett. 38, L02303. http://dx.doi.org/10.1029/2010GL046021.

Frank, W.B., Shapiro, N.M., Husker, A.L., Kostoglodov, V., Romanenko, A., Campillo, M., 2014. Using systematically characterized low-frequency earthquakes as a fault probe in Guerrero, Mexico. J. Geophys. Res. 119 (10), 1686–7700.

Frank, W.B., Shapiro, N.M., Husker, A.L., Kostoglodov, V., Bhat, H.S., Campillo, M., 2015. Along-fault pore-pressure evolution during a slow-slip event in Guerrero, Mexico. Earth Planet. Sci. Lett. 413, 135–143.

Frank, W.B., Shapiro, N.M., Husker, A.L., Kostoglodov, V., Gusev, A.A., Campillo, M., 2016. The evolving interaction of low-frequency earthquakes during transient slip. Sci. Adv. 2 (4), e1501616. http://dx.doi.org/10.1126/sciadv.1501616.

Fromm, R., Zandt, G., Beck, S.L., 2004. Crustal thickness beneath the Andes and Sierras Pampeanas at 30°S inferred from Pn apparent phase velocities. Geophys. Res. Lett. 31, L06625. http://dx.doi.org/10.1029/2003GL019231.

Gans, C.R., Beck, S.L., Zandt, G., Gilbert, H., Alvarado, P., Anderson, M., Linkimer, L., 2011. Continental and oceanic crustal structure of the Pampean flat slab region, western Argentina, using receiver function analysis: new high-resolution results. Geophys. J. Int. 186 (1), 45–58.

Gérault, M., Husson, L., Miller, M.S., Humphreys, E.D., 2015. Flat-slab subduction, topography, and mantle dynamics in south-western Mexico. Tectonics 34. http://dx.doi.org/10.1002/2015TC003908.
Gerbault, M., Cembrano, J., Mpodozis, C., Farias, M., Pardo, M., 2009. Continental margin deformation along the Andean subduction zone: thermo-mechanical models. Phys. Earth Planet. Inter. 177 (3–4), 180–205.
Gerya, T.V., Yuen, D.A., 2003. Characteristics-based marker-in-cell method with conservative finite-differences schemes for modeling geological flows with strongly variable transport properties. Phys. Earth Planet. Inter. 140, 293–318.
Gerya, T.V., Fossati, D., Cantieni, C., Seward, D., 2009. Dynamic effects of aseismic ridge subduction: numerical modelling. Eur. J. Mineral. 21:649–661. http://dx.doi.org/10.1127/0935-1221/2009/0021-1931.
Gilbert, H.J., Beck, S., Zandt, G., 2006. Lithospheric and upper mantle structure of central Chile and Argentina. Geophys. J. Int. 165 (1), 383–398.
Giménez, M., Martinez, M.P., Introcaso, A., 2000. A crustal model based mainly on Gravity data in the Area between the Bermejo Basin and the Sierras de Valle Fértil- Argentina. J. S. Am. Earth Sci. 13 (3), 275–286.
Gómez-Tuena, A., LaGatta, A., Langmuir, C., Goldstein, S., Ortega-Gutiérrez, F., Carrasco-Núñez, G., 2003. Temporal control of subduction magmatism in the Eastern Trans-Mexican Volcanic Belt: mantle sources, slab contributions and crustal contamination. Geochem. Geophys. Geosyst. 4 (8). http://dx.doi.org/10.1029/2003GC000524.
Gómez-Tuena, A., Langmuir, C.H., Goldstein, S.L., Straub, S.M., Ortega-Gutiérrez, F., 2007. Geochemical evidence for slab melting in the Transmexican Volcanic Belt. J. Petrol. 48:537–562. http://dx.doi.org/10.1093/petrology/egl071.
Gorbatov, A., Fukao, Y., 2005. Tomographic search for missing link between the ancient Farallon subduction and the present Cocos subduction. Geophys. J. Int. 160 (3), 849–854.
Goss, A.R., Kay, S.M., 2009. Extreme high field strength element (HFSE) depletion and near-chondritic Nb/Ta ratios in Central Andean adakite-like lavas (~27°S, ~68°W). Earth Planet. Sci. Lett. 270, 97–109.
Goss, A.R., Kay, S.M., Mpodozis, C., 2013. Andean adakite-like high-Mg andesites on the northern margin of the Chilean–Pampean flat-slab (27–28.5°S) associated with frontal arc migration and fore-arc subduction erosion. J. Petrol. 54, 2193–2234.
Grange, F., Hatzfeld, D., Cunningham, P., Molnar, P., Roecker, S.W., Suarez, G., Rodrigues, A., Ocola, L., 1984. Tectonic implications of the microearthquake seismicity and fault plane solutions in southern Peru. J. Geophys. Res. 89 (B7), 6139–6152.
Gurnis, M., Turner, M., Zahirovic, S., DiCaprio, L., Spasojevic, S., Müller, R.D., Boyden, J., Seton, M., Manea, V.C., Bower, D.J., 2012. Plate tectonic reconstructions with continuously closing plates. Comput. Geosci. 38:35–42. http://dx.doi.org/10.1016/j.cageo.2011.04.014.
Gutscher, M.A., 2002. Andean subduction styles and their effect on thermal structure and interplate coupling. J. S. Am. Earth Sci. 15 (1), 3–10.
Gutscher, M.-A., Olivet, J.-L., Aslanian, D., Eissen, J.-P., Maury, R., 1999. The lost Inca Plateau: cause of flat subduction beneath Peru? Earth Planet. Sci. Lett. 171, 335–341.
Gutscher, M.-A., Spakman, W., Bijwaard, H., Engdahl, E.R., 2000. Geodynamics of flat subduction: seismicity and tomographic constraints from the Andean margin. Tectonics 19, 814–833.
Hacker, B.R., 2008. H_2O subduction beyond arcs. Geochem. Geophys. Geosyst. 9 (3), Q03001. http://dx.doi.org/10.1029/2007GC001707.
Hampel, A., 2002. The migration of the Nazca Ridge along the Peruvian active margin: a re-evaluation. Earth Planet. Sci. Lett. 203 (2), 665–679.
Hamza, V.M., Muñoz, M., 1996. Heat flow map of South America. Geothermics 25, 599–646.
Hamza, V.M., Silva Dias, F.J.S., Gomes, A.J.L., Delgadilho Terceros, Z.G., 2005. Numerical and functional representations of regional heat flow in South America. Phys. Earth Planet. Inter. 152, 223–256.
Haschke, M.R., Siebel, W., Günther, A., Scheuber, E., 2002. Repeated crustal thickening and recycling during the Andean orogeny in north Chile (21°–26°S). J. Geophys. Res. 107, 1–18.
Hasegawa, A., Sacks, I.S., 1981. Subduction of the Nazca plate beneath Peru as determined from seismic observations. J. Geophys. Res. 86, 4971–4980.
Heit, B., Yuan, X., Bianchi, M., Sodoudi, F., Kind, R., 2008. Crustal thickness estimation beneath the southern central Andes at 30°S and 36°S form S wave receiver function analysis. Geophys. J. Int. 174 (1), 249–254.
Herrmann, U.R., Nelson, B.K., Ratschbacher, L., 1994. The origin of a terrane: U/Pb zircon geochronology and tectonic evolution of the Xolapa complex (southern Mexico). Tectonics 13 (2), 455–474.
Hildreth, W., Moorbath, S., 1988. Crustal contributions to arc magmatism in the Andes of Central Chile. Contrib. Mineral. Petrol. 98, 455–489.
Honda, S., Uyeda, S., 1983. Thermal process in subduction zones—a review and preliminary approach on the origin of arc volcanism. In: Shimozuru, D., Yokoyama, I. (Eds.), Arc Volcanism—Physics and Tectonics. Terrapublishing, Tokyo, pp. 117–140.
Hu, J., Liu, L., Hermosillo, A., Zhou, Q., 2016. Simulation of late Cenozoic South American flat-slab subduction using geodynamic models with data assimilation. Earth Planet. Sci. Lett. 438, 1–13.
Huesca-Pérez, E., Valenzuela, R.W., Ortega, R., 2016. Crustal anisotropy from tectonic tremor in Guerrero, Mexico. Geochem. Geophys. Geosyst. 17:2323–2335. http://dx.doi.org/10.1002/2016GC006358.
Husker, A., Davis, P.M., 2009. Tomography and thermal state of the Cocos plate subduction beneath Mexico City. J. Geophys. Res. 114, B04306. http://dx.doi.org/10.1029/2008JB006039.
Husker, A.L., Kostoglodov, V., Cruz-Atienza, V.M., Legrand, D., Shapiro, N.M., Payero, J.S., Campillo, M., Huesca- Pérez, E., 2012. Temporal variations of non-volcanic tremor (NVT) locations in the Mexican subduction zone: finding the NVT sweet spot. Geochem. Geophys. Geosyst. 13, Q03011. http://dx.doi.org/10.1029/2011GC003916.
Isacks, B.L., Barazangi, M., 1973. High frequency shear waves guided by a continuous lithosphere descending beneath western South America. Geophys. J. Int. 33 (2), 129–139.
Isacks, B.L., Molnar, P., 1971. Distribution of stresses in the descending lithosphere from a global survey of focal mechanism solutions of mantle earthquakes. Rev. Geophys. Space Phys. 9 (1), 103–174.
Isacks, B., Jordan, T., Allmendinger, R.W., Ramos, V.A., 1982. La segmentación tectónica de los Andes Centrales y su relación con la placa de Nazca subductada, Vth Congreso Latinoamericano de Geología. Universidad de Buenos Aires, Buenos Aires.
Jadamec, M.A., Billen, M.I., 2012. The role of rheology and slab shape on rapid mantle flow: three-dimensional numerical models of the Alaska slab edge. J. Geophys. Res. Solid Earth 117 (B2).
James, D.E., Snoke, J.A., 1990. Seismic evidence for continuity of the deep slab beneath central and Eastern Peru. J. Geophys. Res. 95. http://dx.doi.org/10.1029/89JB03314 (issn: 0148-0227).
Jödicke, H., Jording, A., Ferrari, L., Arzate, J., Mezger, K., Rupke, L., 2006. Fluid release from the subducted Cocos plate and partial melting of the crust deduced from magnetotelluric studies in southern Mexico. Implications for the generation of volcanism and subduction dynamics. J. Geophys. Res. 111, B08102. http://dx.doi.org/10.1029/2005JB003739.
Jordan, T.E., Allmendinger, R.W., 1986. The Sierras Pampeanas of Argentina: a modern analogue of Rocky Mountain foreland deformation. Am. J. Sci. 286 (10), 737–764.
Jordan, T.E., Allmendinger, R.W., Brewer, J.A., Ramos, V.A., Ando, C.J., 1983. Andean tectonics related to geometry of subducted Nazca plate. Geol. Soc. Am. Bull. 94:341–361. http://dx.doi.org/10.1130/00167606.
Jordan, T., Zeitler, P., Ramos, V.A., Gleadow, A.J.W., 1989. Thermochronometric data on the development of the basement peneplain in the Sierras Pampeanas, Argentina. J. S. Am. Earth Sci. 2, 207–222.
Jordan, T.E., Drake, R., Nasser, C., 1993. Estratigrafía del Cenozoico medio en la Precordillera a la latitud del Río Jáchal, San Juan, Argentina. Actas, Congreso Geológico Argentino, 12th, and Congreso de Exploración de Hidro- carburos, 2nd, Mendoza 2. Asociación Geológica Argentina, Buenos Aires, pp. 132–141.
Jordan, T.E., Reynolds III, J.H., Erickson, J.P., 1997. In: Ruddiman, W.F. (Ed.), Variability in Age of Initial Shortening and Uplift in Central Andes, 16-33°30′S. in Tectonic uplift and Climate Change, Part II. Springer, US:pp. 41–61 http://dx.doi.org/10.1007/978-1-4615-5935-1_3.
Jung, H., 2009. Deformation fabrics of olivine in Val Malenco peridotite found in Italy and implications for the seismic anisotropy in the upper mantle. Lithos 109 (3). http://dx.doi.org/10.1016/j.lithos.2008.06.007.
Jung, H., Karato, S., 2001. Water-induced fabric transitions in olivine. Science 293 (5534): 1460–1463. http://dx.doi.org/10.1126/science.1062235.
Jung, H., Katayama, I., Jiang, Z., Hiraga, T., Karato, S., 2006. Effect of water and stress on the lattice preferred orientation (LPO) of olivine. Tectonophysics 421 (1):1–22. http://dx.doi.org/10.1016/j.tecto.2006.02.011.
Kanjorski, N.M., 2003. Cocos Plate structure along the Middle America Subduction Zone off Oaxaca and Guerrero, Mexico: Influence of Subducting Plate Morphology on Tectonics and Seismicity. (PhD Thesis). University of California, San Diego.
Karato, S., Jung, H., Katayama, I., Skemer, P., 2008. Geodynamic significance of seismic anisotropy of the upper mantle: new insights from laboratory studies. Annu. Rev. Earth Planet. Sci. 36 (1):59–95. http://dx.doi.org/10.1146/annurev.earth.36.031207.124120.
Katayama, I., Karato, S., 2006. Effect of temperature on the B- to C-type olivine fabric transition and implication for flow pattern in subduction zones. Phys. Earth Planet. Inter. 157, 33–45.
Kay, S.M., Gordillo, C.E., 1994. Pocho volcanic rocks and the melting of depleted continental lithosphere above a shallowly dipping subduction zone in the Central Andes. Contrib. Mineral. Petrol. 117, 25–44.
Kay, S.M., Abbruzzi, J.M., 1996. Magmatic evidence for Neogene lithospheric evolution of the central Andean "flat-slab" between 30°S and 32°S. Tectonophysics 259, 15–28.
Kay, S.M., Mpodozis, C., 2002. Magmatism as a probe to the Neogene shallowing of the Nazca plate beneath the modern Chilean flat-slab. J. S. Am. Earth Sci. 15, 39–57.
Kay, S.M., Maksaev, V., Moscoso, R., Mpodozis, C., Nasi, C., Gordillo, C.E., 1988. Tertiary Andean magmatism in Chile and Argentina between 28°S and 33°S: Correlation of magmatic chemistry with a changing Benioff zone. J. S. Am. Earth Sci. 1, 21–38.
Kay, S.M., Mpodozis, C., Ramos, V.A., Munizaga, F., 1991. Magma source variations for mid to late Tertiary volcanic rocks erupted over a shallowing subduction zone and through a thickening crust in the Main Andean Cordillera (28–33°S). In: Harmon, R.S., Rapela, C. (Eds.), Andean Magmatism and its Tectonic Setting. Geological Society of America, Special Paper 265, pp. 113–137.
Kim, Y., Clayton, R.W., Jackson, J.M., 2010. Geometry and seismic properties of the subducting Cocos plate in central Mexico. J. Geophys. Res. 115, B06310. http://dx.doi.org/10.1029/2009JB006942.
Kim, Y., Clayton, R.W., Keppie, F., 2011. Evidence of a collision between the Yucatán block and Mexico in the Miocene. Geophys. J. Int. 187:989–1000. http://dx.doi.org/10.1111/j.1365-246X.2011.05191.x.
Kim, Y., Clayton, R.W., Jackson, J.M., 2012a. Distribution of hydrous minerals in the subduction system beneath Mexico. Earth Planet. Sci. Lett. 341-344, 58–67.
Kim, Y., Miller, M.S., Pearce, F., Clayton, R.W., 2012b. Seismic imaging of the Cocos plate subduction zone system in central Mexico. Geochem. Geophys. Geosyst. 13, Q07001. http://dx.doi.org/10.1029/2012GC004033.
Kim, Y., Clayton, R.W., Asimow, P.D., Jackson, J.M., 2013. Generation of talc in the mantle wedge and its role in subduction dynamics in central Mexico. Earth Planet. Sci. Lett. 384:81–87. http://dx.doi.org/10.1016/j.epsl.2013.10.006.
Kneller, E.A., van Keken, P.E., Karato, S.-i., Park, J., 2005. B-type olivine fabric in the mantle wedge: insights from high-resolution non-Newtonian subduction zone models. Earth Planet. Sci. Lett. 237:781–797. http://dx.doi.org/10.1016/j.epsl.2005.06.049.
Kneller, E.A., van Keken, P.E., Katayama, I., Karato, S., 2007. Stress, strain, and B-type olivine fabric in the fore-arc mantle: sensitivity tests using high-resolution steady-state subduction zone models. J. Geophys. Res. 112, B04406. http://dx.doi.org/10.1029/2006JB004544.

Kopp, H., Flueh, E.R., Papenberg, C., Klaeschen, D., 2004. Seismic investigations of the O'Higgins Seamount Group and Juan Fernandez Ridge: aseismic ridge emplacement and lithosphere hydration. Tectonics 23.
Kostoglodov, V., Singh, S.K., Santiago, J.A., Franco, S.I., Larson, K.M., Lowry, A.R., Bilham, R., 2003. A large silent earthquake in the Guerrero seismic gap, Mexico. Geophys. Res. Lett. 30 (15):1807. http://dx.doi.org/10.1029/2003GL017219.
Kostoglodov, V., Husker, A., Shapiro, N.M., Payero, J.S., Campillo, M., Cotte, N., Clayton, R., 2010. The 2006 slow slip event and nonvolcanic tremor in the Mexican subduction zone. Geophys. Res. Lett. 37, L24301. http://dx.doi.org/10.1029/2010GL045424.
Kusky, T.M., Windley, B.F., Wang, L., Wang, Z., Li, X., Zhu, P., 2014. Flat slab subduction, trench suction, and craton destruction: comparison of the North China, Wyoming, and Brazilian cratons. Tectonophysics 630, 208–221.
Lenardic, A., Guillou-Frottier, L., Mareschal, J.-C., Jaupart, C., Moresi, L.-N., Kaula, W.M., 2000. In: Richards, M.A., Gordon, R.G., van der Hilst, R.D. (Eds.), What the Mantle Sees: The Effect of Continents on Mantle Heat FlowThe History and Dynamics of Global Plate Motions, Geophysical Monograph vol. 121. American Geophysical Union, Washington, DC, pp. 95–112.
León Soto, G., Valenzuela, R.W., 2013. Corner flow in the Isthmus of Tehuantepec, Mexico inferred from anisotropy measurements using local intraslab earthquakes. Geophys. J. Int. 195:1230–1238. http://dx.doi.org/10.1093/gji/ggt291.
León Soto, G., Valenzuela, R.W., 2016. Teleseismic measurements of upper mantle shear wave anisotropy in the Isthmus of Tehuantepec, Mexico. Geophys. J. Int. (in preparation).
León Soto, G., Ni, J.F., Grand, S.P., Sandvol, E., Valenzuela, R.W., Guzmán Speziale, M., Gómez González, J.M., Dominguez Reyes, T., 2009. Mantle flow in the Rivera-Cocos subduction zone. Geophys. J. Int. 179 (2):1004–1012. http://dx.doi.org/10.1111/j.1365-246X.2009.04352.x.
Linkimer, L., Beck, S.L., Zandt, G., Alvarado, P.M., Anderson, M.L., Gilbert, H.J., Olsen, K., 2011. In: Linkimer, L. (Ed.), Appendix C: Geometry of the Wadati-Benioff Zone and Deformation of the Subducting Nazca Plate in the Pampean Flat Slab of West- Central Argentina in Lithospheric Structure of Pampean Flat Slab (Latitude 30–33°S) and Northern Costa Rica (Latitude 9–11°N) Subduction Zones. University of Arizona, Tucson (PhD Dissertation). (241 pp).
Litvak, V., Poma, E., Kay, S.M., 2007. Paleogene and Neogene magmatism in the Valle del Cura region: new perspective on the evolution of the Pampean flat slab, San Juan province, Argentina. J. S. Am. Earth Sci. 24, 117–137.
Long, M.D., 2013. Constraints on subduction geodynamics from seismic anisotropy. Rev. Geophys. 51, 76–112.
Long, M.D., Becker, T.W., 2010. Mantle dynamics and seismic anisotropy. Earth Planet. Sci. Lett. Front. 297, 341–354.
Long, M.D., Silver, P.G., 2008. The subduction zone flow field from seismic anisotropy: a global view. Science 319, 315–318.
Long, M.D., Silver, P.G., 2009. Mantle flow in subduction systems: the subslab flow field and implications for mantle dynamics. J. Geophys. Res. 114, B10312. http://dx.doi.org/10.1029/2008JB006200.
Long, M.D., van der Hilst, R.D., 2005. Upper mantle anisotropy beneath Japan from shear wave splitting. Phys. Earth Planet. Inter. 151, 206–222.
Long, M.D., Wirth, E.A., 2013. Mantle flow in subduction systems: the wedge flow field and implications for wedge processes. J. Geophys. Res. 118:583–606. http://dx.doi.org/10.1002/jgrb.50063.
Lonsdale, P., 2005. Creation of the Cocos and Nazca plates by fission of the Farallon plate. Tectonophysics 404, 237–264.
Lowrie, A., Hey, R., 1981. Geological and geophysical variations along the western margin of Chile near latitude 33°S and their relation to Nazca plate subduction. Mem. Geol. Soc. Am. 54, 741–754.
Lynner, C., Long, M.D., 2013. Sub-slab seismic anisotropy and mantle flow beneath the Caribbean and Scotia subduction zones: effects of slab morphology and kinematics. Earth Planet. Sci. Lett. 361:367–378. http://dx.doi.org/10.1016/j.epsl.2012.11.007.
Lynner, C., Long, M.D., 2014a. Sub-slab anisotropy beneath the Sumatra and circum-Pacific subduction zones from source-side shear wave splitting observations. Geochem. Geophys. Geosyst. 15:2262–2281. http://dx.doi.org/10.1002/2014GC005239.
Lynner, C., Long, M.D., 2014b. Testing models of sub-slab anisotropy using a global compilation of source-side shear wave splitting data. J. Geophys. Res. Solid Earth 119: 7226–7244. http://dx.doi.org/10.1002/2014JB010983.
Ma, Y., Clayton, R.W., 2014. The crust and uppermost mantle structure of Southern Peru from ambient noise and earthquake surface wave analysis. Earth Planet. Sci. Lett. 395, 61–70.
MacDougall, J.G., Fischer, K.M., Anderson, M.L., 2012. Seismic anisotropy above and below the subducting Nazca lithosphere in southern South America. J. Geophys. Res. 117, B12306. http://dx.doi.org/10.1029/2012JB009538.
Mamani, M., Wörner, G., Sempere, T., 2010. Geochemical variations in igneous rocks of the Central Andean orocline (13°S to 18°S): Tracing crustal thickening and magma generation through time and space. Geol. Soc. Am. Bull. 122, 162–182.
Manea, V.C., Gurnis, M., 2007. Subduction zone evolution and low viscosity wedges and channels. Earth Planet. Sci. Lett. 264 (1–2), 22–45.
Manea, M., Manea, V.C., 2011a. Curie point depth estimates and correlation with subduction in Mexico. Pure Appl. Geophys. http://dx.doi.org/10.1007/s00024-010-0238-2.
Manea, V.C., Manea, M., 2011b. Flat-slab thermal structure and evolution beneath Central Mexico. Pure Appl. Geophys. http://dx.doi.org/10.1007/s00024-010-0207-9.
Manea, M., Manea, V.C., Kostoglodov, V., 2003. Sediment fill of the Middle America Trench inferred from the gravity anomalies. Geofis. Int. 42 (4), 603–612.
Manea, V.C., Manea, M., Kostoglodov, V., Currie, C.A., Sewell, G., 2004. Thermal structure, coupling and metamorphism in the Mexican subduction zone beneath Guerrero. Geophys. J. Int. 158 (2):775–784. http://dx.doi.org/10.1111/j.1365-246X.2004.02325.x.
Manea, V.C., Manea, M., Kostoglodov, V., Sewell, G., 2005. Thermo-mechanical model of the mantle wedge in Central Mexican subduction zone and a blob tracing approach for the magma transport. Phys. Earth Planet. Inter. 149:165–186. http://dx.doi.org/10.1016/JPEPI2004.08.024.
Manea, V.C., Perez-Gussinye, M., Manea, M., 2012. Chilean flat slab subduction controlled by overriding plate thickness and trench rollback. Geology 40 (1):35–38. http://dx.doi.org/10.1130/G32543.1.
Manea, V.C., Manea, M., Ferrari, L., 2013. Review article: a geodynamical perspective on the subduction of Cocos and Rivera plates beneath Mexico and Central America. Tectonophysics http://dx.doi.org/10.1016/j.tecto.2012.12.039.
Marot, M., Monfret, T., Pardo, M., Ranalli, G., Nolet, G., 2013. A double seismic zone in the subducting Juan Fernandez Ridge of the Nazca Plate (32°S), central Chile. J. Geophys. Res. Solid Earth 118 (7):3462–3475. http://dx.doi.org/10.1002/jgrb.50240.
Marot, M., Monfret, T., Gerbault, M., Nolet, G., Ranalli, G., Pardo, M., 2014. Flat versus normal subduction zones: a comparison based on 3-D regional traveltime tomography and petrological modeling of central Chile and western Argentina (29°–35°S). Geophys. J. Int. 199 (3), 1633–1654.
Martinod, J., Funiciello, F., Faccenna, C., Labanieh, S., Regard, V., 2005. Dynamical effects of subducting ridges: insights from 3-D laboratory models. Geophys. J. Int. 163, 1137–1150.
Matsubara, M., Obara, K., Kasahara, K., 2008. Three-dimensional P-and S-wave velocity structures beneath the Japan Islands obtained by high-density seismic stations by seismic tomography. Tectonophysics 454 (1), 86–103.
McCrory, P.A., Blair, J.L., Waldhauser, F., Oppenheimer, D.H., 2012. Juan de Fuca slab geometry and its relation to Wadati-Benioff zone seismicity. J. Geophys. Res. Solid Earth 117 (B9).
Mégard, F., 1987. Cordilleran Andes and Marginal Andes: a review of Andean geology, north of the Arica elbow (18°S). In: Monger, J.W.H., Francheteau, J. (Eds.), Circum-Pacific Orogenic Belts and Evolution of the Pacific Ocean Basin. American Geophysical Union, Geodynamics Series 18, pp. 71–95.
Melgar, D., Pérez-Campos, X., 2011. Imaging the Moho and subducted oceanic crust at the Isthmus of Tehuantepec, Mexico, from receiver functions. Pure Appl. Geophys. 168: 1449–1460. http://dx.doi.org/10.1007/s00024-010-0199-5.
Mercier de Lepinay, B., Michaud, F., Calmus, T., Bourgois, J., Poupeau, G., Saint-Marc, P., The Nautimate Team, 1997. Large Neogene sub- sidence event along the Middle America Trench off Mexico (18°–19°N): Evidence from submersible observations. Geology 25, 387–390.
Molnar, P., England, P., 1990. Late Cenozoic uplift of mountain ranges and global climate change: chicken or egg? Nature 346 (6279), 29–34.
Molnar, P., Sykes, L.R., 1969. Tectonics of the Caribbean and Middle America regions from focal mechanisms and seismicity. Geol. Soc. Am. Bull. 80 (1639-1384).
Mori, L., Gómez-Tuena, A., Cai, Y., Goldstein, S.L., 2007. Effects of prolonged flat subduction on the Miocene magmatic record of the central Trans-Mexican Volcanic Belt. Chem. Geol. 244 (3–4), 452–473.
Muñoz, M., 2005. No flat Wadati-Benioff zone in the central and southern central Andes. Tectonophysics 395, 41–65.
Nakajima, J., Hasegawa, A., 2004. Shear-wave polarization anisotropy and subduction-induced flow in the mantle wedge of northeastern Japan. Earth Planet. Sci. Lett. 225 (3–4), 365–377.
Norabuena, E.O., Snoke, J.A., James, D.E., 1994. Structure of the subducting Nazca plate beneath Peru. J. Geophys. Res. 99, 9215–9226.
Norabuena, E.O., Dixon, T.H., Stein, S., Harrison, C.G.A., 1999. Decelerating Nazca-South America and Nazca-Pacific Plate motions. Geophys. Res. Lett. 26, 3405–3408.
Obara, K., 2010. Phenomenology of deep slow earthquake family in southwest Japan: spatiotemporal characteristics and segmentation. J. Geophys. Res. 115 (B00A25). http://dx.doi.org/10.1029/2008JB006048.
Obara, K., 2011. Characteristics and interactions between non-volcanic tremor and related slow earthquakes in the Nankai subduction zone, southwest Japan. J. Geodyn. 52: 229–248. http://dx.doi.org/10.1016/j.jog.2011.04.002.
Obara, K., Tanaka, S., Maeda, T., Matsuzawa, T., 2010. Depth dependent activity of non-volcanic tremor in southwest Japan. Geophys. Res. Lett. 37, L13306. http://dx.doi.org/10.1029/2010GL043679.
Obrebski, M., Castro, R.R., Valenzuela, R.W., Van Benthem, S., Rebollar, C.J., 2006. Shear–wave splitting observations at the regions of northern Baja California and southern Basin and Range in Mexico. Geophys. Res. Lett. 33, L05302. http://dx.doi.org/10.1029/2005GL024720.
O'Neill, C., Müller, D., Steinberger, B., 2005. On the uncertainties in hot spot reconstructions and the significance of moving hot spot reference frames. Geochem. Geophys. Geosyst. 6, Q04003. http://dx.doi.org/10.1029/2004GC000784.
Orozco, L.A., Favetto, A., Pomposiello, C., Rossello, E., Booker, J., 2013. Crustal deformation of the Andean foreland at 31°30′S (Argentina) constrained by magnetotelluric survey. Tectonophysics 582, 126–139.
Oxburgh, E.R., Turcotte, D.L., 1970. Thermal structure of island arcs. Bull. Geol. Soc. Am. 81 (6), 1665–1688.
Pacheco, J.F., Singh, S.K., 2010. Seismicity and state of stress in Guerrero segment of the Mexican subduction zone. J. Geophys. Res. 115, B01303. http://dx.doi.org/10.1029/2009JB006453.
Pardo, M., Suárez, G., 1995. Shape of the subducted Rivera and Cocos plates in southern Mexico: seismic and tectonic implications. J. Geophys. Res. 100 (B7), 12,357–12,373.
Pardo, M., Comte, D., Monfret, T., 2002. Seismotectonic and stress distribution in the central Chile. J. S. Am. Earth Sci. 15 (1), 11–22.
Park, J., Levin, V., 2002. Seismic anisotropy: tracing plate dynamics in the mantle. Science 296, 485–489.
Peacock, S.M., 1996. Thermal and petrologic structure of subduction zones. In: Bebout, G.E., et al. (Eds.), Subduction: Top to Bottom. AGU Geophysical Monograph 96, pp. 119–133 (Washington, D.C.).
Peacock, S.M., 2003. Thermal Structure and Metamorphic Evolution of Subducting Slabs. Geophysical Monograph 138. American Geophysical Union, pp. 7–22.

Pennington, W.D., 1981. Subduction of the eastern Panama basin and seismotectonics of northwestern South America. J. Geophys. Res. 86, 10,753–10,770.

Perarnau, M., Gilbert, H., Alvarado, P., Martino, R., Anderson, M., 2012. Crustal structure of the Eastern Sierras Pampeanas of Argentina using high frequency local receiver functions. Tectonophysics 580, 208–217.

Pérez-Campos, X., Kim, Y., Husker, A., Davis, P.M., Clayton, R.W., Iglesias, A., Pacheco, J.F., Singh, S.K., Manea, V.C., Gurnis, M., 2008. Horizontal subduction and truncation of the Cocos Plate beneath central Mexico. Geophys. Res. Lett. 35, L18303. http://dx.doi.org/10.1029/2008GL035127.

Petford, N., Atherton, M.P., 1996. Na-rich partial melts from newly underplated basaltic crust: the Cordillera Blanca batholith, Peru. J. Petrol. 37, 1491–1521.

Phillips, K., Clayton, R.W., 2014. Structure of the subduction transition region from seismic array data in southern Peru. Geophys. J. Int. 196, 1889–1905.

Phillips, K., Clayton, R.W., Davis, P., Tavera, H., Guy, R., Skinner, S., Stubailo, I., Audin, L., Aguilar, V., 2012. Structure of the subduction system in southern Peru from seismic array data. J. Geophys. Res. 117, B11306. http://dx.doi.org/10.1029/2012JB009540.

Pilger Jr., R.H., 1981. Plate reconstructions, aseismic ridges, and low-angle subduction beneath the Andes. Bull. Geol. Soc. Am. 92 (7), 448–456.

Pilger Jr., R.H., 1984. Cenozoic plate kinematics, subduction and magmatism: South American Andes. J. Geol. Soc. Lond. 141, 793–802.

Pollack, H.N., 1980. The heat flow from the Earth: a review. Mechanisms of Continental Drift and Plate Tectonics. Academic Press, London, pp. 183–192.

Ponce-Cortés, J.G., 2012. Medición de la anisotropía de las ondas SKS en el manto superior, debajo de las estaciones permanentes del Servicio Sismológico Nacional instaladas a partir del año 2005. (B. Sc. thesis, 79 pp.). Facultad de Ingeniería, Universidad Nacional Autónoma de México, Mexico City, Mexico.

Porter, R., Gilbert, H., Zandt, G., Beck, S., Warren, L., Calkins, J., Alvarado, P., Anderson, M., 2012. Shear wave velocities in the Pampean flat-slab region from Rayleigh wave tomography: implications for slab and upper mantle hydration. J. Geophys. Res. 117, B11301. http://dx.doi.org/10.1029/2012JB009350.

Radiguet, M., Cotton, F., Vergnolle, M., Campillo, M., Walpersdorf, A., Cotte, N., Kostoglodov, V., 2012. Slow slip events and strain accumulation in the Guerrero gap, Mexico. J. Geophys. Res. 117 (B4), B04305. http://dx.doi.org/10.1029/2011JB008801.

Ramos, V.A., 1999. Plate tectonic setting of the Andean Cordillera. Episodes 22, 183–190.

Ramos, V.A., Folguera, A., 2009. Andean flat-slab subduction through time. In: Murphy, J.B., Keppie, J.D., Hynes, A.J. (Eds.), Ancient Orogens and Modern Analogues. Geological Society, London, Special Publications 327, pp. 31–54 (doi:10.1144/SP327.3).

Ramos, V.A., Munizaga, F., Kay, S.M., 1991. El magmatismo cenozoico a los 33°S de latitud: Geocronología y relaciones tectónicas. VI Congreso Geológico Chileno: Actas 1 pp. 892–896.

Ramos, V.A., Cristallini, E.O., Pérez, D.J., 2002. The Pampean flat slab of the Central Andes. J. S. Am. Earth Sci. 15, 59–78.

Ranero, C.R., Phipps, M.J., McIntosh, K., Reichert, C., 2003. Bending-related faulting and mantle serpentinization at the Middle America trench. Nature 425:367–373. http://dx.doi.org/10.1038/nature01961.

Ratchkovski, N.A., Hansen, R.A., 2002. New evidence for segmentation of the Alaska subduction zone. Bull. Seismol. Soc. Am. 92 (5), 1754–1765.

Ratschbacher, L., Franz, L., Min, M., Bachmenn, R., Martens, U., Stanek, K., Stubner, K., Nelson, B.K., Herrmann, U., Weber, B., López-Martínez, M., Jonckheere, R., Sperner, B., Tichomirowa, M., McWilliams, M.O., Gordon, M., Meschede, M., Bock, P., 2009. In: James, K.H., Lorente, M.A., Pindell, J.L. (Eds.), The North American–Caribbean plate boundary in México–Guatemala–HondurasThe Origin and Evolution of the Caribbean Plate 328. Geological Society of London, pp. 219–293 (Special Publications).

Regnier, M., Chiu, J.M., Smalley Jr., R., Isacks, B.L., Araujo, M., 1994. Crustal thickness variation in the Andean foreland, Argentina, from converted waves. Bull. Seismol. Soc. Am. 84 (4), 1097–1111.

Rodriguez-Gonzales, J., Negredo, A.M., Billen, B.I., 2012. The role of the overriding plate thermal state on slab dip variability and on the occurrence of flat subduction. Geochem. Geophys. Geosyst. 13, Q01002. http://dx.doi.org/10.1029/2011GC003859.

Rodríguez-Pérez, Q., 2007. Estructura tridimensional de velocidades para el sureste de México, mediante el análisis de trazado de rayos sísmicos de sismos regionales. (M. Sc. thesis, 83 pp.). Instituto de Geofísica, Universidad Nacional Autónoma de México, Mexico City, Mexico.

Rojo-Garibaldi, B., 2011. Anisotropía de las ondas *SKS* en el manto superior debajo de un arreglo sísmico entre Guerrero y Veracruz. (B. Sc. thesis, 84 pp.). Facultad de Ciencias, Universidad Nacional Autónoma de México, Mexico City, Mexico.

Rojo-Garibaldi, B., Ponce Cortés, G., Valenzuela Wong, R., Stubailo, I., Davis, P.M., Husker, A., Pérez Campos, X., Iglesias, A., Clayton, R.W., 2011. Anisotropía de la onda *SKS* en el manto superior debajo del arreglo MASE y las nuevas estaciones del Servicio Sismológico Nacional (abstract). Geos Bol. Inf. Unión Geofís. Mex. 31 (1), 116.

Roy, R.F., Decker, E.R., Blackwell, D.D., 1972. Continental heat flow. In: Robertson, E.C. (Ed.), The nature of the solid Earth. McGraw-Hill, New York, pp. 506–543.

Rüpke, L.H., Morgan, J.P., Hort, M., Connolly, J.A.D., 2004. Serpentine and the subduction zone water cycle. Earth Planet. Sci. Lett. 223, 17–34.

Russo, R., Silver, P.G., 1994. Trench-parallel flow beneath the Nazca Plate from seismic anisotropy. Science 263:1105–1111. http://dx.doi.org/10.1126/science.263.5150.1105.

Savage, M.K., 1999. Seismic anisotropy and mantle deformation: what have we learned from shear wave splitting? Rev. Geophys. 37, 65–106.

Schellart, W.,.P., Freeman, J., Stegman, D.R., Moresi, L., May, D., 2007. Evolution and diversity of subduction zones controlled by slab width. Nature 446, 308–311.

Schellart, W.P., Stegman, D.R., Freeman, J., 2008. Global trench migration velocities and slab migration induced upper mantle volume fluxes: constraints to an Earth reference frame based on minimizing viscous dissipation. Earth Sci. Rev. 88:118–144. http://dx.doi.org/10.1016/j.earscirev.2008.01.005.

Schellart, W.P., Stegman, D.R., Farrington, R.J., Moresi, L., 2011. Influence of lateral slab edge distance on plate velocity, trench velocity, and subduction partitioning. J. Geophys. Res. Solid Earth 116.

Sdrolias, M., Muller, R.D., 2006. Controls on back-arc basin formation. Geochem. Geophys. Geosyst. 7 (4), Q04016. http://dx.doi.org/10.1029/2005GC001090.

Sebrier, M., Soler, P., 1991. Tectonics and magmatism in the Peruvian Andes from upper Oligocene to present. In: Harmon, R., Rapela, C. (Eds.), Geological Society of America, Special Paper 265 Andean Magmatism and Its Tectonic Setting, pp. 259–278.

Sedlock, R., Ortega-Gutiérrez, F., Speed, R., 1993. Tectonostratigraphic terranes and the tectonic evolution of Mexico. Geological Society of America Special Paper 278, p. 153.

Shapiro, N.M., Ritzwoller, M.H., 2004. Thermodynamic constraints on seismic inversions. Geophys. J. Int. 157. http://dx.doi.org/10.1111/j.1365-246X.2004.02254.x.

Shelly, D.R., Beroza, G.C., Ide, S., 2007. Non-volcanic tremor and low-frequency earthquake swarms. Nature 446 (7133):305–307. http://dx.doi.org/10.1038/nature05666.

Silver, P.G., 1996. Seismic anisotropy beneath the continents: probing the depths of geology. Annu. Rev. Earth Planet. Sci. 24, 385–432.

Silver, P.G., Chan, W.W., 1988. Implications for continental structure and evolution from seismic anisotropy. Nature 335, 34–39.

Silver, P.G., Chan, W.W., 1991. Shear wave splitting and subcontinental mantle deformation. J. Geophys. Res. 96, 16,429–16,454.

Singh, S.K., Pérez-Campos, X., Espíndola, V.H., Cruz-Atienza, V.M., Iglesias, A., 2014. Intraslab earthquake of 16 June 2013 (M_w 5.9), one of the closest such events to Mexico City. Seismol. Res. Lett. 85:268–277. http://dx.doi.org/10.1785/0220130179.

Skinner, S.M., Clayton, R.W., 2013. The lack of correlation between flat slabs and bathymetric impactors in South America. Earth Planet. Sci. Lett. 371, 1–5.

Smithson, S.B., Brown, S.K., 1977. A model for the lower continental crust. Earth Planet. Sci. Lett. 35, 134–144.

Smithson, S.B., Decker, E.R., 1974. A continental crustal model and its geothermal implications. Earth Planet. Sci. Lett. 22, 215–225.

Song, T.-R.A., Kawakatsu, H., 2012. Subduction of oceanic asthenosphere: evidence from sub-slab seismic anisotropy. Geophys. Res. Lett. 39, L17301. http://dx.doi.org/10.1029/2012GL052639.

Song, T.-R.A., Kim, Y., 2012a. Anisotropic uppermost mantle in young subducted slab underplating central Mexico. Nat. Geosci. 5:55–59. http://dx.doi.org/10.1038/ngeo1342.

Song, T.-R.A., Kim, Y., 2012b. Localized seismic anisotropy associated with long-term slow-slip events beneath southern Mexico. Geophys. Res. Lett. 39, L09308. http://dx.doi.org/10.1029/2012GL051324.

Song, T.A., Helmberger, D.V., Brudzinski, M.R., Clayton, R.W., Davis, P., Pérez-Campos, X., Singh, S.K., 2009. Subducting slab ultra-slow velocity layer coincident with silent earthquakes in Southern Mexico. Science 324:502–506. http://dx.doi.org/10.1126/science.1167595.

Soyer, W., Unsworth, M., 2006. Deep electrical structure of the northern Cascadia (British Columbian, Canada) subduction zone: implications for the distribution of fluids. Geology 34 (1), 53–56.

Stern, C.R., 1991. Role of subduction in the generation of Andean magmas. Geology 19, 78–81.

Stern, C.R., 2011. Subduction erosion: rates, mechanisms, and its role in arc magmatism and the evolution of the continental crust and mantle. Gondwana Res. 20, 284–308.

Stoiber, R.E., Carr, M.J., 1973. Quaternary volcanic and tectonic segmentation of Central America. Bull. Volcanol. 37-3, 304–325.

Stubailo, I., 2015. Seismic anisotropy below Mexico and its implications for mantle dynamics. (Ph.D. thesis, 119 pp.). University of California, Los Angeles, CA, USA.

Stubailo, I., Davis, P., 2007. Shear wave splitting measurements and interpretation beneath Acapulco-Tampico transect in Mexico. EOS Trans. Am. Geophys. Union 88 (52) (Fall Meeting Supplement Abstract T51B-0539).

Stubailo, I., Davis, P.M., 2012a. Anisotropy of the Mexico subduction zone based on shear-wave splitting analysis (abstract). Seismol. Res. Lett. 83 (2), 379.

Stubailo, I., Davis, P.M., 2012b. Anisotropy of the Mexico Subduction Zone Based on Shear-wave Splitting and Higher Modes Analysis, Abstract T11A-2538 Presented at 2012 Fall Meeting, American Geophysical Union, San Francisco, CA, 3–7 December.

Stubailo, I., Davis, P., 2014. Seismic Anisotropy of the Mexican Subduction Zone Based on the Surface Waves, Shear Wave Splitting, and Higher Modes, Abstract DI33A-4302 Presented at 2014 Fall Meeting, American Geophysical Union, San Francisco, CA, 15–19 December.

Stubailo, I., Davis, P.M., 2015. The surface wave, shear wave splitting, and higher mode seismic anisotropy comparison of the Mexican subduction zone (abstract). Seismol. Res. Lett. 86 (2B), 677.

Suárez, G., Molnar, P., Burchfiel, B.C., 1983. Seismicity, fault plane solutions, depth of faulting, and active tectonics of the Andes of Peru, Ecuador and southern Colombia. J. Geophys. Res. 88, 10403–10428.

Suárez, G., Gagnepain, J., Cisternas, A., Hatzfeld, D., Molnar, P., Ocola, L., Roecker, S.W., Viodé, J.P., 1990. Tectonic deformation of the Andes and the configuration of the subducted slab in central Peru: results from a microseismic experiment. Geophys. J. Int. 103, 1–12.

Tan, E., Choi, E., Thoutireddy, P., Gurnis, M., Aivazis, M., 2006. GeoFramework: coupling multiple models of mantle convection within a computational framework. Geochem. Geophys. Geosyst. 7. http://dx.doi.org/10.1029/2005GC001155 Q06001 (14 pp).

Taramon, J.M., Rodriguez-Gonzalez, J., Negredo, A.M., Billen, M.I., 2015. Influence of cratonic lithosphere on the formation and evolution of flat slabs: insights from 3-D time dependend modeling. Geochem. Geophys. Geosyst. 16. http://dx.doi.org/10.1002/2015GC005940.

Tavera, H., Buforn, E., 2001. Source mechanism of earthquakes in Peru. J. Seismol. 5, 519–539.

Thomas, W.A., Astini, R.A., 2003. Ordovician accretion of the Argentine Precordillera terrane to Gondwana: a review. J. S. Am. Earth Sci. 16:67–79. http://dx.doi.org/10.1016/S0895-9811(03)00019-1.

Toksöz, M., Nafi, J., Minear, W., Julian, B.R., 1971. Temperature field and geophysical effects of a downgoing slab. J. Geophys. Res. 76, 1113–1138.
Tommasi, A., Vauchez, A., Godard, M., Belley, F., 2006. Deformation and melt transport in a highly depleted peridotite massif from the Canadian Cordillera: Implications to seismic anisotropy above subduction zones. Earth Planet. Sci. Lett. 252, 245–259.
Turcotte, D.L., Schubert, G., 1973. Frictional heating of the descending lithosphere. J. Geophys. Res. 78 (26), 5876–5886.
Turcotte, D.L., Schubert, G., 2014. Geodynamics. Cambridge University Press.
Unsworth, M., Rondenay, S., 2013. Actively observing fluid movement in the mid to deep crust and lithospheric mantle utilizing geophysical methods, solicited chapter. In: Harlov, D., Austrheim, H. (Eds.), Metasomatism and Metamorphism: The Role of Fluids in Crustal and Upper Mantle Processes. Lecture Notes in Earth System Sciences. Springer, pp. 535–598 (ISSN: 2193-8571).
Uyeda, S., Kanamori, H., 1979. Back-arc opening and the mode of subduction. J. Geophys. Res. 84 (B3), 1049–1061.
van Benthem, S.A.C., 2005. Anisotropy and Flow in the Uppermantle Under Mexico. (M. Sc. thesis, 41 pp.). Utrecht University, Utrecht, The Netherlands.
van Benthem, S.A.C., Valenzuela, R.W., Obrebski, M., Castro, R.R., 2008. Measurements of upper mantle shear wave anisotropy from stations around the southern Gulf of California. Geofis. Int. 47 (2008), 127–143.
van Benthem, S.A.C., Valenzuela, R.W., Ponce, G.J., 2013. Measurements of upper mantle shear wave anisotropy from a permanent network in southern Mexico. Geofis. Int. 52, 385–402.
van den Beukel, J., Wortel, R., 1988. Thermo-Mechanical modelling of arc-trench regions. Tectonophysics 154, 177–193.
van Hunen, J., van den Berg, A.P., Vlaar, N.J., 2000. A thermomechanical model of horizontal subduction below an overriding plate. Earth Planet. Sci. Lett. 182, 157–169.
van Hunen, J., van den Berg, A.P., Vlaar, N.J., 2002. On the role of subducting oceanic plateaus in the development of shallow flat subduction. Tectonophysics 352, 317–333.
van Hunen, J., van den Berg, A.P., Vlaar, N.J., 2004. Various mechanisms to induce present-day shallow flat subduction and implications for the younger Earth: a numerical parameter study. Earth Planet. Sci. Lett. 146, 179–194.
Vannucchi, P., Sak, P.B., Morgan, J.P., Ohkushi, K., Ujiie, K., the IODP Expedition Shipboard Scientists, 2013. Rapid pulses of uplift, subsidence, and subduction erosion offshore Central America: implications for building the rock record of convergent margins. Geology 41 (9), 995–998.
Vauchez, A., Tommasi, A., Barruol, G., Maumus, J., 2000. Upper mantle deformation and seismic anisotropy in continental rifts. Phys. Chem. Earth Solid Earth Geod. 25 (2), 111–117.
Vinnik, L.P., Kind, R., 1993. Ellipticity of teleseismic *S*-particle motion. Geophys. J. Int. 113, 165–174.
Vitorello, I., Hamza, V.M., Pollack, H.N., 1980. Terrestrial heat flow in the Brazilian highlands. J. Geophys. Res. 85, 3778–3788.
Wagner, L.S., Beck, S., Zandt, G., 2005. Uppermantle structure in the south central Chilean subduction zone (30° to 36°S). J. Geophys. Res. 110. http://dx.doi.org/10.1029/2004JB003238.
Wagner, L.S., Beck, S.L., Zandt, G., Ducea, M., 2006. Depleted lithosphere, cold, trapped asthenosphere, and frozen melt puddles above the flat slab in central Chile and Argentina. Earth Planet. Sci. Lett. 245, 289–301.
Wagner, L.S., Anderson, M., Jackson, J.M., Beck, S.L., Zandt, G., 2008. Seismic evidence for orthopyroxene enrichment in the continental lithosphere. Geology 36, 935–938.
Wallace, P., Carmichael, I., 1999. Quaternary volcanism near the Valley of Mexico: implications for subduction zone magmatism and the effects of crustal thickness variations on primitive magma compositions. Contrib. Mineral. Petrol. 135:291–314. http://dx.doi.org/10.1007/s004100050513.
Ward, K.M., Porter, R.C., Zandt, G., Beck, S.L., Wagner, L.S., Minaya, E., Tavera, H., 2013. Ambient noise tomography across the Central Andes. Geophys. J. Int. http://dx.doi.org/10.1093/gji/ggt166.
Wech, A.G., Bartlow, N.M., 2014. Slip rate and tremor genesis in Cascadia. Geophys. Res. Lett. 41 (2):392–398. http://dx.doi.org/10.1002/2013GL058607.
Wech, A.G., Creager, K.C., Melbourne, T.I., 2009. Seismic and geo- detic constraints on Cascadia slow slip. J. Geophys. Res. 114, B10316. http://dx.doi.org/10.1029/2008JB006090.
Wortel, R., Cloetingh, S., 1981. On the origin of the Cocos-Nazca spreading center. Geology 9, 425–430.
Wright, N.M., Seton, M., Williams, S.E., Müller, R.D., 2016. The Late Cretaceous to recent tectonic history of the Pacific Ocean basin. Earth-Sci. Rev. 154:138–173. http://dx.doi.org/10.1016/j.earscirev.2015.11.015.
Yáñez, G., Ranero, C., von Huene, R., Díaz, J., 2001. Magnetic anomaly interpretation across the southern Central Andes (32°–33.5°S): the role of the Juan Fernández ridge in the late Tertiary evolution of the margin. J. Geophys. Res. 106, 6325–6345.
Yang, X., Fischer, K.M., Abers, G.A., 1995. Seismic anisotropy beneath the Shumagin Islands segment of the Aleutian-Alaska subduction zone. J. Geophys. Res. 100, 18,165–18,177.
Yang, T., Grand, S.P., Wilson, D., Guzmán-Speziale, M., Gómez-González, J.M., Domínguez-Reyes, T., Ni, J., 2009. Seismic structure beneath the Rivera subduction zone from finite-frequency seismic tomography. J. Geophys. Res. 114, B01302. http://dx.doi.org/10.1029/2008JB005830.
Yepes, H., Audin, L., Alvarado, A., Beauval, C., Aguilar, J., Font, Y., Cotton, F., 2016. A new view for the geodynamics of Ecuador: Implication in seismogenic source definition and seismic hazard assessment. Tectonics.
Zhao, D., 2007. Seismic images under 60 hotspots: Search for mantle plumes. Gondwana Res. 12, 335–355.
Ziagos, J., Blackwell, D., Mooser, F., 1985. Heat flow in southern Mexico and the thermal effects of subduction. J. Geophys. Res. 90, 5410–5420.
Zigone, D., Rivet, D., Radiguet, M., Campillo, M., Voisin, C., Cotte, N., Walpersdorf, A., Shapiro, N., Cougoulat, G., Roux, P., Kostoglodov, V., Husker, A., Payero, J.S., 2012. Triggering of tremors and slow slip event in Guerrero, Mexico, by the 2010 Mw 8.8 Maule, Chile, earthquake. J. Geophys. Res. 117, B09304. http://dx.doi.org/10.1029/2012JB009160.
Zimmerman, M.E., Zhang, S.Q., Kohlstedt, D.L., Karato, S., 1999. Melt distribution in mantle rocks deformed in shear. Geophys. Res. Lett. 26:1505–1508. http://dx.doi.org/10.1029/1999GL900259.